ERRATA SHEET

Page	Line No.	Word No.	Error	Read Instead
2	23	2	downward	downwards
3	11	4	, (missing)	, (after hence)
5	last	(after last word)	: (missing)	:
16	20	8	cms	cm
29; 60	9,15; 4,13	5,3; 2→7, 1→2	1.5→1.10	1.6→1.11
20	Fig.1.4	-	(β appears twice)	erase one β
34	24	9	if	of
35	12	last	V/V_2	V_e/V_g
36	26	1	experiments	experiment
42	26	11	(missing word)	same (after 10th word)
45	15	2	3.2.1.2	3.2.1.3
47	24	6	dimater	diameter
50	13	3	(3.3)	3.3
52	5	last	Consequetly	and
59	5	4	or	of
60	7	(last)	1.9	1.10
91	25	2	untruly	(omit)
92	12	(last)	(missing)	are:
93	last	(last)	$m' = m_w$	$m' = \frac{1}{2}M_w$
94	3	(second product from left)	$\frac{\rho_s-\rho}{\rho} W\frac{D}{2}\cos(\beta_1+\beta_2)$	$\frac{\rho_s-\rho}{\rho_s} W\frac{D}{2}\cos(\beta_1+\beta_2)$
94	5	(second product from right)	$(\rho_s-\rho)\frac{g\pi D^2}{6}\cos(\beta_1+\beta_2)$	$\frac{g\pi D^3}{12}(\rho_s-\rho)\cos(\beta_1+\beta_2)$
95	6,18	6,4	Fig	Fig.
100	one before the last	8	gms	gm
103	7	11	cms	cm
107	1,4,6	4,7,5	cms	cm
117	last	2	510c	5.10c
123	23	10	5.14e,f and g	5.13a,b and c
137	23	13	beding	bending
167	6	-	(missing symbol)	min Minute

THE STABILITY OF STONES IN STEEP SHALLOW STREAMS

by

Atallah Y. Abu-Sayf, BE(Civil Engineering)
DIC & MSc(Civil Engineering Hydraulics)

Thesis submitted for the degree of
Doctor of Philosophy to the University of London
and to the Imperial College of Science and Technology
(Civil Engineering Department, Hydraulics)
London SW7

March 1976

Acknowledgements

This work was carried out under the supervision of Professor P. Ackers to whom the author expresses thanks and appreciation for his encouragement and invaluable advice.

The author would like also to express his gratitude to Professor J.R.D. Francis for his advice, continuous interest in this work and encouragement.

The author must thank:-

Dr J.D. Hardwick for his help and many hours of discussion about the dynamic properties of the force transducer.

Mr A. Scott-Moncrieff for his help in the electronic set-up.

Mr G. Thomas for his help in the design and construction of the flume.

Miss J. Gurr for taking photographs.

Also all the technical staff of the hydraulics laboratory who helped in one way or another.

The financial support of the Ministry of Higher Education, SYRIA, is highly appreciated.

A B S T R A C T

The stability of stones when used as a cheap lining material in steep open channels is a civil engineering problem of practical and economic importance. The little known information about this problem stimulated the pursuit of a research programme which consisted of two stages.

Stage I dealt with devising a simple theory by which the stability of irregular stones could be related to a steady stream power. This theory was tested by conducting a series of experiments on a mobile section of loose stones. The critical stream power that would produce no scour in the mobile section was determined statistically by regression analysis.

Froude model similarity criteria was employed to extend the results obtained from Stage I to apply to prototype tumbling streams and bigger stone sizes. Two empirical relationships were discovered. The first one predicts the critical stream power and the second predicts low stone transport stages once the critical stream power is exceeded.

In Stage II, a force measuring transducer was developed to isolate and measure (instantaneously and simultaneously) the hydrodynamic drag, lift and torque on a sphere suspended in a steep shallow stream. Being an idealized model, Stage II improved the understanding of the mechanics of removal of a sphere from a bed of similar spheres. Statistical analysis of the force measurements (on a very light sphere attached to the force transducer) showed that: drag generally increases with stream power and sphere protrusion, lift becomes predominantly negative in a shallow steep stream and torque due to the uneven distribution of skin friction stresses on the surface of the sphere is an equally significant contributor to the initial removal of a sphere

as drag and lift.

Stage II also included measurements of the critical stream power that dislodged a loose sphere placed at different locations and exposures.

Finally, the link between Stages I and II was established through the similarity of results of both stages.

List of Contents

		Page
List of Contents		v
List of Plates		xi
List of Figures		xiii
List of Tables		xvi
Chapter 1	Introduction.	1
1.1	A basic physical picture.	2
1.1.1	Definitions.	2
1.1.2	Forces acting on a particle.	2
1.1.2.1	Static forces.	2
1.1.2.2	Hydrodynamic forces.	3
1.1.2.2.1	Subcritical deep flows.	3
1.1.2.2.2	Supercritical shallow flows.	7
1.2	Literature Survey.	9
1.2.1	Methods followed in deep supercritical streams.	9
1.2.1.1	Classical approaches.	10
1.2.1.1.1	Outline of some classical approaches.	10
1.2.1.1.2	Brief discussion of classical approaches.	11
	(i) Shields' approach;	11
	(ii) Limitations of Shields'approach;	13
	(iii) Critical velocity criteria.	13
1.2.1.2	Idealized approaches.	15
1.2.1.2.1	Discussion of some idealized approaches.	15
1.2.2	Literature survey in shallow supercritical flows.	18
1.3	Scope of the present investigation.	23
Stage I (includes Chapters 2 and 3)	"The initial instability of irregular stones and scour experiments".	25a

List of Contents Continued

		Page
Chapter 2	Theoretical Considerations in Stage II.	25
2.1	Purpose.	25
2.2	Hydraulics of a steady fast flow in a rough steep channel.	26
2.2.1	Preliminary observations.	26
2.2.2	Available knowledge.	29
2.3	Choice of the method of analysis.	29
2.4	Outline of the author's method of analysis.	30
2.5	The stream as a transporting machine.	30
2.5.1	Available stream power.	30
2.5.2	Solid friction.	31
2.5.3	Work rate.	32
2.5.4	Efficiency of the stream.	33
2.5.5	$\overline{U}$, an average speed of a dislodged solid.	34
2.5.6	Ω_c, the critical stream power.	35
2.5.6.1	Independent variables describing the flow.	36
2.5.6.2	Independent variables describing the solid mixture.	37
2.5.6.3	Dependent variables.	37
2.5.6.4	A functional relationship of Ω_c.	38
2.5.7	A general equation for the efficiency of the stream.	38
2.5.8	Elimination of some variables from eq. 2.10 .	38
2.5.8.1	μ, viscosity of water.	39
2.5.8.2	ϵ, surface tension.	39
Chapter 3	Experiments and Results in Stage I	41
3.1	The experiments needed.	41

List of Contents Continued

		Page
3.2	Description of equipment and experimental results.	41
3.2.1	Experiments kind 1.	41
3.2.1.1	ρ_s, the mass density of solids.	41
3.2.1.2	The angle of sliding friction; α.	43
3.2.1.3	Size distribution; $(Dn)_d$.	43
3.2.1.4	Shape factor distirubtion; $(S.F)_d$.	44
3.2.1.5	Fall velocity distribution; $(Vg)_d$.	44
3.2.2	Experiments kind 2.	45
3.2.2.1	Apparatus.	45
3.2.2.2	Simplifications.	50
3.2.2.3	Experimental procedure.	52
3.2.2.4	Observations.	53
3.2.2.5	Experimental results.	55
3.2.2.5.1	Tables 3.4 and 3.5.	55
3.2.2.5.2	Determination of Ω_c.	57
3.2.2.5.3	Table 3.6; Comparison with previous investigations.	59
3.2.2.5.4	Testing scour equation.	61
3.2.2.5.5	Prediction of Ω_c and $\frac{w_k}{\Omega}$ for larger solids than those tested.	61
Stage II (includes Chapters 4 and 5)	"Force measurements on a sphere in a shallow stream and the initial instability of a loose sphere.	79a
Chapter 4	Hydrodynamic forces on a sphere in a super-critical rough flow and their statistical analysis.	79
4.1	Purpose.	79

List of Contents Continued

		Page
4.2	Isolation of drag, lift and skin friction forces.	79
4.3	Desirable dynamic properties of the force transducer.	82
4.4	Analysis of random data.	83
4.4.1	Basic Descriptive properties of random waves.	85
4.4.2	Digital analysis procedure for random waves.	86
4.5	Stability of a sphere.	92
Chapter 5	Experiments and Discussion of Results of Stage II.	95
5.1	Scope of experiments.	95
5.2	Modification of existing flume.	95
5.3	Description of force transducer.	96
5.3.1	Choice of dimensions.	96
5.3.2	Straingauges.	96
5.3.3	Block diagram of electronic set up.	99
5.3.4	Natural frequency.	100
5.3.5	Static calibration of force transducer.	100
5.4	Experimental procedure.	102
5.4.1	Simultaneous records.	102
5.4.2	Digitization and Filtering of simultaneous records.	105
5.4.3	Experiments on the initial instability of a loose sphere.	106
5.5	Experimental results and discussion.	107

List of Contents Continued

		Page
5.5.1	Force measurements.	107
5.5.1.1	Instantaneous values of FD, FL and TM.	108
5.5.1.2	Mean values and standard deviations.	108
5.5.1.2.1	Drag.	108
5.5.1.2.2	Lift.	114
5.5.1.2.3	Skin friction drag.	116
5.5.1.2.4	Angular acceleration.	118
5.5.1.3	Probability distributions.	122
5.5.1.4	Autocorrelation Functions.	129
5.5.1.5	Spectral density functions.	129
5.5.2	Sources and relative magnitudes of error in force measurements.	137
5.5.3	The critical stream power in the case of a loose sphere.	139
Chapter 6	Conclusions.	147
6.1	Stage I.	147
6.2	Stage II.	149
6.2.1	Mean values and standard deviations.	149
6.2.1.1	Drag.	149
6.2.1.2	Lift.	150
6.2.1.3	Torque due to skin friction.	
6.2.1.4	Angular acceleration.	150
6.2.2	Probability distributions.	151
6.2.3	Autocorrelation functions.	151
6.2.4	Spectral density functions.	152
6.3	The critical stream power in the case of a loose sphere.	152
6.4	The link between Stages I and II.	153

List of Contents Continued

		Page
6.4.1	Link in geometry and hydraulic conditions.	153
6.4.2	Link in results.	153
6.5	An outlook for future research.	153
List of Symbols		165
References		171
Appendix I; Curve fitting by the least square method.		176
Appendix II; Computer programs for the statistical analysis of force measurements.		178

List of Plates

		Page
Plate 1	Top view of flume (looking upstream) showing the bed roughened with granite stones. Scale indicator: width of flume = 50 cm.	157
Plate 2	Top view of flume (looking upstream) showing the roughness of the water surface. Scale indicator: width of flume = 50 cm. Q = 24.63 litres/sec, slope = 30%.	158
Plate 3	Profile of flow (direction of flow is from right to left) showing a distorted water surface. Scale indicator: depth of flow is in the order of 6 to 8 cm. Q = 24.63 litres/sec, slope = 30%.	159
Plate 4	Top view of flume (looking upstream) showing the force transducer, the idealized bed of spheres and the hexagonal packing. Scale indicator: diameter of each sphere = 5.1 cm.	160
Plate 5	Top view of flume (looking upstream) showing the force transducer mounted in position and a rough, shallow and supercritical stream over the idealized bed of spheres. Air entrainment is clearly indicated by the white spots on the water surface. Q = 24.63 litres/sec, slope = 20.8%.	161
Plate 6	Profile of a shallow supercritical stream over a steep bed of spheres. Scale indicator: diameter of sphere = 5.1 cm. Q = 24.63 litres/sec, slope = 20.8%.	162
Plate 7	Profile of force transducer showing the mounting arrangement and the point gauge. Scale indicator: diameter of sphere = 5.1 cm.	163

List of Plates Continued

Page

Plate 8 A close view of force transducer showing the strain gauges glued and waterproofed. Scale indicator: diameter of sphere = 5.1 cm. 164

List of Figures

		Page
Chapter 1		
1.1	Boundary layer development along a rough flat bed.	4
1.2	Production of shear forces in a turbulent boundary layer (from Francis (1958).	5
1.3	Hydrodynamic forces on a particle.	7
1.4	Profile of a shallow supercritical flow over a rough steep bed.	8
1.5	Shields Diagram (from Graf, 1971).	12
1.6	Critical water velocities for quartz sediment as function of mean grain size (from Graf, 1971).	14
1.7	A simple force diagram of forces acting on a stone in a supercritical shallow stream (after Hartung et al, 1970).	20
1.8	Variation of the critical modified Shields parameter with D_{50}/d in supercritical flows (after Ashida et al, 1973).	22
Chapter 2		
2.1	Velocity profiles, So = 23%, Q = 17.41 litres/sec, x = 50 cm.	27
2.2	Lines of equal velocity. So = 23%, Q = 17.41 litres/sec, x = 50 cm.	28
2.3	A large solid just sliding in air over a rough surface.	31
2.4	A large solid pulled by a force F_1 with constant speed.	31
Chapter 3		
3.1	Weight distribution of 100 granite stones.	46
3.2	Shape factor distribution of 100 granite stones.	46
3.3	Fall velocity distribution of 100 granite stones.	46
3.4	Plan and profile of flume.	48
3.5	Orifice plate and connections of manometers.	49

List of Figures Continued

		Page
Chapter 4		
4.1a	Profile of an ideal bed of spheres and a supercritical flow over it.	80
4.1b	Plan of hexagonal pattern of spheres.	80
4.2	Diagram of bending moments.	81
4.3a&b	Frequency response functions of a mechanical system with a force input. (a) Gain factor, (b) Phase factor. (From Bendate, 1971).	84
4.4	Simultaneous records of stress at sections S_1, S_3 and S_7.	85
4.5	Sampling of a continuous record.	86
4.6	Sampling of a stationary random record with a zero mean.	88
4.7	Forces acting on a loose sphere.	92
Chapter 5		
5.1a,b&c	Dimensions of force transducer (a) Profile, (b) Side view, (c) Plan.	97
5.2a,b&c	(a) Loading diagram, (b) One-armed bridge, (c) Four-armed bridge.	99
5.3	Block diagram of electronic set-up.	99
5.4a&b	Free vibrations of force transducer (a) In air, (b) In water.	101
5.5a&b	Static calibration of force transducer (a) Loading diagram, (b) Deflections of signals S_1, S_3 and S_7 after loading.	102
5.6	Simultaneous records of S_1, S_3 and S_7.	104
5.7	Digital filtering of a record.	106
5.8a,b, c&d	Time versus (a) drag, (b) torque, (c) lift, (d) angular acceleration.	109-112
5.9a,b&c	Ω versus $\overline{F_D}$ (a) p_r = 2.84 cm, (b) p_r = 3.84 cm, (c) p_r = 4.84 cm.	115
5.10a,b &c	Ω versus $\overline{FL}$ (a) p_r = 2.84 cm, (b) p_r = 3.84 cm, (c) p_r = 4.84 cm.	117

List of Figures Continued

		Page
5.11a,b &c	Ω versus $\overline{TM}$ (a) p_r = 2.84 cm, (b) p_r = 3.84 cm, (c) p_r = 4.84 cm.	119
5.12	Actual and assumed suspension locations of the test sphere.	118
5.13	Ω versus $\overline{a}$ (a) p_r = 2.84 cm, (b) p_r = 3.84 cm, (c) p_r = 4.84 cm.	121
5.14a,b, c&d	Probability that:-	
	(a) Drag is exceeded;	124
	(b) lift is exceeded;	125
	(c) torque is exceeded;	126
	(d) angular acceleration is exceeded.	127
5.14e,f &g	Ω versus % stability	
	(a) p_r = 2.84 cm ;	128
	(b) p_r = 3.84 cm ;	128
	(c) p_r = 4.84 cm .	128
5.15a,b &c	Lag time versus autocorrelation coefficient for (a) drag, (b) lift, (c) torque.	130-132
5.16a,b &c	Frequency versus power spectral density function for (a) drag, (b) lift, (c) torque.	134-136
5.17a,b &c	Slope versus Ω_c	
	(a) x = 66.25 cm ;	141
	(b) x = 110.42 cm ;	141
	(c) x = 154.58 cm .	141

List of Tables

		Page
Chapter 3		
3.1	Measurements of the mass density of solids, ρ_s.	63
3.2	Measurement of the angle of sliding friction α.	64
3.3	Calibration of orifice plate.	65
3.4	Details of experimental results.	66
3.5	Contains e_o, Ω_{co}, r_o, e_1, Ω_{c1} and r_1 as defined in equations 3.7.3 and 3.7.4 .	76
3.6	Comparison of Ω_c versus S_o as computed by the author based on data from different sources.	77
Chapter 5		
5.1	Summary of instantaneous force measurements.	142
5.2	Summary of initiation of motion experimental results on a loose sphere, D = 5.1 cm, ρ_s = 2.65 gm/cm^3.	146

CHAPTER 1

Introduction

What happens when a stream of water flows over a bed of cohesionless particles like sand or quarried rock? Tracing the first answers to this question shows that channel and river hydraulics began as an art. When and where this art has started remains hidden in antiquity. However, scientific attempts have been made to systemize that art from the Sixteenth Century till now; qualitative as well as quantitative knowledge has been accumulating about erosion, transport and deposition of cohesionless materials when subjected to a stream of fluid. The fluid is mainly water or air and the stream is conveyed by an open channel or a closed conduit.

Initiation of motion of cohesionless particles by a stream is usually understood as a threshold condition after which a continuous flow of sediment commences. Although an immense volume of knowledge has been gained about the initiation phenomenon in relatively deep and subcritical streams, little is known about it in relatively shallow and supercritical ones. It is the object of this research to investigate the critical hydraulic conditions under which large cohesionless particles start moving when subjected to a shallow and supercritical stream.

The practical application of this investigation is to devise a rational method by which the minimum weight of individual solids could be chosen to line spillway chutes of small dams, steep highway ditches and other similar civil engineering works where artificial steep open channels are to be lined with cheap available material such as gravel, natural stones or quarried rock.

The first part of this chapter will consist of a basic physical picture of subcritical and supercritical steady flows in alluvial wide channels. A brief review of literature will next be discussed. Finally the scope of this investigation will be outlined.

1.1 A Basic Physical Picture

1.1.1 Definitions

The term subcritical flow in open channels physically means that, if a small disturbance is created on the water surface, it travels both upstream and downstream; while in supercritical flows, such a disturbance travels only downstream. On the other hand, a flow is described as deep when the mean depth of flow d is large compared to the mean sediment size D_{50}, say $\frac{d}{D_{50}} > 10$, hence, there is a thick cover of fluid moving over the loose particles (see Fig. 1.1); a shallow flow implies that both d and D_{50} are of the same order of magnitude, say $\frac{d}{D_{50}} < 10$ (see Fig. 1.4).

1.1.2 Forces Acting on a Particle

Consider a stream and the forces acting on a particle deposited in the top layer of a loose bed. These forces could be divided into two categories: A - Static Forces. B - Hydrodynamic Forces.

1.1.2.1 Static Forces

(i) The weight of the particle which could be represented by a vector passing through its centre of mass and pointing vertically downwards.

(ii) The buoyancy force which is the weight of the fluid displaced by the particle. The buoyancy force acts also through the centre of mass of the particle but its direction is vertically upwards.

(iii) Constraint forces transmitted from the neighbouring grains. These forces are unknown in magnitude, direction or point of application.

Since it is difficult to locate the centre of mass of irregular-shaped particles, the point of application of the weight and buoyancy forces is unknown.

1.1.2.2 Hydrodynamic Forces

These forces are due to the movement of the fluid over the loose bed of particles. It is the set of hydrodynamic forces in a region close to the particle that may set it to roll, slide or be ejected from its recess. Hence, a close look at the flow structure near the loose bed is indispensable. A distinction has to be made between subcritical deep flows on the one hand and supercritical shallow ones on the other.

1.1.2.2.1 Subcritical deep flows

Boundary layer characteristics near a rough bed

Most of the discussion in this article is strongly influenced by a simple account of the boundary layer characteristics given by Francis(1958).

A boundary layer is the extent of retarded fluid due to the presence of a solid boundary when that fluid is flowing. Fig. 1.1 shows a profile of a steady two dimensional flow along a rough flat bed.

Since there can be no slip between the fluid particles and the solid boundary, the velocity of the fluid at a certain level below the summits of the roughness elements of the solid boundary should be zero. This level is usually referred to as the theoretical bed level. In the boundary layer, fluid elements are continuously sheared one relative

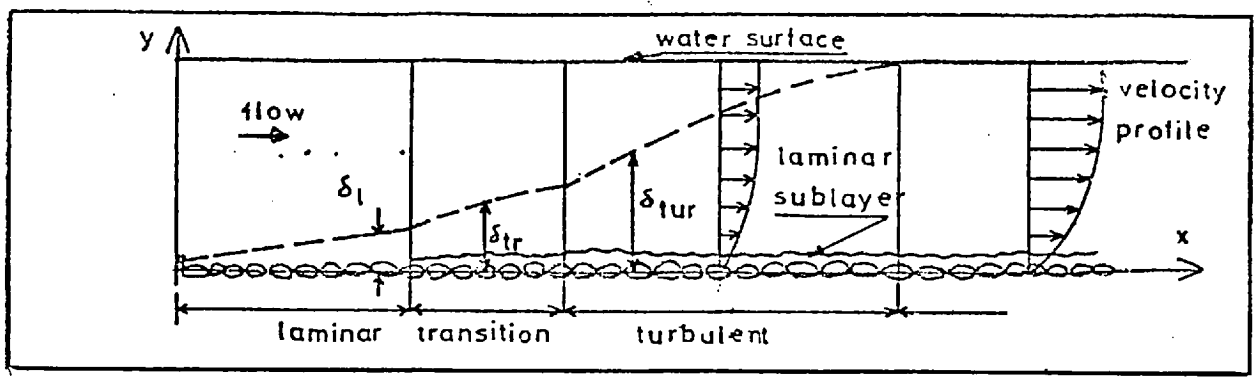


FIG. 1.1 , Boundary layer development along a rough flat bed

to the other and the flow could be thought of as sluggish layers of fluid near the solid boundary and faster ones away from it.

The production of a shear stress in the boundary layer needs the essential assumption that a shear stress at a point produces a rate of strain there. The rate of strain is equivalent to a gradient of velocity at the same point. Hence, production of shear forces culminates wherever velocity gradients are large.

If the flow in the boundary layer is purely laminar, then there is a simple linear relationship between τ (the shear stress at a point) and $\frac{dv}{dy}$ (the velocity gradient at the same point) such that

$\tau = \mu \frac{dv}{dy}$, where μ is the coefficient of viscosity of the fluid. If τ is assumed to decrease from τ_o at the bed to zero at a distance $y = \delta_l$ (δ_l is the thickness of the laminar boundary layer) and the differential equation $\tau = \mu \frac{dv}{dy}$ is integrated, the well-known parabolic velocity distribution in a laminar boundary layer is obtained

$$V - v = \frac{\tau_o}{2 \mu \delta_l} (\delta_l - y)^2 \quad \text{..... Eq . 1.1}$$

where V is the free stream velocity and v is the velocity at a point in the boundary layer.

In a turbulent boundary layer, a shear stress at a point could

be thought to be produced by momentum exchange between fast and slow moving fluid layers. The agent responsible for this momentum exchange is an eddy of mean size l , see Fig. 1.2 .

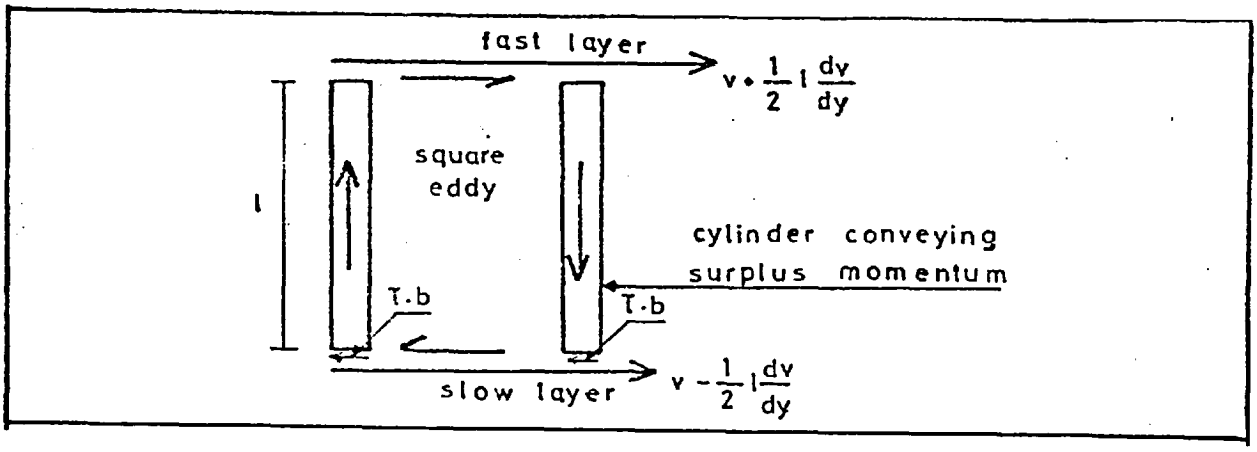


FIG. 1.2 , Production of shear forces in a turbulent boundary layer (from Francis 1958)

The rate of change of momentum between the two layers is proportional to the shear forces at the ends of the two cylinders which are assumed to convey the surplus momentum from the fast moving to the slow moving one. On the other hand, the rate of change of momentum between the two layers is equal to the mean slip velocity of the eddy: $\frac{1}{2} l \frac{dv}{dy}$, multiplied by the mass per unit time transferred on each side of the eddy: $2(b \rho \frac{1}{2} l \frac{dv}{dy})$. The shear force at the end of the cylinders is $2b\tau$. Therefore

$$\tfrac{1}{2} l \frac{dv}{dy} \left(2 b \rho \tfrac{1}{2} l \frac{dv}{dy}\right) \propto 2 b \tau \qquad \text{Hence}$$

$$\left(\frac{\tau}{\rho}\right)^{\frac{1}{2}} = \left(\frac{k}{2}\right)^{\frac{1}{2}} l \frac{dv}{dy} \qquad \ldots\ldots\ldots\ldots\ldots\ldots\ldots \text{Eq. 1.2}$$

where k is a constant that accounts for the variation of size of the eddies encountered in both space and time.

Schlichting (1955) reports Prandtl's hypothesis that the mixing length is proportional to the mean eddy size (mentioned previously).

Prandtl integrated equation 1.2 based on the following assumptions:

1. $l\,(\frac{k}{2})^{\frac{1}{2}} = 0.4y$

2. The shear stress τ at any point in the turbulent boundary layer is assumed to be constant and equal to τ_o, the shear stress at the solid boundary.

Integration of equation 1.2 yields the well-known logarithmic velocity distribution

$$v = 5.75\,(\frac{\tau}{\rho})^{\frac{1}{2}} \log \frac{y}{C_1} \qquad \text{..... Eq. 1.3}$$

where C_1 is a constant of integration and depends on the ratio of the roughness size to the thickness of the laminar sublayer and v is a time average velocity at a point in the turbulent boundary layer.

Schlichting (1955) also reports that Nikuradse has shown by experiments on rough pipes that the thickness of the laminar sublayer is $\delta' = 11.5\ \nu\,\{\frac{\tau_o}{\rho}\}^{\frac{1}{2}}$, where ν is the kinematic viscosity of the fluid. The laminar sublayer is observed to exist next to a smooth solid boundary even if the boundary layer as a whole is a turbulent one.

A transition boundary layer is that region just downstream of the wholly laminar one, where intermittent unsteadiness of the flow characteristics prevails.

List of Hydrodynamic Forces

With the laws of the velocity distributions in laminar, transition and turbulent boundary layers established, the mean hydrodynamic forces on a particle could be predicted.

Consider a particle in a fully developed turbulent boundary layer, where x - x' and y - y' are perpendicular axes passing through its centre of gravity c.g. See Fig. 1.3 . The mean hydrodynamic forces on the irregular particle could be tentatively listed as follows:

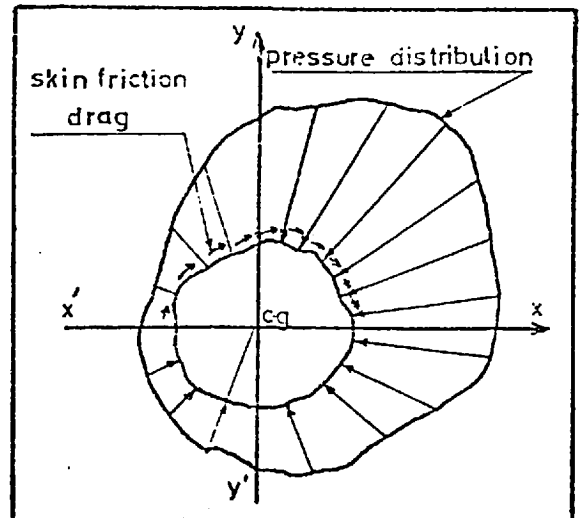


FIG 1.3 . Hydrodynamic forces on a particle

1. A mean drag force $\overline{FD}$ due to the unbalance of pressures upstream and downstream of the y - y' axis.

2. A mean lift force $\overline{FL}$ due to the unbalance of pressures above and below the x - x' axis.

3. A mean torque $\overline{TM}$ due to unevenly distributed skin friction stresses on the surface of the particle. In a highly turbulent flow, these skin friction stresses could be due to the collapse of turbulent eddies on the surface of the particle.

The instantaneous hydrodynamic forces which act on a particle are mathematically expressed by the following set of equations:

$$FD = \overline{FD} + FD'$$
$$FL = \overline{FL} + FL' \qquad \text{Equations 1.4}$$
$$TM = \overline{TM} + TM'$$

where FD', FL' and TM' are turbulent fluctuating components of FD, FL and TM respectively, superimposed on the mean values.

The irregular shape of the solid particles making up a loose bed and the turbulent characteristics of a turbulent boundary layer throw some uncertainties whether equations 1.4 could be exactly determined.

1.1.2.2.2 Supercritical Shallow Flows

In contrast to Fig. 1.1 , Fig. 1.4 shows a profile of a shallow steady flow in a wide rectangular open channel, the bed of which is

lined with layers of large and loose solids. The term steady flow implies that the volumetric discharge of water per unit time is constant.

Such a flow picture is radically different from that of a deep subcritical stream. The main differences are as outlined below:

1. The flow is supercritical and shallow and the size of a loose solid is of the same order of magnitude as the water depth. The water depth could be locally defined as the normal distance between a point on the surface of the particle and the water surface (normal in this context means normal to the main slope of the channel).

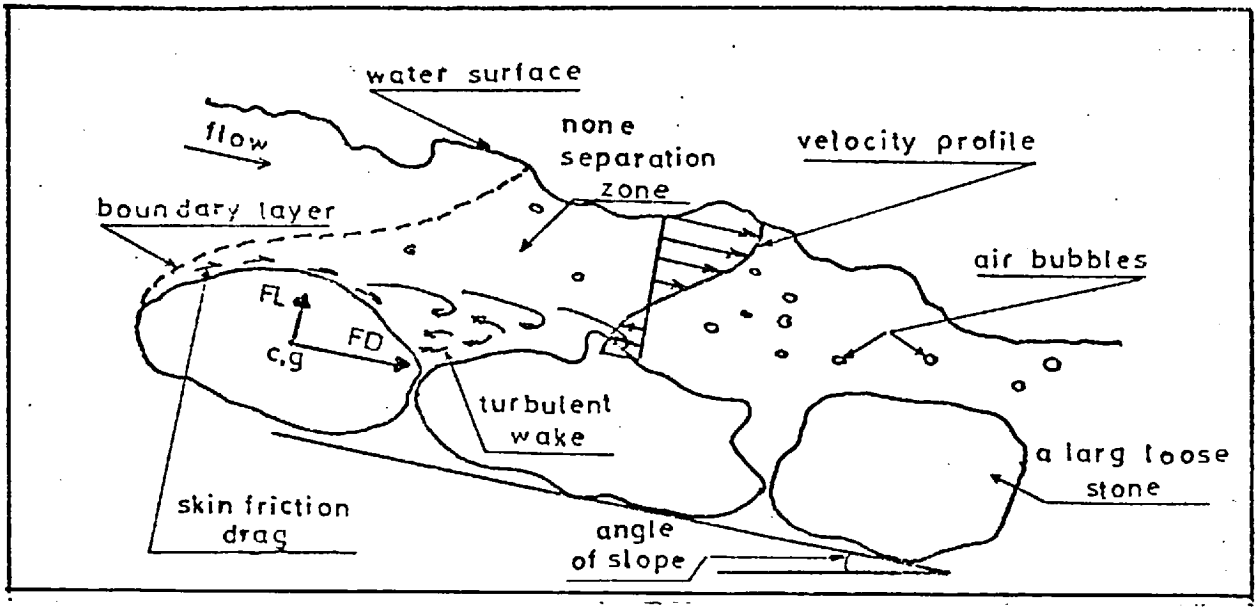


FIG. 1.4 , Profile of a shallow supercritical flow over a rough steep bed

2. A boundary layer grows from the leading edge of the first solid and fills the whole depth of the stream within a short longitudinal distance. This fast growth of the boundary layer is attributed to the high velocities encountered and the shallowness of the stream. Sharp edges located on the surface of the particle are edges of separation of the boundary layer. Turbulent wakes downstream of the

separation edges are also of an appreciable size relative to the depth of the flow. Hence, the boundary layer is severely interrupted.

3. The streamlines in the non-separation zones are radically distorted due to the presence of a very rough bed indeed. Consequently, the water surface is a complex combination of humps and depressions and any attempt to measure the stream depth could be impractical.

4. Distortion of the streamlines together with the presence of high velocities near the water surface, may cause some water lumps to leave that surface temporarily and come back to it again entraining some air from the atmosphere.

5. A mean velocity traverse at one cross-section of the channel may be an irregular curve with varying velocity gradients or even negative mean velocities in the turbulent wakes.

The instantaneous hydrodynamic forces on a solid are schematically shown in Fig. 1.4 . They are similar to the ones previously enumerated in the case of a deep subcritical stream and are mathematically expressed by equations 1.4 . But, more uncertainty is encountered if the tentative list of hydrodynamic forces is to be determined in the case of a shallow supercritical stream. This uncertainty is due to the complex characteristics of a tumbling flow as was described previously.

1.2 Literature Survey

This survey will outline and discuss the contemporary methods of dealing with the initial movement problem, firstly in a deep subcritical stream and secondly in a shallow supercritical one.

1.2.1 Methods Followed in Deep Subcritical Streams

Generally speaking, such methods could be classified into two

categories: A - Classical Approaches, B - Idealized Approaches.

1.2.1.1 Classical Approaches

Where the threshold condition for initiating the motion of a certain grain size is correlated to critical hydraulic parameters of the stream (such as τ_c and $\overline{V}_c$). The critical hydraulic parameters are those associated with zero sediment transport rate.

The majority of researchers, like Shields (1936), have conducted flume experiments in which the cross-section of the flume is rectangular, the side walls are made of glass and the bed consists of uniform loose particles such as sand or gravel. The hydraulic parameters of the stream are maintained so as to produce some sediment transport rate and the critical hydraulic parameters that produce zero transport rate are extrapolated.

Other researchers like Kramer (1935) and Vanoni (1964) have subjectively observed the initial motion of single grains or the occurrence of small bursts of scour along the loose bed and defined the associated hydraulic parameters as the critical ones.

In the above mentioned classical approaches, no sophisticated instrumentation was employed, but simply measuring mean flow depths, mean velocity profiles and the slope of the channel was considered adequate for describing the flow.

1.2.1.1.1 Outline of Some Classical Approaches

1. Critical mean shear stress criteria; as developed by Shields (1936) and later checked or criticized by White (1940), Lane (1955), Eginzaroff (1957 and 1965), Vanoni (1964), Bogardi (1968) and recently by White (1970) and Mantz (1973 and 1975).

2. Critical mean velocity criteria, as reported by Lelliavsky (1955) to be first due to Brahams who developed a critical velocity equation

in 1753. Other classical works are those by Fortier and Scobey (1926), Hjustrom (1935) and Mavis (1949). Recently, Neill (1967) and Yang (1973) have developed similar criteria.

1.2.1.1.2 Brief Discussion of Typical Classical Approaches

(i) Shields' Approach

Sheilds considered the stability of a sand grain among similar grains which make up the bed of a wide rectangular channel conveying a deep subcritical flow. He equated the mean drag force on the grain to its weight under water. By making use of the velocity distribution in a fully developed boundary layer and dimensional analysis he obtained the following functional relationship:

$$\tau_{*c} = \frac{\tau_c}{\rho g\left(\frac{\rho_s}{\rho} - 1\right)D_n} = f\left(\frac{D_n V_{*c}}{\nu}\right) \quad \text{..... Eq. 1.5}$$

where $V_{*c} = \left(\frac{\tau_c}{\rho}\right)^{\frac{1}{2}}$ and is known as the critical shear velocity.

$\frac{D_n V_{*c}}{\nu} = Re_*$ is known as the grain Reynolds number and could be thought of as the ratio between the nominal diameter of the particle D_n and the thickness of the laminar sublayer.

τ_c is the critical mean shear stress at the bed level that is just sufficient to set the grain into motion.

See the list of symbols for the rest of the variables.

Shields determined the functional relationship: Eq. 1.5 , by experiment. His experimental results are shown in Fig .1.5 .

The main characteristics of Shields' approach are:

1. The critical mean shear stress is extrapolated from plots of sediment transport rates versus the bed shear stress in a uniform flow region. The mean bed shear stress that corresponds to zero transport

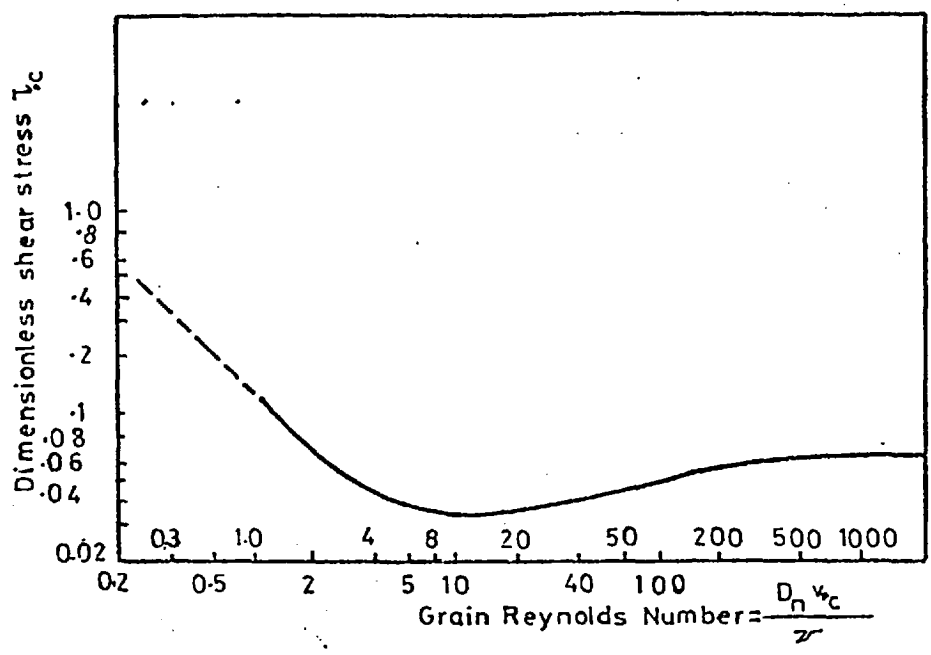


FIG. 1.5 , Shields Diagram. (from Graf(1971))

rate is defined as τ_c.

2. The general shape of Shields Curve is similar to that of a drag coefficient of a fixed sphere versus the Reynolds number in an infinitely deep flow.

Three regions in Shields Curve can be distinguished:

A. $Re_* < 2$, this region reveals a linear increase of the critical shear stress τ_{*c} with decreasing Re_* and is not backed up by experimental data. To get down to such low values of Re_*, the flow is usually laminar and the size of the sand is fine.

B. $2 < Re_* < 1000$, here, τ_{*c} decreases with increasing Re_* until the former reaches a minimum value of 0.033 at $Re_* = 10$ and increases again to level off at a value of 0.06 when $Re_* = 1000$.

C. $Re_* > 1000$, τ_{*c} becomes independent of Re_*. Hence, for the special conditions of uniform particles, a plain channel bed, uniform flow conditions and $\frac{\rho_s}{\rho} = 2.6$, the following simple relationship holds:

$$D_n = 11\ d\ S_o$$

where D_n is the minimum size of a particle that is not eroded by a stream of uniform depth d and slope S_o.

(ii) Limitations of Shields' Approach

Shields criteria has been mainly criticized from the following points of view:

1. When the density difference between the solid and the fluid is large, disagreement with Shields criteria is distinct, as was shown in the experiments conducted by White (1940).

2. Shields criteria apply to uniform sediment sizes and have to be modified for sediment mixtures as was suggested by Gessler (1965 and 1971).

3. Experiments conducted recently by White (1970) and Mantz (1973 and 1975) explored the region $Re_* < 2$.

4. In the case of shallow supercritical flows, some investigators like Neill (1967) and Ashida et al (1973) have suggested that Shields criteria could be modified to suit these particular flow conditions. It will be shown in this investigation that such a modification is not adequate especially when the sediment size and the depth of flow are of the same order of magnitude.

(iii) Critical Velocity Criteria

On of the earliest expressions of a critical mean stream velocity $\overline{V}_c$ is due to Brahams in 1753 which reads:

$\overline{V}_c = K\, W^{0.125}$, where K is an empirical constant, and W is the weight of the grain. The Task Committee of the ASCE on Sedimentation (1966) and Graf (1971) have presented a chronological survey of the works of many investigators in the field of initiation of motion of sediments.

Hjulstrom (1935) in an extensive data analysis on the initiation of motion of sediments in deep streams (depth in excess of 1 metre), obtained a diagram as an erosion-deposition criterion, where he related $\overline{V}_c$ to D_n as shown in Fig. 1.6 .

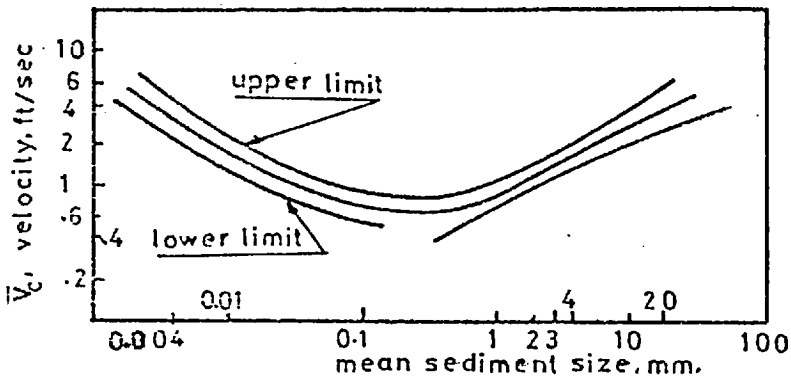


FIG 1.6 , Critical water velocities for quartz sediment as function of mean grain size. (from Graf (1971))

The work of Mavis et al (1949) is a correlation between critical velocities near the bed of a stream v_{bc} and D_n. His critical velocities were obtained by extrapolating actual velocity distributions measured in rivers. Mavis obtained the following equation: $v_{bc} = \frac{1}{2}(D_n)^{4/9}(\frac{\rho_s}{\rho} - 1)^{\frac{1}{2}}$, where v_{bc} is measured in cm/sec and D_n in mm.

Neill (1967) used dimensional analysis to write a functional relationship that describes the initiation of motion of a grain of size D_n, Neill's relationship reads:

$$\frac{\rho \bar{V}_c}{(\rho_s-\rho)gD_n} = f\left(\frac{\bar{V}_c D_n}{\nu}, \frac{D_n}{d}\right)$$

Neill obtained by experiment:

$$\frac{\rho \bar{V}_c}{(\rho_s-\rho)gD_n} = 2.5\left(\frac{D_n}{d}\right)^{-0.2} \quad \text{for} \quad \frac{\bar{V}_c D_n}{\nu} > 800$$

The previous equation shows that $\bar{V}_c$ is dependent on the shallowness of the stream as expressed by the ratio $\frac{D_n}{d}$. Later Neill (1968) attributed the effect of $\frac{D_n}{d}$ on $\bar{V}_c$ to systematic errors in his experiments.

Yang (1973) used the equations of velocity distribution in a boundary layer and conducted multiple regression analysis on experimental data obtained from different sources. He deduced the following

equations:

$$\frac{\overline{V}_c}{V_g} = \frac{2.5}{\log (Re_* - 0.06)} \quad , \text{For } 0 < Re_* < 70$$

and $$\frac{\overline{V}_c}{V_g} = 2.05 \quad , \qquad \text{For } Re_* > 70$$

where V_g is the terminal fall velocity of a particle of size D_n.

Yang's equations apply to sands with a size range of

$0.02 \text{ mm} < D_n < 2 \text{ mm}$

1.2.1.2 Idealized Approaches

Both the lack of understanding of the structure of turbulence and the complexity of geometry of naturally deposited sediment beds have stimulated researchers to introduce the following aids and simplifications to solve the initiation problem:

1. Line the channel bed with fixed geometrical elements (such as spheres or cylinders).
2. Concentrate on the understanding of flow structure around one geometrical element.
3. Explore the effect of turbulence by using sophisticated instrumentation.
4. Infer the stability of one geometrical solid and hence, the stability of irregular ones.

1.2.1.2.1 Discussion of Some Idealized Approaches

Einstein and El-Samni (1949) have built a flume, where the bed is lined with hemispheres 2.7 inches in diameter D . The hemispheres were glued in a hexagonal pattern to a flat bed. A fully developed boundary layer was maintained over the roughened bed. The pressure

difference Δp between the top and base of the hemispheres was measured instantaneously by a pressure transducer and the following conclusions drawn:

1. The pressure near the summit of a hemisphere fluctuates and is always less than the pressure at the base. The pressure at the base is virtually constant with time.

2. The probability distribution of the pressure difference Δp is normal.

3. There is a unique relationship between Δp and the coefficient of lift of a hemisphere (C_L) such that

$\overline{\Delta p} = C_L \rho \frac{v^2}{2}$ where $\overline{\Delta p}$ is the mean pressure difference, v is the stream velocity measured at 0.35 D above the theoretical bed level and C_L is found to be constant and equal to 0.178.

4. Experiments to locate the theoretical bed level in the case of natural gravel were conducted and it was found that the theoretical bed level is located 0.2 D_{67} below the summits of the natural grains. D_{67} is the sediment size where 67% by weight of the material is finer than that size.

Chepil (1958) measured mean pressures on hemisphere surfaces. The hemispheres ranged from 0.16 to 5.08 cm. in diameter and were placed in a wind tunnel in a hexagonal pattern but three diameters apart. Integrating the pressure distribution over the surface of the test hemisphere, he obtained the lift and drag forces and concluded that lift is approximately 75% of the drag force, hence lift is an important contributor to the initial instability of a loose grain.

Chepil (1959) obtained records of instantaneous drag and lift on a sphere. He used straingauges, but the drag and lift records were taken individually, so there is no direct information on the total instantaneous force. However, he concluded that the ratio of maximum

to mean values of drag and lift is approximately 2.5, he also found that the instantaneous lift and drag forces are statistically distributed according to a skewed normal error law.

Chepil (1961) measured the mean pressure distribution on a sphere placed at different elevations above the bed of a wind tunnel. He found that the mean lift force decreases with elevation above the bed becoming nearly zero at 3 to 4 grain diameters above the bed.

Using straingauges, Apperley (1968) measured the instantaneous drag and lift forces on a quarter of an inch sphere. The test sphere was placed in a five-foot working section where similar spheres were glued to a flat bed in a hexagonal pattern. The rest of the flume bed was roughened with natural gravel of a mean size of $\frac{1}{4}$ inch.

Apperley has investigated only one hydraulic condition, namely one discharge and one slope of the channel. The test sphere was exposed 4 times to the flow with protrusions ranging from $\frac{1}{4}$D to 1.5 D. His main conclusions are:

1. The mean lift force starts positive with no protrusion of the test sphere, increases to a maximum at $\frac{1}{2}$D and becomes negative at 0.9 D and at least up to 1.5 D.
2. The mean drag force increases with the protrusion of the sphere.
3. The instantaneous drag and lift forces are statistically distributed according to a skewed normal error law. Auto-correlation calculations for both drag and lift show a rapid decay of the auto-correlation function after a lag time of approximately 1 sec. The frequency content of the instantaneous records of drag and lift was obtained by calculating the power spectral density function. On the whole, low frequency components of drag and lift contain more energy than high frequency ones. The range of frequencies explored is from 0 to 25 Hz.

Chen and Clyde (1972) conducted instantaneous force measurements on a one-foot diameter sphere placed among closely packed ones of a similar size. The flume used was 50 ft long, 8 ft wide. Their main conclusions are:

1. The theoretical bed level is located 0.15 D below the summits of the spheres.

2. The Chezy Coefficient for the bed is independent of the channel slope and depth of flow and has a constant value of $35.3 ft^{\frac{1}{2}}/sec$.

3. The probability densities of the fluctuating lift and drag forces are approximately normally distributed.

4. The relative intensity of lift (ratio of the mean square value to the mean value) was found to be independent of the depth of flow and slope of the channel and is approximately equal to 0.18. The relative intensity of drag was found to be a weakly increasing function of the depth of flow.

Chen and Carsten (1973) used a sphere-pin model in a wind tunnel to determine the probability distribution of the fluid driving moment (which is the result of drag, lift and skin friction contributions to roll a sphere). They concluded that the contribution of skin friction drag is of the same order of magnitude as that of lift and drag, especially if the sphere is exposed one sphere diameter above the flat bed of the tunnel. They also found that the fluid driving moment is normally distributed and increases with the protrusion of the sphere.

1.2.2 Literature Survey in Shallow Supercritical Flows

Initiation of motion of large solids in a shallow supercritical stream constitutes a special problem that has only recently attracted the attention of few researchers. Only few works have been found to have direct relevance to the present study; they are briefly discussed

subsequently:

A. Hartung and Scheuerlein's Approach

Hartung and Scheuerlein (1967 and 1970) have dealt with the problem of finding a resistance equation to apply to shallow super-critical flows in a wide rectangular channel with a rough bed. They have assumed that an equation of the following form applies:

$$(\lambda)^{-\frac{1}{2}} = A_1 \log \left(c \frac{K_m}{d_m} \right) \quad \text{.....Eq. 1.6}$$

where λ is a resistance factor, A_1 is a constant, K_m is the mean roughness height of the solids making up the channel bed. K_m is arbitrarily chosen to be equal to $\frac{D_{50}}{3}$.

d_m is an imaginary mean depth of flow.

c is a rougness factor which is defined in terms of the following empirical equation:

$$c = \sigma(1.7 + 8.1(P.F1)\sin \beta) \quad \text{.....Eq. 1.7}$$

P.F1 is a packing factor defined as a ratio of the D_{50} of the solid mixture to the longitudinal distance between two roughness elements.

σ is an aeration factor and is equal to the ratio of the mass density of the air-water mixture to the mass density of pure water.

β is the angle the channel bed makes with the horizontal.

The aeration factor σ is given by the following empirical equation:

$$\sigma = 1 - 1.3 \sin \beta + 0.08 \frac{d_m}{K_m} \quad \text{.....Eq. 1.8}$$

Considering a unit width of the stream and assuming a uniform steady flow, a formula for the average stream velocity (similar to the Chezy formula) is adopted, hence;

$$\overline{V}_m = (8g\, d_m \sin \beta)^{\frac{1}{2}}/\lambda \quad \text{.....Eq. 1.9}$$

and the discharge of pure water per unit width of the channel is:

$$q = \sigma\, d_m\, \overline{V}_m \qquad \text{..... Eq. 1.10}$$

The stability of a single solid is next considered:

Fig 1.7 shows a simple force diagram acting on one solid in a shallow supercritical stream.

The forces consist of:

G the submerged weight of the solid;

I is a hydrodynamic impact force given by

$I = \rho_m (\overline{V}_c)^2 S$

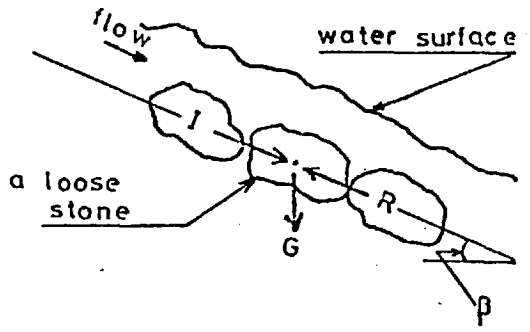


FIG. 1.7 , A simple diagram of forces acting on a stone in a supercritical shallow stream.

(after Hartung et al (1970))

where ρ_m is the mass density of the air-water mixture, S is the striking area of the solid, assumed equal to $\frac{1}{2}\frac{\pi}{4} D_{50}^2$.

$\overline{V}_c$ is the critical average stream velocity which just sets a solid of size D_{50} into motion.

R is a resistance friction force given by:

$$R = G \cos\beta \tan\alpha$$

where α is the angle of sliding friction of the solid.

Finally, the stability equation is written as:

$$I + G \sin\beta \leq G \cos\beta \tan\alpha$$

After several algebraic manipulations the following equation for $\overline{V}_c$ is obtained:

$$\overline{V}_c = \left\{2g \frac{\rho_s - \rho}{\rho} D_{50} \cos\beta \frac{2}{3} (\tan\alpha - \tan\beta)\right\}^{\frac{1}{2}}$$

For steep slopes and large solids $\frac{2}{3}(\tan\alpha - \tan\beta) \cong 1.2$

where α is assumed equal to 65° and β equal to 20°.

Hence:

$$\overline{V}_c = \left(1.2 \frac{2g(\rho_s - \rho)\, D_{50} \cos \beta}{\rho} \right)^{\frac{1}{2}} \quad \text{..... Eq. 1.11}$$

Equations 1.6 to 1.11 can only be solved by trial and error if q, D_{50}, ρ, ρ_s, β and P.F are known quantities.

No experiments were conducted by Hartung et al to check the stability of loose stones when a shallow supercritical stream actually flows over them. It was also stated in the above mentioned investigation that $\overline{V}_m$ and d_m are imaginary quantities that did not actually occur but were helpful only for the estimation of an average impact force on the individual solids.

B. Initiation of Motion Experiments

Some of Neill's experiments to which reference has been made previously, have been conducted under supercritical flow conditions. The maximum values of the channel slope , mean sediment size, Froude number and (D_{50}/d) were: 2.7%, 2 cm, 1.3 and 0.35 respectively. But, the flow - as Neill put it - was always uniform and the water surface was defined and undisturbed. Hence, some of Neill's experiments could be classified under a threshold class of investigations where the shallowness of the stream just starts to show some influence on the initial instability of solids.

Ashida and Bayazit (1973) have suggested that dimensional analysis, when applied to the initial instability of a solid by a shallow supercritical stream, gives the following functional relationship:

$$\tau_{*c} = f(Re_* , D_{50}/d)$$

They have modified Shields' parameter to account for steep channel slopes and used the following one instead:

$$\tau_{*s} = \tau_{*c}/(\cos\beta \tan\alpha - \frac{\rho_s}{\rho_s - \rho} \sin\beta) = f(Re_* , D_{50}/d)$$

Experiments were run to determine the above mentioned relationship. Fig . 1.8 shows a distinct increase of τ_{*s} with (D_{50}/d). The maximum channel slope and sediment mean size used in their experiments were 20% and 2.25 cm respectively.

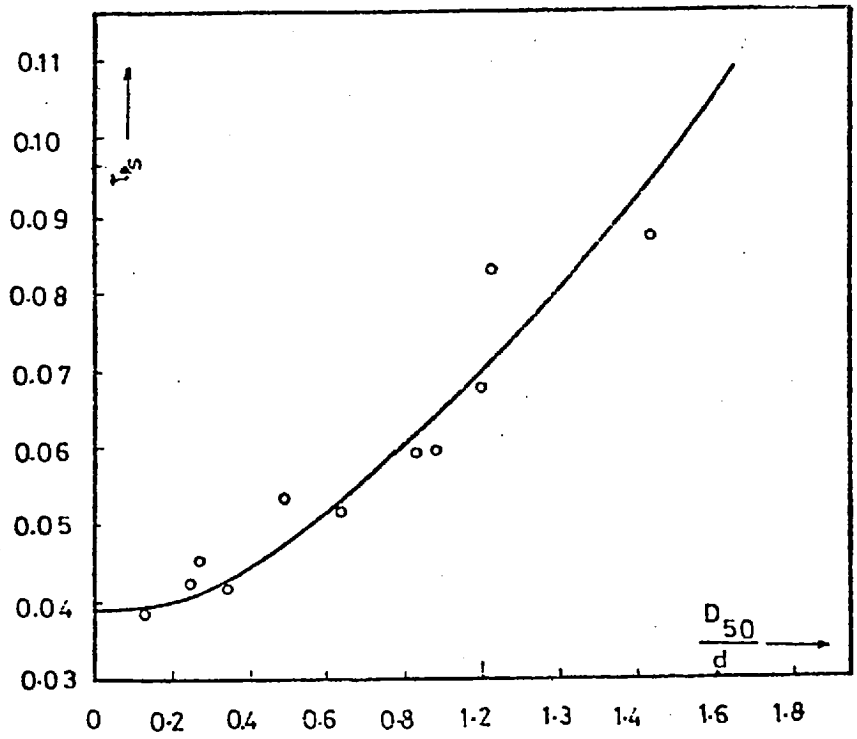


FIG.(1·8) · Variation of the critical modified Shields parameter with $\frac{D_{50}}{d}$ in supercritical flows. (after Ashida et al(1973))

The following comments are made about Ashida and Bayazit's experiments.

1. It is doubtful whether water depths of the same order of magnitude as the sediment size could be reliably measured.

2. The assumption of the existence of a logarithmic velocity distribution (as in a turbulent boundary layer) in a shallow supercritical stream with a rough steep bed is questionable.

3. Nothing is mentioned about the reproduceability of the experimental data, i.e. do different observers obtain the same results under similar hydraulic conditions?

In a recent study, Hollingsworth (1971) measured the distribution of mean pressures on the surface of single hemispheres placed individually on a flat bed in a supercritical stream. He concluded:

1. The lift force coefficient C_L increases with the ratio of the depth of the stream to the radius of the hemisphere. C_L is also found to be an increasing function of the Froude number of the stream.
2. The Drag force coefficient C_D is essentially constant over the range of flows tested:

$$1.84 < Fr < 5.91$$

$$1.11 \times 10^5 < Re < 4.96 \times 10^5$$

1.3 Scope of the Present Investigation

The main purpose of this investigation is to determine the stability of stones when used as a cheap lining material in steep open channels. The literature survey presented previously revealed the necessity to pursue a research programme the scope of which is outlined below:

The main body of this investigation will be carried out in two stages. Stage I will deal with devising a simple theory by which the stability of irregular solids could be related to a steady stream power. Testing of this theory by experiment is next done by running a series of scour experiments where the critical stream power is extrapolated. Stage I will be the subject of chapters 2 and 3.

Stage II will consist of Chapters 4 and 5 and will deal with instantaneous force measurements on an idealized particle (a sphere) placed in a steep shallow stream. Being an idealized model, Stage II will tend to improve the understanding of the mechanics of removal of a spherical particle from the bed of a steep channel lined with similar spheres. Stage II will investigate also the statistical nature of the

fluid driving forces.

The link between Stages I and II and the main conclusions of the present research will be the subject of Chapter 6.

STAGE I

(includes Chapters 2 and 3)

"The initial instability
of irregular stones and
scour experiments."

CHAPTER 2

Theoretical Considerations in Stage I

2.1 Purpose

Briefly, a shallow fast stream flows in a wide rectangular channel, the bed of which is steep and lined with a mixture of large stones and the problem is to devise a simple theory by which a representative size of the stone mixture (say D_{50}) is just set into motion under a critical set of hydraulic conditions.

Any theoretical analysis of the problem should be initiated with the following aims in mind:

1. How can a shallow fast stream, conveyed by a wide rectangular channel whose bed is rough and steep, be hydraulically described?
2. Is there a way of correlating the hydraulic parameters of such a stream to the damage done to the solids lining the channel bed? (Damage in this context means that some solids are dislodged by the stream.)
3. A definition of a threshold (or a critical) hydraulic property of the flow just to initiate motion of a representative size of a solid mixture is needed.
4. What is the nature of the initiation of motion problem? Is it a balance between static forces, or is it statistical in nature?

The answers to the first two questions will be tentatively given in this chapter, while the answers to the remaining two should await testing the theoretical approach by experiment.

2.2 Hydraulics of a Steady Fast Flow in a Rough Steep Channel

2.2.1 Preliminary Observations

Preliminary experiments were run to measure average velocity distributions at a channel cross-section. The channel has a rectangular cross-section 50 cm wide, 40 cm high. The length of the channel is 300 cm and its slope is adjustable; up to sin β = 50%. The channel bed is roughened with a layer of crushed granite stones (D_{50} = 5 cm). See Fig. 3.4 and Plates 1 and 2 .

The purpose of those experiments was to detect whether a logarithmic velocity distribution exists in such tumbling flows and to get an idea about the curvature or distortion of the stream lines and the lines of equal velocity at a cross-section.

Fig. 2.1 shows velocity profiles at one cross-section in the flume described above. These profiles were obtained by a Pitot tube which was always parallel to the channel bed with its tip pointing upstream. Each profile is an irregular curve with different velocity gradients or even with negative mean velocities in the turbulent wakes of the solids. Hence, no universal velocity distribution law could be considered to apply to such a flow.

Fig. 2.2 shows lines of equal velocities (isovels) at the same cross-section mentioned above, pockets of reverse flow regions could be detected, crowding and distortion of isovels, especially near the summits of the glued solids, indicate that the stream lines in the longitudinal direction of the flow are radically distorted.

Velocity distributions were also measured at greater channel slopes than 23.3% (23.3% is the channel slope associated with Figs. 2.1 and 2.2) but are not included for the sake of brevity. Generally speaking, for one solid mixture, the greater the channel slope is the greater are the water surface disturbances (see Plate 3), the more is air entrained

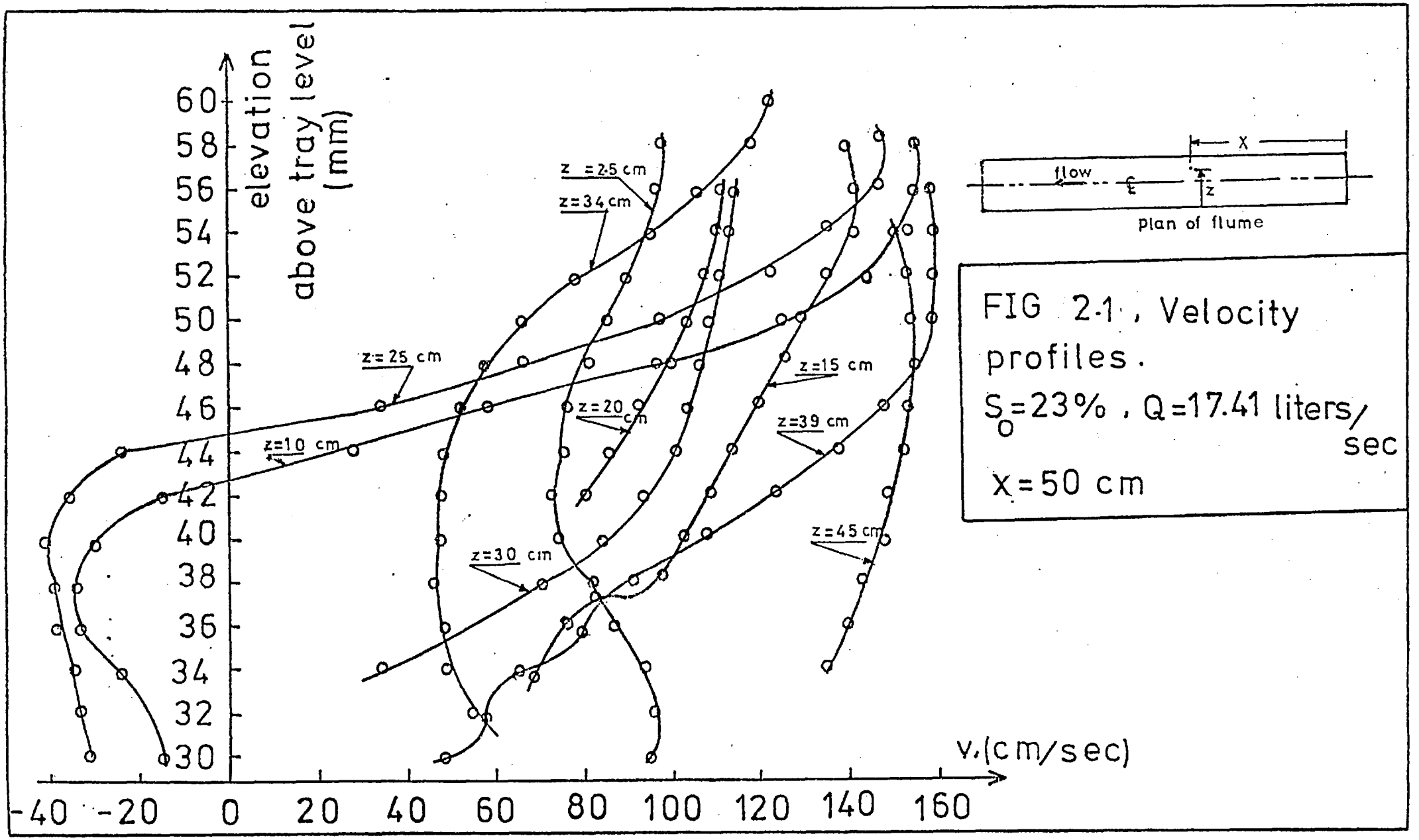


FIG 2.1 , Velocity profiles.
S_o=23% , Q=17.41 liters/sec
X=50 cm

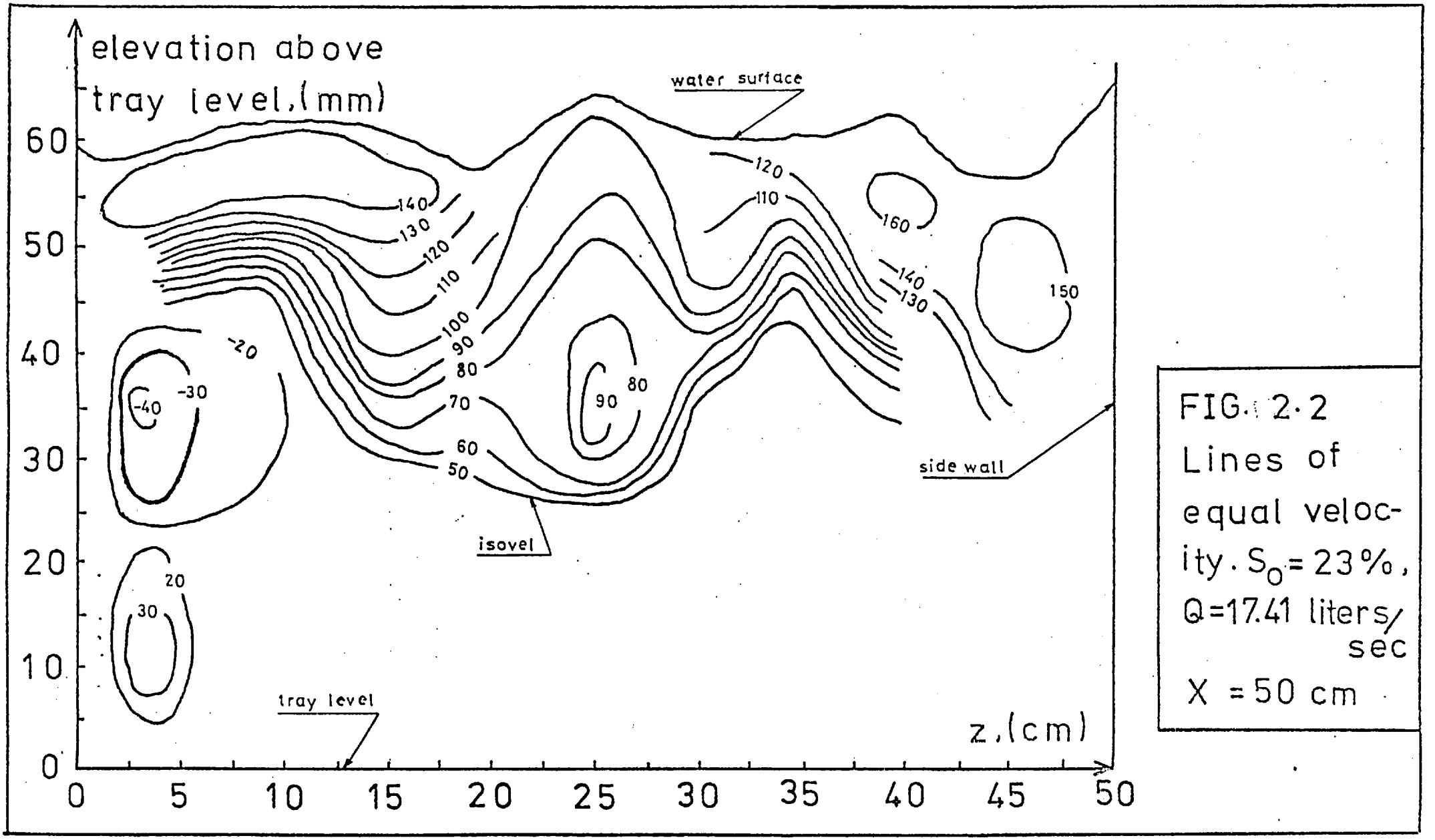


FIG. 2.2
Lines of equal velocity. S_o = 23%, Q = 17.41 liters/sec
X = 50 cm

by the flow (see Plate 2) and the more is the distortion in the isovels.

The above mentioned preliminary observations show that the hydraulic parameters that can be measured practically in such tumbling flows are:

1. The volumetric discharge Q.
2. The channel slope S_o.

2.2.2 Available Knowledge

It was mentioned in the previous chapter that Hartung and Scheuerlein (1970) have developed equations 1.6 → 1.11. These equations allow the estimation of the following variables:

σ, $\overline{V}_m$, $\overline{V}_c$ and d_m

if q, $\sin\beta$, D_{50} and P.F 1 are known.

The author does not find in the literature a more comprehensive analysis of the hydraulics of a tumbling flow. Therefore, he has adopted equations 1.6 → 1.11 as an available guide when need arises to check the results of this research.

2.3 Choice of the Method of Analysis

The contemporary methods of analysing the initiation of motion problem in deep slow flows as well as in shallow fast ones has been outlined previously. The researcher has to make a decision as to which method of analysis should be pursued or should a new one be devised.

The above mentioned contemporary methods of analysis are generally based on the following assumptions:

1. An uninterrupted boundary layer fills the whole stream depth.
2. The water surface is smooth or identifiable.
3. Some or all of the following classical hydraulic parameters can be practically measured: τ_o, v, $\overline{V}$, d.

Due to the fact that the three assumptions mentioned above are violated (in the case of a fast shallow flow conveyed by a wide rectangular rough channel) the following new method of analysis was devised.

2.4 Outline of the Author's Method of Analysis

Consider the stream as a machine that transports irregular solids. When a certain power input is available to that machine, it produces a useful work rate (useful in the sense that the machine is able to dislodge solids from the loose channel bed at a certain efficiency).

The ultimate aim is not to establish an equation for the rate of sediment transport, but rather to discover by experiment what the critical (or threshold) input power is, that would just produce no useful work at all.

2.5 The Stream as a Transporting Machine

2.5.1 Available Stream Power

The idea of the stream power, introduced to sediment transport by Bagnold (1966, 1973), is to be modified and adopted for this research.

Consider a fast shallow stream as a machine transporting irregular solids which line a wide rectangular channel bed. The available power input per unit length of the channel is: $P = \rho g Q S_o$, where Q is the volumetric discharge; $S_o = \sin \beta$, the channel slope; ρ the mass density of unaerated water; and g is the acceleration due to gravity. Hence, the available power input per unit bed area is:

$$\Omega = \rho g q S_o \qquad \text{..... Eq. 2.1}$$

where q is the pure water discharge per unit width of the channel.

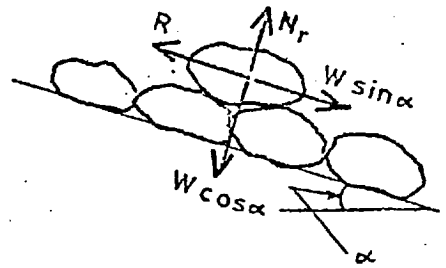


FIG. 2.3 , A large solid just sliding in air over a rough surface.

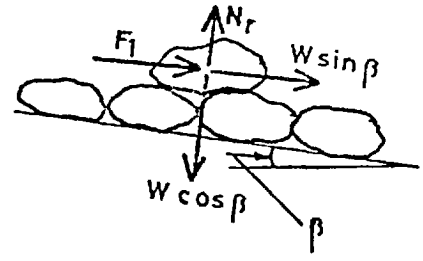


FIG. 2.4 , A large solid pulled by a force F_1 with constant speed.

2.5.2 Solid Friction

Let a stone of weight W be on the verge of sliding in air when placed over an inclined bed of closely packed stones of a similar shape, density and size. See Fig. 2.3 . Let the underlying bed of stones be also considered as a rough plane surface of inclination α^o with the horizontal.

Consequently, it could be assumed that the resultant of contact forces transmitted from the underlying bed of stones to the stone on top, be represented by the following two components:

The first one is R, which is a resultant friction force parallel to the line of the greatest slope of the rough bed (i.e. R acts up the slope and makes an angle α^o with the horizontal); the second component is a resultant normal force N_r perpendicular to R.

Consider both R and N_r to pass through the centre of mass of the stone.

Under the limiting conditions mentioned above and applying Newton's first law, the equations of statics of the stone on the verge of sliding could be written as:

$$R \leqslant W \sin \alpha$$

$$N_r = W \cos \alpha$$

Therefore

$R = N_r \tan \alpha$, where $\tan \alpha$ could be thought of as a limiting

coefficient of sliding friction.

If the angle of inclination of the rough bed of stones is $\beta < \alpha$, see Fig. 2.4 , and the stone is dragged by a force F1 at a constant speed $\overline{U}$, then the following simple relationship holds:

$$F_1 = W \cos \beta \tan \alpha - W \sin \beta$$

or

$$F_1 = W \cos \beta (\tan \alpha - \tan \beta) \quad \ldots\ldots\ldots\ldots\ldots \text{Eq. 2.2}$$

2.5.3 Work Rate

If, in Fig. 2.4 , a fast shallow stream is responsible for the maintenance of a steady motion of the solid (say by sliding, rolling or short saltations), then the fluid thrust provided by the stream should overcome the contact solid to solid friction forces encountered. If the assumption that the angle of internal friction α_1 during sliding, rolling or short saltations is constant and is equal to α, the fluid thrust is given by the following equation:

$$F.T = W\left(1 - \frac{\rho}{\rho_s}\right) \cos \beta (\tan \alpha - \tan \beta) \quad \ldots\ldots \text{Eq. 2.3}$$

The above mentioned assumption that α_1 is constant and = α is backed by Francis' experiments (1973) and was also suggested by Bagnold (1973)*.

The work done by the stream per unit time to move a solid with a constant speed $\overline{U}$ parallel to the channel bed is:

$$\overline{U}\, W\left(\frac{\rho_s - \rho}{\rho_s}\right) \cos \beta (\tan \alpha - \tan \beta)$$

Considering the work rate per unit area of the channel bed:

---

* See Francis (1973) for the definition and measurement of α_1.

$$w_k = \overline{U}\, w \frac{(\rho_s - \rho)}{\rho_s} \cos\beta\, (\tan\alpha - \tan\beta) \quad \ldots\ldots\ldots \text{Eq. 2.4}$$

where w is the average weight of solids dislodged per unit area of the channel bed.

The work rate term w_k could be thought of as a low transport rate of solids per unit bed area.

The following three assumptions are considered to hold in establishing equation 2.4.

1. $\overline{U}$, the speed of the solids dislodged is constant for each discharge Q and the associated slope of the channel S_o.
2. Assume that there is no upstream feed of stones (due to the difficulty encountered if an upstream feed of stones is to be maintained in an experimental flume).
3. The area from which the stones are dislodged is the area of a working mobile section, upstream and downstream of which there are fixed stones of similar sizes and shapes. The area of the mobile section is considered to be large enough, such that, for one set of hydraulic conditions, similar work rates w_k would be produced in both the mobile section and in a very long and wide steep channel (the bed of which is lined with similar stones as those in the mobile section.).

2.5.4 Efficiency of the Stream

Now, the work rate w_k and the available power Ω are related to each other by the following general equation:

$$w_k = \Omega\, E \quad \ldots\ldots\ldots\ldots\ldots\ldots \text{Eq. 2.5}$$

where E is the efficiency of the stream and could be tentatively expressed by the following function:

$$E = f_1 \left(\frac{\Omega - \Omega_c}{\Omega}\right) \quad \ldots\ldots\ldots\ldots\ldots\ldots \text{Eq. 2.6}$$

where $\frac{\Omega - \Omega_c}{\Omega}$ is a ratio of the excess stream power above a critical

value to the available one. This ratio could also be thought of as a transport stage (i.e. it is an indicator that tells whether the solids are just moving, saltating or eventually in suspension).

Substituting equations 2.1, 2.4 and 2.5 into equation 2.6 one obtains:

$$f_1\left(\frac{\Omega - \Omega_c}{\Omega}\right) = \frac{\overline{U}\, w\, \frac{\rho - \rho_s}{\rho_s} \cos\beta\, (\tan\alpha - \tan\beta)}{\Omega} \qquad \text{.... Eq. 2.7}$$

Equation 2.7 could be tested by experiment if Ω_c and $\overline{U}$ are further defined in terms of hydraulic parameters describing the flow, physical properties of the fluid and geometrical and physical properties of the solids lining the channel bed.

2.5.5 $\overline{U}$, An Average Speed of a Dislodged Solid

The trajectories of a solid dislodged by a fast stream (as observed in the flume mentioned in article 2.2.1) vary from rolling or sliding along the channel bed to short ballistic jumps (saltations).

There is no experimental evidence on those trajectories nor on the average speed of solids in the case of shallow fast flows, but there is an interesting experimental study on the same subject in slow flows by Francis (1973). From that study the following functional relationship could be written:

$$\overline{U} = f_2\left(V_g, \overline{V}, V_*, \frac{D_n}{d}, \text{shape of solids, adjacent solids in motion}\right),$$

where

$\overline{U}$ is the average speed of a solitary solid particle when performing saltations in water.

V_g is the fall velocity in still water of a solid particle of a nominal diameter D_n and mass density ρ_s.

$\overline{V}_{water}$ is the average speed in a flume where a turbulent boundary layer is fully developed.

V_* is the shear velocity,

and

$\frac{D_n}{d}$ is the ratio of the nominal diameter of the solid particle to the depth of flow d.

d is defined as the normal distance from the theoretical bed level to the water surface.

The following main conclusions were made:

1. Angular and flat solids spin more during saltation but are slower than well rounded ones.

2. Satisfactory correlation is obtained when $\frac{\overline{U}}{\overline{V}}$ as ordinates versus $\frac{V_*}{V_g}$ as abscissa are plotted. All curves are concave downwards and are displaced to the left for increasing depths of the flow.

3. $\overline{U}$ is reduced due to the presence of other solids in saltation.

Based on Francis' experiments, a functional relationship is tentatively written for $\overline{U}$ in the case of a fast stream as:

$\overline{U} = f_3(V_g,$, shallowness of the stream, physical properties of the fluid, geometrical and physical properties of the solid mixture) ... Eq. 2.8

It will be shown in the next article that Ω_c is generally expressed in terms of a function similar to $f_3(....)$, hence, the discussion of each of the variables on the right hand side of equation 2.8 is adjourned.

2.5.6 Ω_c, The Critical Stream Power

If the percentage damage, %dg, (as defined below) to a steep channel bed lined with loose solids is correlated with increasing stream powers, the stream power that corresponds to zero % dg could be extrapolated and defined as the critical (or threshold) stream power Ω_c.

The independent variables that cause the damage are tentatively listed and discussed.

2.5.6.1 Independent Variables Describing the Flow

The independent variables decribing the flow are as follows:

1. The stream power per unit channel bed area Ω .

2. The shallowness of the stream, usually expressed as a ratio of a representative solid size (say D_{50}) to a mean stream depth d. Since d can not be practically measured in this problem, the slope of the channel bed; $S_o = \sin \beta$ may be substituted to define shallowness, provided Ω and D_{50} associated with S_o are also stated.

3. The time T the solids are exposed to the stream.

The time T is a variable that accounts for the change in hydrodynamic forces exerted on each stone as a result of the following factors:

(a) The turbulent hydrodynamic forces exerted on each stone are expected to be time dependent.

(b) As a result of the movement of some stones, the forces exerted on others are expected to change because the bed geometry upstream or downstream of them has been altered. This feature is usually referred to as the interaction between the stream and the loose boundary (i.e. the loose bed of stones).

4. Randomness in space of the forces causing initiation of motion of solids. This variable is a function of the random shapes and orientations of the solids. An account of the randomness of the driving forces could be made by subjecting a solid mixture to similar hydraulic conditions but changing the orientations of the solids each time an experiment is repeated. Call this variable N_o.

5. Physical properties of the fluid, such as: viscosity μ, density ρ and surface tension ε .

2.5.6.2 Independent Variables Describing the Solid Mixture

1. Mass density of solids ρ_s, which is the mass per unit volume of a representative sample of the solid mixture.

2. Shape factor distribution $(S.F)_d$. For one solid S.F is defined as: $S.F = a_1/(a_2a_3)^{\frac{1}{2}}$, where a_1, a_2, a_3 are three dimensions of the solid in three perpendicular directions passing through its centre of mass, a_1 is the least dimension.

3. Size distribution $(D_n)_d$

4. Packing factor is defined in this investigation as a ratio of the actual number of solids per unit bed area per layer to the number of spheres per unit area per layer. The diameter of each sphere D is equal to D_{50} of the mixture and the spheres are arranged in a square pattern. The symbol chosen for the packing factor is P.F2.

5. The angle α, which is the minimum angle at which a layer of a solid mixture starts to slide over an inclined plane surface roughened with a layer of a similar mixture.

6. The number of layers of the loose solids placed as a slope protection to the channel bed. Call this variable N_L.

7. The under layer condition U_L, such as permeability and grading of the materials under the slope protection layers.

2.5.6.3 Dependent Variables

1. %dg; the percentage damage defined as a ratio of the number of solids per unit bed area dislodged from the top layer to the number of solids per unit bed area per layer placed with a packing factor P.F2 = 100%.

2. σ , the aeration factor.

3. The terminal fall velocity distribution of a representative sample from the solid mixture, $(V_g)_d$. For one solid, the balance between the

submerged weight and the fluid drag on it gives:

$$V_g = \left(\frac{4g}{3C_D} \left(\frac{\rho_s}{\rho} - 1 \right) D_n \right)^{\frac{1}{2}}$$, where C_D is the coefficient of drag of the solid when it is moving in still fluid at a speed V_g.

2.5.6.4 A Functional Relationship for Ω_c

A functional relationship for Ω_c is suggested in terms of the independent variables listed previously. First let

$$\% \, dg = f_4(\Omega, S_o, T, N_o, \mu, \rho, \varepsilon, \rho_s, (S.F)_d, (D_n)_d, P.F2, \alpha, N_L, U_L) \quad \ldots\ldots \text{Eq. 2.9}$$

when $\%dg = 0$, $f_4(\ldots) = 0$, and $\Omega = \Omega_c$,

hence

$$\Omega_c = f_5(S_o, T, N_o, \mu, \rho, \varepsilon, \rho_s, (S.F)_d, (D_n)_d, P.F2, \alpha, N_L, U_L) \quad \ldots\ldots\ldots \text{Eq. 2.10}$$

2.5.7 A General Equation for the Efficiency of the Stream

Going back to equation 2.7 and substituting equations 2.8 and 2.10 into it one obtains:

$$f_1\left(\frac{\Omega - f_5(\ldots)}{\Omega} \right) = \frac{w(\rho_s - \rho) \cos \beta \, (\tan \alpha - \tan \beta) \, f_3(\ldots)}{\rho_s \, \Omega} \quad \ldots\ldots \text{Eq. 2.11}$$

Equation 2.11 describes the scour problem in its most general form. But, $f_3(\ldots)$ and $f_5(\ldots)$ in that equation are defined in terms of the same variables, hence, only one of them has been retained; $f_5(\ldots)$.

In order to retain the dimensionlessness form of equation 2.11 $f_3(\ldots)$ is substituted by $\overline{V}_g$ which is the fall velocity of a solid whose size is D_{50} of the solid mixture.

2.5.8 Elimination of Some Variables from Equation 2.10

Equation 2.10 contains 13 variables, some of which can hardly affect Ω_c. Such irrelevant variables are thus discussed and eliminated

from the analysis.

2.5.8.1 μ, Viscosity of Water

It was mentioned previously in Shields approach that τ_{*c} is independent of Re_* in the range $Re_* > 1000$. This implies that initiation of motion of solids is independent of viscosity in turbulent flows. The flows encountered in this problem are highly turbulent and viscosity is thus eliminated from this analysis.

A word of caution might however be added that when experiments are conducted in well heated laboratories, viscosity of water could be up to 6 times less than that of water in real streams near the freezing point.

2.5.8.2 ε, Surface Tension

The surface tension stress ε, that prevails on both sides of a water strip of a unit width, could only be relevant to our problem from the following point of view:

Due to the existence of high velocities in a fast stream, surface tension forces are overcome by viscous forces, hence, the water surface loses its smooth skin and air is entrained by the stream. The presence of fluctuating air bubbles in a fast stream might have an effect on the initial motion of solids. However, one might consider air entrainment as a dependent variable; dependent perhaps on the stream power, slope of the channel, the physical properties of the solids and the relative magnitude of viscous forces to surface tension forces. Kenn and Zanker (1967) and Kenn (1969) suggest that air-entraining water flows can only be modelled if full scale velocities (assuming the same fluid is used in model and prototype) are also maintained. On this basis, if a Froude model is employed to study the initial movement of large solids

by a shallow fast stream, air entrainment may not be correctly scaled. However, other researchers like Straub and Anderson (1960) and the ASCE Task Committee on Aerated Flows in Open Channels (1961) have concluded from experiments in rough steep open channels the following equation:

$$\overline{C} = 0.743 \log_{10}(S_o/q^{1/5}) + 0.876$$

where $\overline{C}$ is the mean concentration of air defined as the ratio of the volume of air to the volume of the air-water mixture.

$S_o = \sin \beta$ and β is the angle the channel makes with the horizontal.

q is the discharge per unit width in $ft^3/sec/ft$.

Based on the above mentioned experimental evidence, air entrainment is a dependent variable on S_o and q, hence it is concluded that ε can be eliminated.

CHAPTER 3

Experiments and Results of Stage I

The main topics discussed in this chapter are:

1. The experiments needed.
2. Description of equipment used and the procedure followed in conducting the experiments.
3. Experimental results and analysis of data.

3.1 The Experiments Needed

Two kinds of experiments are needed in Stage I:

1. Experiments to determine the physical and geometrical properties of an irregular solid mixture such as:

ρ_s, $(D_n)_d$, $(S.F)_d$, $(V_g)_d$ and α.

2. Experiments to test equations 2.10 and 2.11 .

3.2 Description of Equipment and Experimental Results

3.2.1 Experiments, Kind 1

3.2.1.1 ρ_s; The Mass Density of Solids

A small number of solids (10 was considered sufficient) was picked up randomly from a mixture of crushed granite stones, the solids were dried in an oven at a temperature of 100° Centigrade for 6 hours and weighed individually in air by an electric sensitive balance (sensitivity of the Mettler, K7 balance used is 9.81 dynes).

Each solid was suspended by a light string and immersed in water with a temperature 20° centigrade. The water was contained in a container but the solid did not touch the base or the sides of it.

The buoyancy force on a solid is the difference between two weights; the first is the weight of the container plus the water in it after the solid was immersed and the second is that of the container plus water before the solid was immersed.

The volume of the irregular solid is thus:

$$\frac{\text{Buoyance force}}{\text{Weight density of water at } 20^{\circ}C}$$

and the weight density of the solid is:

$$\gamma_s = \frac{\text{Dry weight of the solid in air}}{\text{Volume of the solid}}$$

hence, the mass density of the solid ρ_s is:

$$\rho_s = \frac{\gamma_s}{g}$$

Light-weight replicas of 100 granite stones, picked up at random from the solid mixture, were made to conduct initiation of motion experiments on light-weight solids. The technique followed in making these replicas is subsequently described:

A granite stone was covered with a coat of grease and immersed in warm wax contained in a shallow wooden tray. The flattest surface of the stone was kept uncovered and flush with the wax surface. The solid was removed from the wax after approximately 10 minutes. The cavity in the wax was greased and prepared for casting.

Gypsum (plaster of Paris) was mixed with water (one volume water to one volume gypsum) and a homogeneous mix was thus ready to be poured in the cavity. One hour after the cavity was cast, the wax around it was broken and removed. The light-weight replicas thus obtained were dried in an oven at $100^{\circ}C$ for 2 hours and then painted with two coats of polyurethane and one coat of rubber paint for water proofing.

The mass density of 10 replicas was obtained in the same way followed for the real stones.

The results of the mass density experiments are shown in Table 3.1 at the end of this Chapter.

3.2.1.2 The Angle of Sliding Friction; α

Measurements of the angle of sliding friction α were conducted by spreading a loose layer of solids over a layer of similar solids glued to a metal tray. The inclination of the tray (as read from an inclinometer attached to the tray) was increased gradually until the loose layer started to avalanche down the slope. Similar tests were conducted under still water, but no apparent difference in the limiting angle of inclination (i.e. the angle α) was noticed. See Table 3.2.

3.2.1.3 Size Distribution; $(D_n)_d$

Determination of the size distribution of a solid mixture by sieve analysis was abandoned because the sizes of the solids were large and standard sieve sizes would only allow few points to be plotted on a size distribution curve.

A distribution by weight of 100 solids, picked up at random, was done instead. The solids were labelled from 1 to 100, weighed individually on the Mettler electric balance and a weight distribution curve was thus obtained as explained subsequently:

The weights of the solids were arranged in an ascending order, the cumulative weights from the lightest to the heaviest ones were calculated, the ratio of the cumulative weight to the total weight of the sample is defined as the percentage smaller of the mixture (relative to the solid weight under consideration).

Fig. 3.1 is a plot of % smaller as ordinate and the logarithm of the weight of each solid as abscissa. Fig. 3.1 could be converted

into a size distribution curve by converting the W scale into a D_n scale, where D_n is the nominal diameter of the solid given by:

$$D_n = (6W/\pi\rho_s g)^{1/3}.$$

3.2.1.4 Shape Factor Distribution; $(S.F)_d$

The shape factor of an irregular solid (as defined in article 2.5.6.2) was measured in the following way:

The outside dimensions of a solid in three perpendicular directions was measured by a compass. Identification of the three perpendicular directions was done by eye, hence the shape factor of a solid obtained is an approximate value that provides some idea about the flatness of an irregular solid.

Fig. 3.2 is a plot of the percentage flatter as ordinate and the logarithm of S.F as abscissa. The percentage flatter than a given value of S.F is obtained from cumulative weights in the same way followed to determine the percentage smaller in the weight distribution curve; Fig. 3.1.

3.2.1.5 Fall Velocity Distribution; $(V_g)_d$

The terminal fall velocity of a solid in still water is reached when there is a balance between its immersed weight and the drag force on it. A visual tank 3 m wide, 6 m long and 3 m high provided just enough depth of water so that the time measured for one solid to cross the 3 m depth of the tank is in the order of 2 to 5 seconds. Unfortunately, there was no deeper tank available in the laboratory to increase the time measured.

The method of measuring the fall velocity of one solid was done in the following way:

A stand carrying a vertical scale is immersed in the visual tank

opposite one of its transparent windows. A transverse mark was fixed to the scale at a known height, the solid was released at the water surface and the time elapsed between passing the transverse mark and reaching the tank base was recorded by a stop watch. Each experiment was repeated three times and the arithmetic mean of the three time readings was adopted as the reliable time reading. The fall velocity of the solid under consideration is the ratio of the known distance the solid has moved to the time elapsed.

Observations during these experiments showed that some solids followed an inclined path and spun before they hit the base of the tank, others followed a vertical path without spinning at all, still others followed a helical path without much spinning.

Fig. 3.3 is a plot of % slower as ordinate against log (V_g) as abscissa, % slower is defined in the same way % smaller was defined in article 3.2.1.3. The same solids were used to establish Figs. 3.1, 3.2 and 3.3 .

3.2.2 Experiments, Kind 2

3.2.2.1 Apparatus

General

The apparatus is a short rectangular flume with perspex glass side walls, an adjustable slope and dimensions shown in Fig. 3.4, see also Plate 1. The geometry of the flume entrance was improved by fitting a streamlined plate upstream of the leading edge of the flume bed. Two flat parallel plates were also clamped to the leading edges of the perspex side walls on one end and to the perforated baffle in the reservoir tank on the other. The purpose of the above mentioned improvements was to prevent standing waves from occurring and persisting downstream of the flume entrance (see Plate 2).

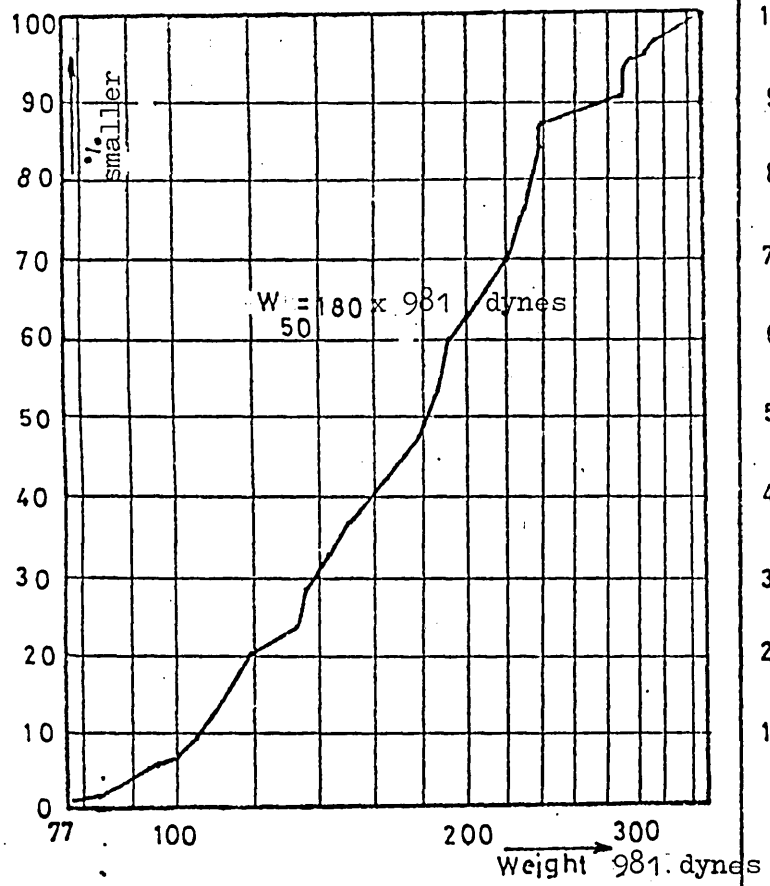


FIG. 3.1 , Weight distribution of 100 granite stones.

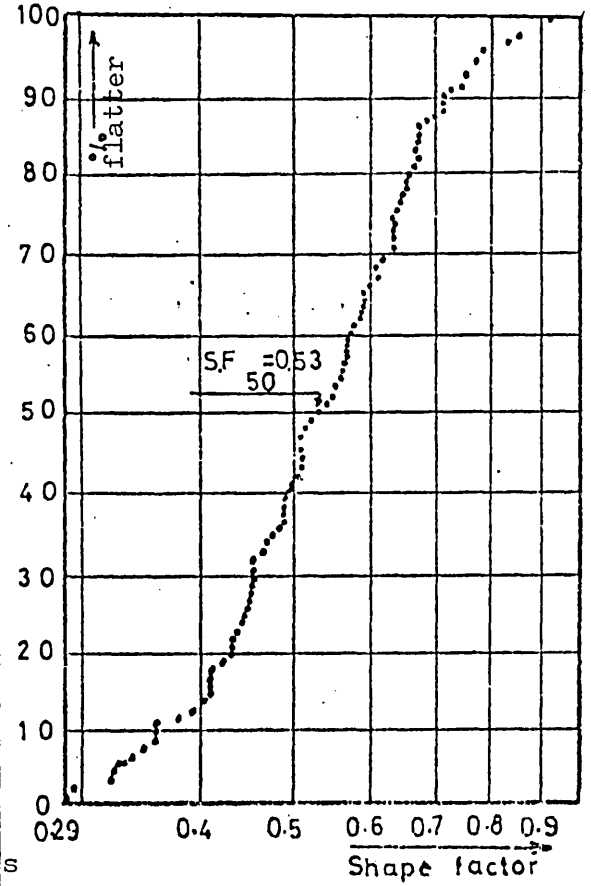


FIG. 3.2 , Shape factor distribution of 100 granite stones.

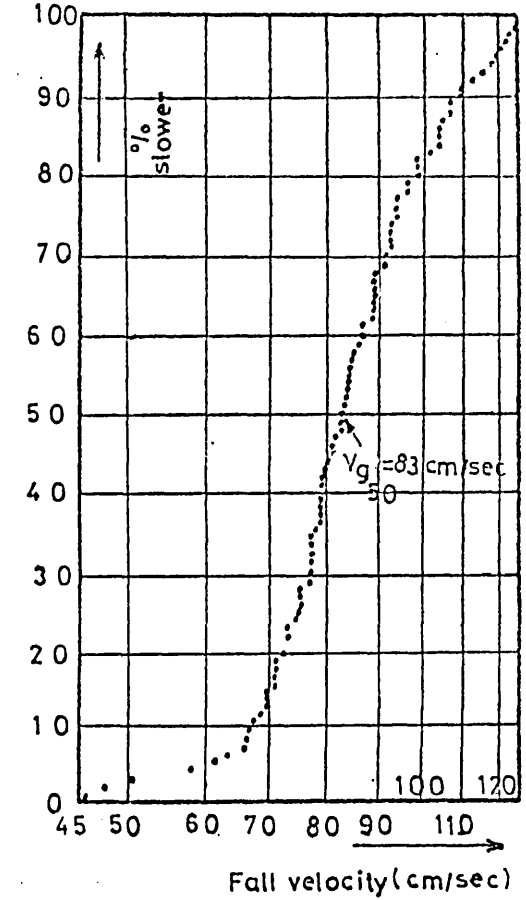


FIG. 3.3 , Fall velocity distribution of 100 granite stones.

The Roughened Bed and the Mobile Section

A false bed of inverted steel trays was built in the flume, the trays were 50 by 50 cm in plan area and had a 10 cm high edge. A layer of granite stones with a D_{50} = 5 cm was glued to the trays with 100 stones on each tray approximately, see Plate 1.

The mobile section was a layer or more of loose solids placed on top of a glued one in a shallow tray. The shallow tray was 50 by 50 cm in plan area and had a 2 cm high edge. The elevation and the longitudinal position of this tray could be changed in relation to the inverted trays of glued stones. The elevations of the shallow tray were always adjusted so that the top loose layer in the mobile section was flush with the glued one on the inverted trays upstream and downstream.

Supply and Disposal of Water

A 6 inch plastic pipe supplied water to an open steel box (the reservoir tank in Fig. 3.4). A control butterfly valve was fitted two metres upstream of the pipe outlet in the box. A baffle 10 cm thick was constructed across the steel box to dissipate any disturbances in the flow after it leaves the pipe outlet.

The outlet of the flume was directed to an underground measuring tank where excess water was spilled to the lab sumps over a longitudinal weir built in the underground measuring tank.

Calibration of Orifice Plate

A circular orifice plate (the diameter of the orifice was 4.5 inches) was fitted in a horizontal piece of the supply pipe. Two pressure-measuring tapping points p_1 and p_2 were located on the under side of the supply pipe and two air-relief ones b_1 and b_2 were located on the upper side of it, see Fig. 3.5 .

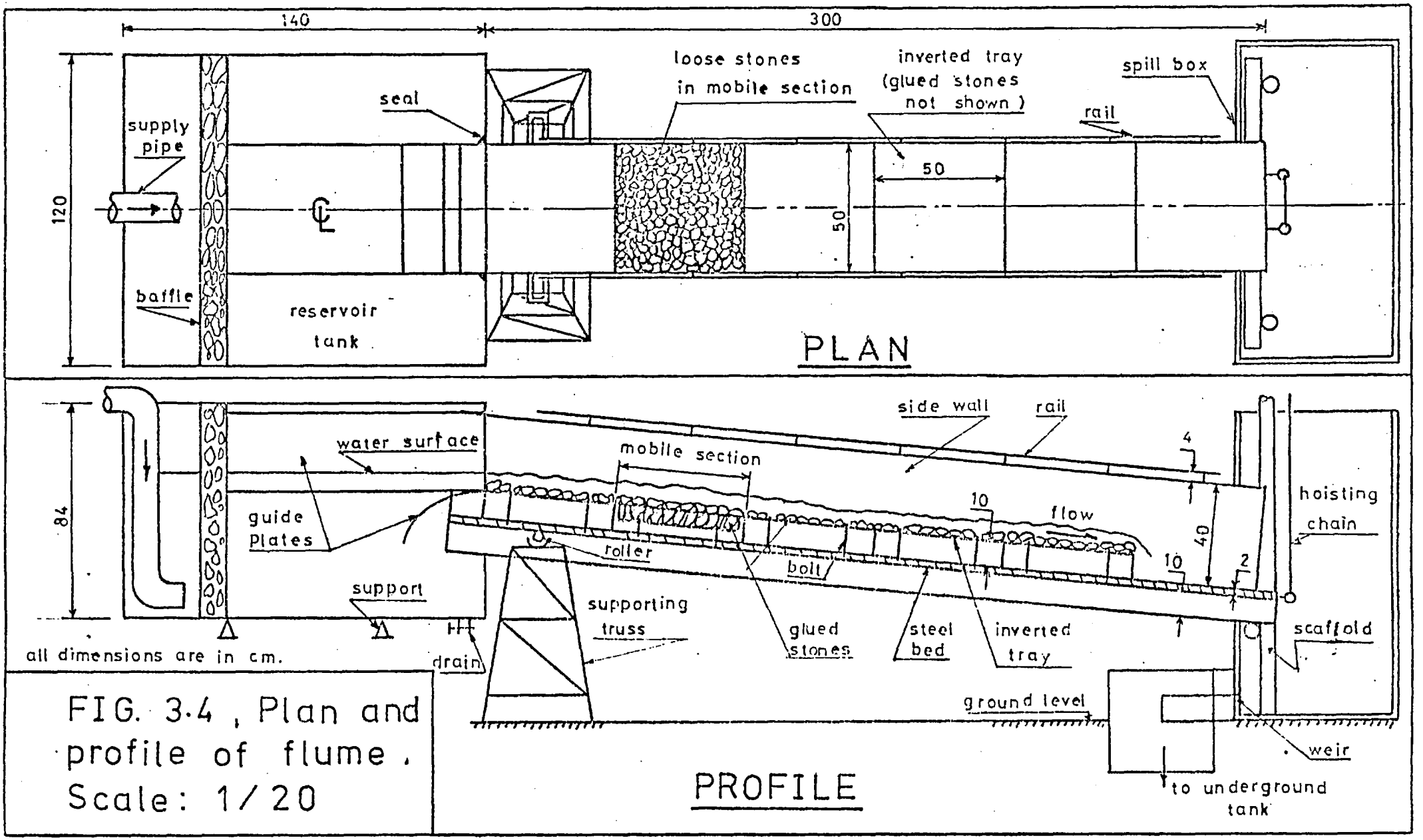


FIG. 3.4, Plan and profile of flume. Scale: 1/20

The pressure difference between the tapping points p_1 and p_2 was measured by a water or a mercury manometer depending upon whether the pressure difference was small or large respectively.

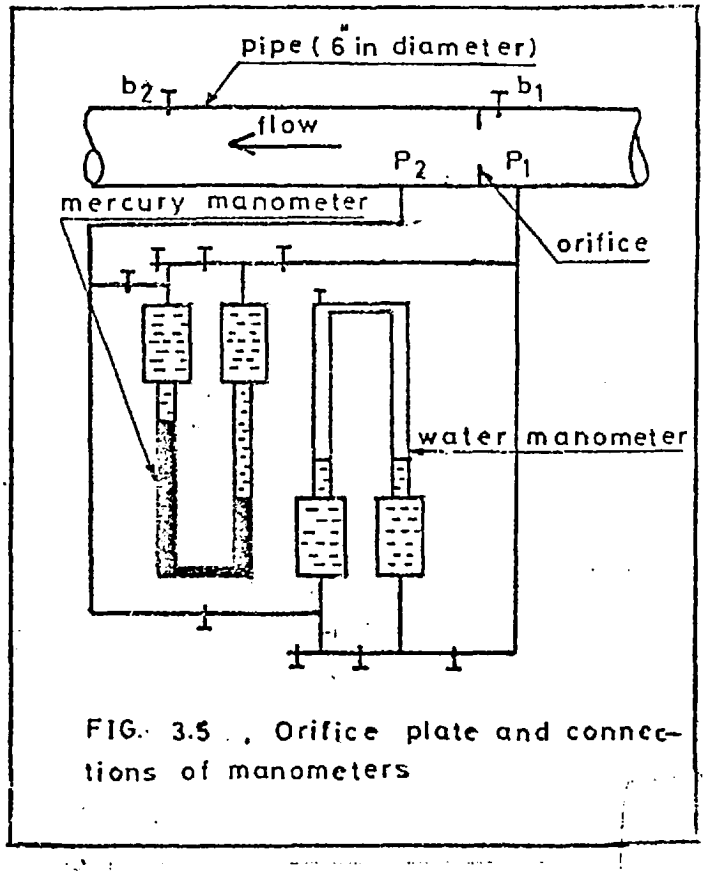


FIG. 3.5 , Orifice plate and connections of manometers

Calibration of the orifice was done as follows:

1. A valve opening was chosen, and air, if any, was relieved from the supply pipe by opening tapping points b_1 and b_2 until air bubbles ceased to escape from the pipe.

2. A point gauge was mounted over the underground measuring tank opening. The water level in the tank was read by the first appearance of a signal which is only activated when a direct current electric circuit was closed as the point gauge tip touched the water surface.

The impact of the water outflow from the flume generated irregular waves on the water surface in the underground tank. A vertical steel pipe 1 m long, 10 cm in diameter, surrounded the point gauge and damped down the irregular disturbances (water in the underground tank gained access to the pipe through a 2 cm gap near its lower end).

3. The time to fill a known volume of the measuring tank, the plan area of which is 41.30 m^2 , was measured by a stop watch. This step was repeated 3 times and the arithmetic mean of the three readings was considered as the reliable time reading.

4. The level difference between the two limbs of the manometer (the water or the mercury one) was recorded, hence the pressure difference

between the tapping points p_1 and p_2 was calculated.

5. The equation of the volumetric discharge through the orifice was assumed to have the form:

$$Q = c_d A_f (2gH)^{\frac{1}{2}} \quad \text{..... Eq. 3.1}$$

where c_d is the coefficient of discharge of the orifice plate;

A_f is the area of the orifice and

H is the pressure difference between the two tapping points p_1 and p_2.

If an overall coefficient of discharge C_d is substituted for the product $c_d A_f (2g)^{\frac{1}{2}}$ equation 3.1 becomes:

$$Q = C_d (H)^{\frac{1}{2}} \quad \text{..... Eq. 3.2}$$

Table 3.3 shows the measured values of Q and $(H)^{\frac{1}{2}}$.

Fitting an equation of the same form as equation 3.2 to the data in table 3.3 , by the least square method, gave the following equation:

$$Q = 3291 (H)^{\frac{1}{2}} \quad \text{..... Eq. 3.3}$$

where Q is measured in cm^3/sec and H in cm of water.

The coefficient of correlation of equation 3.3 is 99.0%.

3.2.2.2 Simplifications

Some preliminary experiments were run in the flume shown in Fig. 3.4 to simplify the functional relations proposed in the previous chapter i.e. equations 2.9, 2.10 and 2.11 . These experiments consisted of subjecting several (2 or 3) layers of the granite stone mixture (whose physical and geometrical properties were described in Figs.3.1, 3.2 and 3.3 and Tables 3.1 and 3.2) to a fast shallow stream. The observations made during these experiments led to the following simplifications:

1. An impermeable underlayer condition would simplify the main experimental flume.

2. The variable N_o determining the number of random placings to be

tested (mentioned previously in article 2.5.6.1) was arbitrarily fixed at 10.

3. The number of layers in the mobile section should be restricted to one for the following reason:

If the mobile section contained more than one loose layer of solids, a standing wave would form over that section due to the flow gaining access locally to the lower layers in the tray, thus creating a special flow condition over it

4. The time T was arbitrarily chosen to be 10 minutes. The justification for this choice was based on the following observations: under these test conditions, there appeared to be no continuous flow of solids after the first solids were dislodged by the stream. There could have been very low rates of solid transport, but if so, the rate was so low that a reliable count of solids might have required several days to obtain.

5. The geometrical and physical properties of any solid mixture could be expressed in the following way:

The size $(D_n)_d$ of a solid mixture could be thought of as a pair of variables; D_{50} being the median size of the mixture and $\left(\frac{D_n}{D_{50}}\right)_d$ being the non dimensional distribution about the median value. The same argument applies to the distribution of the fall velocity $(V_g)_d$ but not to the distribution of the shape factor $(S.F)_d$, because the shape factor S.F is already non dimensional.

What Figs. 3.1, 3.2 enable one to do is to obtain the relative distributions about the median value, i.e. $\left(\frac{D_n}{D_{50}}\right)_d$ and $\left(\frac{V_g}{V_{g_{50}}}\right)_d$

If the assumption is made that larger or smaller (in size) stone mixtures have the same relative distribution curves of $\left(\frac{D_n}{D_{50}}\right)_d$, $\left(\frac{V_g}{V_{g_{50}}}\right)_d$.

as well as the same shape factor distribution $(S.F)_d$ as the stone mixture tested in this investigation, then the remaining variables expressing the geometrical and physical properties of a mixture are: D_{50}, $V_{g_{50}}$, $S.F_{50}$, ρ_s.

6. The packing factor P.F2 was kept constant at 100%, and the number of loose stones per layer in the mobile section was always 100.

Based on the above simplifications, equations 2.9 , 2.10 and 2.11 in Chapter 2 are simplified and have the following forms respectively:

$$\% \text{ dg(during time T = 10 minutes)} = f_6(\Omega, S_o, D_{50}, S.F_{50}, \rho_s) \quad \text{..... Eq. 3.4}$$

$$\Omega_c = f_7(S_o, D_{50}, S.F_{50}, \rho_s) \quad \text{..... Eq. 3.5}$$

and

$$\frac{W_k}{\Omega} = f_1\left(\frac{\Omega - \Omega_c}{\Omega}\right) = \frac{w \overline{V}_g \frac{(\rho_s - \rho)}{\rho_s} \cos\beta(\tan\alpha - \tan\beta)}{\Omega} \quad \text{..... Eq. 3.6}$$

Equations 3.4, 3.5 and 3.6 were tested by experiment as will be discussed subsequently in the following articles.

3.2.2.3 Experimental Procedure

A typical experiment to determine the percentage damage within 10 min (%dg) was run in the following way:

1. The channel bed was set at a known slope.
2. The mobile section was located at a chosen distance from the flume entrance.
3. A loose layer of solids was placed on the glued one in the shallow tray of the mobile section. The tray elevation was adjusted so that

the loose solids were flush with the glued ones on the upstream and downstream inverted trays; this was estimated by eye.

4. The control valve was opened slowly (within a period of 1 min) to the desired valve opening and the discharge was increased gradually (in increments of 1000 cm^3/sec approximately). The aim of opening the valve slowly was to prevent a bore (like that of a flood wave) from occurrence over the mobile section. Each valve opening was maintained for 10 minutes and at the end of this period the dislodged solids were counted and their identifying labels recorded (each solid was identified so that its weight could be obtained). The corresponding manometer reading (to allow calculation of Q) was also recorded.

5. The flow was stopped when damage exceeded 15% approximately, since after that stage, the geometry of the bed at the mobile section radically changed.

6. The loose solids were reorientated again as in step 3 above and the experiment was repeated 10 times for each slope to demonstrate whether or not there was scatter in the experimental results due to ten different random placings of the stones.

7. A range of slopes of the channel bed was tested.

8. The longitudinal position of the mobile section was then changed to demonstrate whether an undeveloped boundary layer had any influence on the erosion of large solids.

9. Experiments with light-weight replicas also followed the same steps mentioned above.

3.2.2.4 Observations

(i) The Beginning of Motion of Solids

Solids in the mobile section were observed before they were dislodged by the stream. Some solids adjusted their positions to safer

shelters. Others were in a critical static balance beforehand and began a random rocking movement, still others looked stable in their recesses.

Dislodgement of the first solid occurred after a certain discharge, Q, and an accompanying slope, S_o, were exceeded. New solids were also dislodged once Q and/or S_o were increased. The removed solids could have been rocking, adjusted their positions or looked stable before they were dislodged.

When the loose layer of the mobile section was reorientated randomly and subjected to the same Q and S_o values that dislodged the first, second and subsequent solids, the following observations were made:

(a) For Q and S_o values that dislodged only one solid in a previous experiment, one of the subsequent events occurred:

1. No solid was dislodged at all.
2. A different first solid moved.
3. More than one solid moved (not more than 2 or 3).

(b) For Q and S_o values that dislodged two solids only, the following events occurred:

1. Less than two solids moved (including no movement at all).
2. Different two solids moved.
3. More than two solids moved (though not more than 5 or 6).

These observations showed that the threshold condition for the first solid to be dislodged from a mixture can not be defined unless one resorts to a statistical approach. Such an approach will be discussed when the experimental data is analysed.

(ii) <u>The Longitudinal Location of the Mobile Section</u>

For one channel slope and one solid mixture, changing the longitudinal position of the mobile section did not show any distinct

and consistent influence on the number of stones dislodged by a stream of a certain stream power .

These experiments demonstrated that, in the case of a shallow fast flow over a steep rough channel bed, the region of developing boundary layer is so short that its influence on the initial movement of large solids is overshadowed by the irregular shapes of the solids and the randomness in space and/or time of the hydrodynamic forces. Hence, it was decided to fix the longitudinal location of the mobile section in the remaining tests at $50 < x < 100$ cm.

The experimental results regarding this part of the work are not included in the thesis.

3.2.2.5 Experimental Results

Experimental results are shown in Tables 3.4, 3.5 and 3.6. Each of these tables will be described in detail.

3.2.2.5.1 Tables 3.4 and 3.5

Each column heading of Table 3.4 was obtained in the following way:

1. Column 1; q, dimensions: $cm^3/sec-cm$.

q is the volumetric discharge of water per unit width of the flume. First the total discharge Q was obtained by using the calibration equation of the orifice plate, equation 3.3; then $q = Q/50$, where 50 cm is the width of the flume.

2. Column 2; Ω , dimensions: 981 dynes/(cm-sec)

Ω is the stream power per unit bed area, each value in this column was obtained by using the equation $\Omega = \rho g q S_o$, where $\rho g = 981$ dynes/cm^3 for water at 20°C. q is found in column 1 and S_o in column 7.

3. Column 3; 2500w, dimensions: 981 dynes.

This term represents the total weight of solids dislodged from the mobile section whose area is 2500 cm^2. Each value in this column was obtained by adding up the weights of all solids dislodged from the start of an experiment to the experimental run under consideration. As an example, the weight of solids dislodged due to the stream power in experiment 4, run 4 is the sum of the weights of dry solids in air dislodged during runs 1, 2, 3 and 4.

4. Column 4; %dg, dimensionless.

For one experimental run, %dg is given by the cumulative number of solids actually dislodged from the start of the first experiment to the run under consideration. This is because the number of spherical solids that could be placed in one loose layer in the 50 cm x 50 cm mobile section with square packing(P.F2 = 100%) is 100, as D_{50}, the median diameter of the equivalent sphere was 5.00 cm. It is assumed that the area of the mobile section is large enough to give a fair indication about %dg in a long flume. As an example of how %dg was calculated, consider experiment 4, run 4 again: the number of solids dislodged from the whole area of the mobile section during runs 1, 2, 3 and 4 were: 0, 1, 3, 2 respectively, hence %dg that corresponds to the stream power in run 4 is (0 + 1 + 3 + 2)/100 = 6%.

5. Column 5; w_k/Ω , dimensionless.

Equation 3.6 is employed to calculate this ratio, where:
w was calculated by dividing the values in column 3 by 2500 cm^2; the area of the mobile section, $\frac{\rho_s}{\rho}$ and sin β are tabulated in column 7 of Table 3.4 . Average values of α under water are found in Table 3.2 . $\overline{V}_g$ was calculated using the following equation:

$$\overline{V}_g = \left(\frac{4gD_{50}}{3C_D} \left(\frac{\rho_s}{\rho} - 1 \right) \right)^{\frac{1}{2}}$$, where C_D is assumed to be 1 due to the

angular shapes of the solids. $\overline{V}_g$ was checked against Vg_{50} as obtained from the fall velocity distribution curve Fig. 3.3 . Vg_{50} is defined as the fall velocity of a solid where 50% of the solids in a mixture have slower fall velocities. For the crushed granite stones, $\overline{V}_g$ = 104 cm/sec, compared with Vg_{50} = 83 cm/sec. The disagreement between the two values led the author to adopt $\overline{V}_g$ to be used in equation 3.6 instead of Vg_{50}, since the former is a more practical parameter to define when the size of a solid becomes large.

Ω values are found in column 2.

6. Column 6; $\frac{\Omega - \Omega_c}{\Omega}$,dimensionless.

This parameter is calculated from a knowledge of Ω and Ω_c (Ω_c the stream power at initial motion,as will be described in the following section3.2.2.5.2

7. Column 7; variables kept constant during one set of experiments. These variables are:

- slope of the channel bed; $S_o = \sin \beta$;
- the longitudinal location of the mobile section as expressed by the inequality < x < , where x = 0 coincides with the leading edge of the flume and x is measured in cm;
- N; the number of solids per layer placed loose in the mobile section.
- average physical and geometrical properties of a solid mixture as expressed by ρ_s/ρ and D_{50}. In addition, figures 3.1,3.2 and 3.3 show the size distribution by weight, shape factor and its distribution and fall velocity and its distribution.

3.2.2.5.2 Determination of Ω_c

For one channel slope and one solid mixture, equation 3.4 could be written in the following form:

$$\% \text{ dg(during 10 min)} = f_8(\Omega) \quad \ldots\ldots\ldots\ldots \text{Eq. 3.7}$$

Two alternative functions were fitted to the data in columns 4 and 2 of Table 3.4 namely:

1. % dg (during 10 min) = $e_o \log (\Omega) + C_o$, ... Eq. 3.7.1

   where e_o and C_o are constants.

2. log (% dg(during 10 min)) = $e_1 \log (\Omega) + C_1$ ..... Eq. 3.7.2

   where e_1 and C_1 are constants also.

   Let $C_o = e_o \log (1/ \Omega_{co})$ and

   $C_1 = e_1 \log (1/ \Omega_{cl})$, where Ω_{co} and Ω_{cl} are the critical stream powers corresponding to 0% and 1% damage respectively. Hence equations 3.7.1 and 3.7.2 could alternatively be written in the following forms:

$$\% \text{ dg(during 10 min)} = e_o \log \frac{\Omega}{\Omega_{co}} \quad , \ldots\ldots\ldots\ldots \text{Eq. 3.7.3}$$

and

$$\% \text{ dg(during 10 min)} = \left(\frac{\Omega}{\Omega_{cl}}\right)^{e_1} , \quad \ldots\ldots\ldots\ldots \text{Eq. 3.7.4}$$

The method of the least square was used in the fitting procedure and a computer program was fed to a Hewlett calculator* to find the constants: e_o, Ω_{co}, e_1 and Ω_{cl}.

The coefficients of correlation (see Appendix I) r_o and r_1 associated with equations 3.7.3 and 3.7.4 respectively were also determined by the calculator.

Table 3.5 summarizes the results obtained from this regression analysis, where a pair of equations of the same form as equations 3.7.3 and 3.7.4 , were fitted for each channel slope and solid mixture tested.

Although Ω_{co} and Ω_{cl} correspond to 0% dg and 1% dg respectively, Table 3.5 shows that Ω_{cl} for the different slopes tested is slightly

---

* Hewlett Packard Calculator, Model 9100B

less than the corresponding values of Ω_{co}. This anomaly is thought to be due to the scatter in the data and due to the function chosen in the fitting procedure. However, Ω_{co} has been adopted as the critical stream power and hence was used to evaluate the ratio $(\Omega - \Omega_c)/\Omega$ in column 6 of Table 3.4.

3.2.2.5.3 Table 3.6; Comparison with Previous Investigations

Data from three different investigations have been collected to compute the critical stream powers Ω_c and compare them with those obtained in this investigation ; Table 3.5 . Table 3.6 shows the results of these computations and the following comments are made regarding them.

Computations of Ω_c Based on Neill's Data

1. For one sediment mixture Ω_c does not show a consistent increase or decrease with the channel slope. However, an average Ω_c could be computed and assumed to be a criterion for the initiation of motion of solids for the limited range of slopes tested.

2. The larger the D_n of a solid, the larger is Ω_c.

3. Identification of the threshold condition of motion of a solid was based on a subjective method where a small number of grains only moved when the threshold hydraulic conditions prevailed.

Computations of Ω_c Based on Ashida and Bayazit's Data

1. Comments 1 and 2 made about Ω_c based on Neill's data also apply.

2. Definition of the threshold condition of motion of a solid mixture was based on extrapolation from non-dimensional shear stress versus transport rate plots. Although this method is more objective than Neill's, there was no mention in Ashida and Bayazit's experiments about the number of times the same experiments were repeated. In other words, it is not known whether different transport rates would have been

measured by different investigators even if the same hydraulic conditions prevailed in the test flume.

Computation of Ω_c Based on Hartung and Scheuerlein's Equations

Equations 1.6, 1.7, 1.8, 1.9, 1.10 and 1.11 were solved for the case of $\rho_s/\rho = 2.65$, $D_{50} = 5$ cm and a packing factor P.F1 = 1. The critical stream power Ω_c was computed based on the equation:

$\Omega_c = \rho g q \sin \beta$, where q is given in equation 1.10.

The computations of Ω_c are shown in Table 3.6 and they reveal the following trends:

1. For a particular solid mixture, Ω_c increases with S_o. This trend was also revealed by the results shown in Table 3.5.
2. It could be shown that similar reiteration solutions to equations 1.6 to 1.11 for increasing D_{50} and/or ρ_s/ρ reveal an increase in Ω_c.

Ω_c Based on the Author's Experiments

Table 3.6 shows that, for the crushed granite stone mixture ($D_{50} = 5$ cm and $\rho_s/\rho = 2.65$), Ω_c increases with S_o. The following empirical equation was fitted by the least square method to the 4 data points obtained:

$$\Omega_c = 235 (S_o)^{0.516} \quad \text{..... Eq. 3.8}$$

The coefficient of correlation of equation 3.8 is 91.7%.

The limitations on equation 3.8 are:

1. It does not apply to subcritical flows.
2. It applies to a particular solid mixture.
3. The number of points which led to its establishment is small and it might prove fruitful to increase the number of experimental runs.

Table 3.6 also shows that Ω_c for the light-weight replicas increases with S_o. Unfortunately, slopes greater than 15.82% could not be tested because initiation of motion occurred when the volumetric discharges

were too small to measure (in the order of 1000 cm^3/sec or less).

3.2.2.5.4 Testing Scour Equations

The validity of equation 3.6 is now tested in the following way: All positive value of w_k/Ω and $\frac{\Omega - \Omega_c}{\Omega}$ in Table 3.4 were fed into the Hewlett calculator so that an equation of the form

$$\frac{w_k}{\Omega} = e_2\left(\frac{\Omega - \Omega_c}{\Omega}\right)^{e_3}, \quad (e_2 \text{ and } e_3 \text{ are constants})$$

can be fitted by the least square method.

Feeding in 193 data points gave the following equation:

$$\frac{w_k}{\Omega} = 12\left(\frac{\Omega - \Omega_c}{\Omega}\right)^{0.236}, \quad \text{..... Eq. 3.9}$$

The coefficient of correlation of equation 3.9 is only 25.8%, which means that such an equation predicts the weight of solids dislodged by a stream with a very poor degree of correlation.

3.2.2.5.5 Prediction of Ω_c and $\frac{w_k}{\Omega}$ for Larger Solids than those Tested

The experimental results obtained in Stage I of this investigation, could be regarded as results obtained from a Froude model that simulates the hydraulic conditions in a prototype wide channel lined with loose solids of $\rho_s/\rho = 2.65$. The major criticism of this assumption is that air entrainment in the prototype is greater than that in the model.

If the linear dimensions of the prototype are L times larger than those of the model, then the ratio of the stream powers per unit bed area is:

$$\frac{\Omega_c(\text{of model})}{\Omega_c(\text{of prototype})} = L^{-1.5} \quad \text{..... Eq. 3.10}$$

Consider a prototype stone mixture with a certain D_{50} but of a similar

weight distribution curve as Fig. 3.1 , assume also that the prototype solids are geometrically similar to those tested in the model and $\rho_s/\rho = 2.65$ is common between both model and prototype. Based on these assumptions, the following relations are written:

$$\frac{D_{50}(\text{of model})}{D_{50}(\text{of prototype})} = \frac{1}{L} \qquad \ldots\ldots\ldots\ldots\ldots\ldots \text{Eq. 3.11}$$

since D_{50} (of the model) = 5 cm and by substituting equation 3.11 into equation 3.10 one obtains:

$$\Omega_c(\text{of prototype}) = \Omega_c(\text{of model}) \left(\frac{D_{50}(\text{of prototype})}{5} \right)^{1.5} \quad \ldots\ldots \text{Eq. 3.12}$$

where D_{50}(of the prototype) is measured in cm.

Substituting the empirical equation 3.8 into equation 3.12 one obtains the following equation for Ω_c in a prototype:

$$\Omega_c = 235(S_o)^{0.516} \left(\frac{D_{50}}{5} \right)^{1.5} \qquad \ldots\ldots\ldots\ldots\ldots\ldots \text{Eq. 3.13}$$

Substituting equation 3.13 into equation 3.9 , one obtains the following equation for w_k/Ω in a prototype:

$$\frac{w_k}{\Omega} = 12 \left(\frac{\Omega - 235\,(S_o)^{0.516}\,(D_{50}/5)^{1.5}}{\Omega} \right)^{0.236} \quad \ldots \text{Eq. 3.14}$$

The same limitations on equations 3.8 and 3.9 also apply to equations 3.13 and 3.14 respectively.

Table 3.1 ; Measurements of the Mass Density of Solids, ρ_s

Solid mixture	Weight of solid in air 981 dynes	Weight of container + water before solid is immersed 981 dynes	Weight of container + water after solid is immersed 981 dynes	Buoyancy force 981 dynes	ρ_s gm/cm^3
Crushed granite stones D_{50}= 5cm	219.46	522.90	606.22	83.32	2.63
	317.57	618.32	737.80	119.48	2.66
	104.17	594.70	633.70	39.00	2.67
	138.06	595.50	646.90	51.40	2.68
	107.12	596.30	636.60	40.30	2.66
	116.29	596.75	640.85	44.10	2.64
	107.97	597.30	639.20	41.90	2.58
	103.49	524.20	562.92	38.72	2.67
	161.51	521.40	582.60	61.20	2.64
	118.15	599.71	644.11	44.40	2.66
				Average ρ_s	2.65
Light-weight replicas D_{50}= 5cm	76.10	634.80	688.00	53.20	1.43
	62.50	633.00	681.00	48.00	1.30
	115.50	642.50	727.40	84.90	1.36
	89.10	639.70	699.60	59.90	1.48
	105.90	642.50	709.00	66.50	1.59
	75.90	638.00	689.20	51.20	1.48
	161.10	650.00	752.10	102.10	1.58
	164.00	652.10	753.50	101.40	1.61
	169.20	655.20	765.50	110.31	1.53
				Average ρ_s	1.48

Table 3.2 ; Measurements of the Angle of Sliding Friction, α

Experiment No.	Solid Mixture	α in air degrees	α under water degrees
1	Crushed Granite	66	65
2	Stones	63.5	62
3	D_{50}= 5cm	62.5	62
4		64	66
5	$\frac{\rho_s}{\rho}$ = 2.65	66.5	60
6		65	63
7		63.5	66.5
8		64	65
9		66	64.5
10		63	62
	Average	63.6	64.4
1	Light-Weight	63	64
2	Replicas	64	61.5
3	D_{50}= 5cm	63.5	62.5
4		61	60.5
5	$\frac{\rho_s}{\rho}$ = 1.48	63	62.5
7		63.5	64
8		62	65
9		61.5	63.5
10		62	63
	Average	62.85	63.10

Table 3.3 ; Calibration of Orifice Plate

Q cm^3/sec	$(H)^{\frac{1}{2}}$ $(cm\ of\ water)^{\frac{1}{2}}$	Q cm^3/sec	$(H)^{\frac{1}{2}}$ $(cm\ of\ water)^{\frac{1}{2}}$
8816	2.68	58792	17.75
12149	3.73	60439	18.58
15143	4.70	63791	19.44
15142	4.63	65936	20.02
16950	5.16	67202	20.64
17288	5.69	70779	21.53
19834	6.10	74526	22.78
21413	6.49		
24183	7.42		
2.6302	8.02		
29477	8.96		
32859	10.03		
36369	11.13		
39031	11.97		
39887	12.09		
47745	14.64		
53717	16.27		
42457	12.90		
44544	13.56		
52318	15.55		
55427	17.13		

Table 3.4 ; Details of Experimental Results

Column: 1		2	3	4	5	6	7
Exp./Run	$\frac{q}{\text{sec-cm}}$ cm^3	$\frac{\Omega}{981 \text{ dynes}}$ cm-sec	2500w 981 dynes	%dg in 10 min	$\frac{w_k}{\Omega}$	$\frac{\Omega-\Omega_c}{\Omega}$	Variables kept constant during each experiment
1/1	1044.80	71.50	149.95	1	9.29	22.45	S_o = 6.8%
1/2	1374.30	93.45	494.84	3	23.45	40.66	$\frac{\rho_s}{\rho}$ = 2.65
1/3	1425.00	96.85	625.19	4	28.59	42.75	
2/1	542.90	36.90	0	0	0	-	D_{50}= 5cm
2/2	781.90	53.17	718.10	3	59.83	-	50cm< x< 100cm
2/3	1132.60	77.00	893.70	4	51.40	27.99	N = 100
2/4	1440.00	97.90	1255.70	7	57.05	43.36	
3/1	476.20	31.77	346.38	2	48.31	-	
3/2	874.20	59.44	533.12	3	39.74	6.71	
3/3	1227.40	83.50	821.60	5	43.58	33.59	
3/4	1329.40	90.43	1155.75	7	56.61	38.68	
3/5	1382.21	93.99	1262.95	8	59.54	41.00	
4/1	898.80	61.12	0	0	0	-	
4/2	1018.40	69.25	175.60	1	11.23	19.93	
4/3	1222.90	83.15	915.36	4	48.76	33.31	
4/4	1305.00	88.74	1184.51	6	59.14	37.51	
4/5	1390.00	94.52	1546.77	9	72.51	41.33	
5/1	904.00	61.53	0	0	0	-	
5/2	1070.66	72.80	129.18	1	7.87	23.83	
5/3	1266.80	86.14	365.38	3	18.78	35.63	
5/4	1382.20	94.00	546.20	4	25.72	41.01	
6/1	795.74	54.11	376.25	2	30.79	-	
6/2	949.04	64.53	522.28	3	35.85	14.07	
6/3	1034.35	70.33	820.40	5	51.67	21.16	
6/4	1258.17	85.55	1152.85	7	59.70	35.18	
6/5	1378.26	93.72	1410.56	9	66.68	40.83	
7/1	996.75	67.77	0	0	0	-	
7/2	1050.07	71.40	186.74	1	11.64	22.34	
7/3	1100.82	74.85	620.36	3	36.72	25.92	
7/4	1280.50	82.85	727.56	4	38.84	33.07	
7/5	1503.30	102.20	822.31	5	35.65	45.74	
8/1	572.30	38.91	0	0	0	-	
8/2	723.90	49.23	190.32	1	17.10	-	

Table 3.4 continued

Column: 1	2	3	4	5	6	7
9/1	907.88	143.63	777.71	6	22.64	20.13	S_o = 15.82%
9/2	1068.11	168.98	1126.24	8	27.86	32.11	$\frac{\rho_s}{\rho}$ = 2.65
9/3	1193.61	188.83	1338.30	10	29.64	39.25	
9/4	1382.21	218.67	1519.12	11	29.04	47.54	D_{50}= 5cm
10/1	874.20	138.30	413.49	2	12.48	17.05	50cm< x< 100cm
10/2	977.37	154.62	918.00	5	24.82	25.81	N = 100
10/3	1191.32	188.47	2099.11	11	46.58	39.14	
10/4	1281.81	202.78	2502.86	14	51.60	43.43	
11/1	595.66	94.23	0	0	0	-	
11/2	788.85	124.79	526.04	3	17.61	8.00	
11/3	871.06	137.80	697.64	4	21.16	16.75	
12/1	735.12	116.29	1233.36	7	44.34	1.36	
12/2	982.95	155.50	1772.13	10	47.64	26.23	
12/3	1191.32	188.46	2338.50	13	51.88	39.14	
13/1	988.48	156.38	760.27	4	20.32	26.65	
13/2	1436.40	227.24	1475.02	9	27.14	49.52	
14/1	681.17	107.76	297.08	2	11.51	-6.0	
14/2	874.19	138.29	1735.02	11	52.46	17.05	
14/3	1174.49	186.27	2488.81	15	55.87	38.42	
15/1	745.25	120.90	225.68	1	7.80	5.12	
15/2	954.77	151.04	1180.70	7	32.00	24.06	
15/3	1085.85	171.78	1401.67	8	34.11	33.22	
15/4	1186.73	187.74	2017.62	12	44.94	38.90	
16/1	874.20	138.30	109.30	1	3.30	17.06	
16/2	991.24	156.81	288.28	2	7.61	26.85	
16/3	1177.50	186.28	468.28	3	10.50	38.42	
16/4	1279.70	202.45	575.43	4	11.86	43.33	
16/5	1434.45	226.94	926.13	6	17.05	49.45	
17/1	609.25	96.38	0	0	0	-	
17/2	723.90	114.52	254.23	2	-	-	
17/3	861.61	136.30	385.41	3	11.83	15.84	
17/4	1091.30	172.97	1131.66	8	27.36	33.68	
17/5	1175.17	185.91	3420.00	19	76.93	38.28	

Table 3.4 continued

Column: 1		2	3	4	5	6	7
18/1	723.90	114.52	0	0	0	-	S_o = 15.82%
18/2	858.44	135.81	1030.72	6	31.72	15.53	$\frac{\rho_s}{\rho}$ = 2.65
18/3	968.96	153.29	1267.43	7	34.58	25.17	
18/4	1191.32	188.47	2693.60	17	59.76	39.14	D_{50}= 5cm
19/1	511.87	80.98	0	0	-	-	50cm< x< 100cm
19/2	720.12	113.00	129.00	1	-	-	N = 100
19/3	864.72	136.80	1381.06	9	42.22	16.15	
19/4	974.58	154.18	1726.52	12	46.83	25.60	
20/1	609.25	96.38	256.68	2	-	-	
20/2	858.44	135.81	524.28	4	16.14	15.53	
20/3	1095.86	173.37	857.28	6	20.68	33.83	
20/4	1268.98	200.75	984.00	7	20.49	42.86	
20/5	1352.28	213.93	1120.35	8	21.89	46.38	
21/1	547.93	86.68	0	0	0	-	
21/2	738.83	116.88	304.06	2	10.88	1.85	
21/3	858.44	135.81	1150.91	6	35.44	15.53	
21/4	1083.34	171.38	2914.73	18	71.12	33.06	
22/1	572.29	90.53	563.68	3	-	-	
22/2	889.66	140.74	682.63	4	20.28	18.50	
22/3	1083.33	171.38	2167.68	11	52.89	33.06	
23/1	295.80	46.80	0	0	-	-	
23/2	470.05	74.36	188.12	1	-	-	
23/3	649.59	102.76	505.34	3	-	-	
23/4	1191.32	188.46	1766.81	12	39.06	39.14	
24/1	473.08	74.84	324.67	2	-	-	
24/2	595.66	94.23	878.40	5	-	-	
24/3	672.29	106.35	1027.13	6	-	-	
24/4	746.18	118.04	3238.59	20	-	-	
25/1	618.15	97.79	752.86	4	-	-	
25/2	1031.72	163.21	4534.03	28	-	-	
26/1	338.57	53.56	0	0	-	-	
26/2	572.29	90.54	472.02	3	-	-	
26/3	738.83	116.88	1457.27	7	52.13	1.85	
26/4	977.38	154.62	1939.70	10	52.46	25.81	

Table 3.4 continued

Column: 1		2	3	4	5	6	7
27/1	280.02	65.35	0	0	0	-	S_o = 23.34%
27/2	317.71	74.15	162.38	1	1.81	-11.24	$\frac{\rho_s}{\rho}$ = 2.65
27/3	386.60	90.23	298.78	2	13.06	2.90	
27/4	446.41	104.19	393.53	3	14.89	13.65	D_{50}= 5cm
27/5	479.17	111.84	500.68	4	17.65	19.55	
27/6	634.74	148.15	1388.41	10	36.96	39.27	50cm<x<100cm
27/7	713.47	166.52	5505.60	34	-	45.97	N = 100
28/1	277.00	64.65	0	0	0	-	
28/2	401.44	93.69	215.57	2	9.06	3.97	
28/3	502.56	117.30	1136.39	8	38.19	23.29	
28/4	552.26	128.90	1247.03	9	38.18	30.20	
28/5	599.64	139.96	2649.06	18	74.63	35.72	
29/1	280.74	65.52	0	0	0	-	
29/2	336.91	78.63	149.45	1	-	-	
29/3	394.92	92.17	384.13	3	16.44	2.39	
29/4	527.79	123.19	1447.91	9	46.34	26.96	
29/5	565.82	132.06	1543.08	10	46.06	31.87	
29/6	617.45	144.11	2339.04	15	64.02	37.57	
29/7	650.58	151.85	2423.64	16	62.94	40.74	
30/1	446.89	104.30	0	0	0	-	
30/2	508.56	118.70	423.40	2	14.06	24.20	
30/3	562.36	131.25	559.80	3	16.81	31.45	
30/4	631.32	147.35	773.80	4	20.70	38.94	
30/5	675.09	157.56	1132.96	6	28.35	42.90	
30/6	1029.06	240.18	5343.68	33	-	62.54	
31/1	382.66	89.31	0	0	0	-	
31/2	447.38	104.42	642.31	3	24.29	13.84	
31/3	489.02	114.14	753.97	4	26.05	21.17	
31/4	526.97	122.94	1326.12	9	42.53	26.84	
32/1	252.35	58.90	0	0	0	-	
32/2	322.45	75.25	171.60	1	-	-	
32/3	511.96	119.49	342.30	2	11.30	24.71	
32/4	568.11	132.60	1943.02	12	57.78	32.15	
32/5	608.61	142.10	2554.36	16	70.91	36.66	

Table 3.4 continued

Column: 1		2	3	4	5	6	7
33/1	228.00	58.90	0	0	0	-	S_o = 23.34%
33/2	241.83	56.44	118.15	1	-	-	$\frac{\rho_s}{\rho}$ = 2.65
33/3	271.83	63.45	226.14	2	-	-	
33/4	392.16	91.53	420.24	3	18.11	1.70	D_{50}= 5cm
33/5	480.53	112.16	551.69	4	19.39	19.80	50cm<x<100cm
33/6	509.84	118.99	664.00	5	22.00	24.39	N = 100
33/7	656.55	153.23	1728.06	11	44.48	41.29	
33/8	705.84	164.67	3724.38	23	-	-	
34/1	303.77	70.90	0	0	0	-	
34/2	412.64	96.31	303.38	3	12.43	6.57	
34/3	465.41	108.63	751.13	6	27.28	17.18	
34/4	524.49	122.42	2043.17	12	65.81	26.50	
34/5	584.28	136.37	4210.17	26	-	34.03	
35/1	352.61	82.30	0	0	0	-	
35/2	425.55	99.32	643.53	5	25.56	9.42	
35/3	591.28	138.00	1050.50	8	30.09	34.81	
35/4	624.42	145.74	1954.93	13	52.89	38.26	
35/5	691.26	161.34	8258.41	51	-	44.24	
36/1	449.79	104.98	1643.18	9	63.59	14.30	
36/2	522.43	121.94	3886.31	24	-	26.21	
37/1	410.00	95.69	768.48	6	31.68	5.98	
37/2	518.27	120.96	944.58	7	30.78	25.62	
37/3	565.82	132.06	1730.36	11	51.67	31.87	
37/4	592.38	138.26	3076.66	19	-	34.93	
38/1	359.51	83.86	531.95	4	-	-	
38/2	465.41	108.63	782.00	6	28.39	17.18	
38/3	695.32	162.29	4695.96	29	-	49.56	
39/1	203.93	100.42	0	0	0	-	S_o = 49.24%
39/2	306.61	150.57	94.75	1	1.81	-	$\frac{\rho_s}{\rho}$ = 2.65
39/3	386.84	190.48	223.75	2	3.40	11.83	
39/4	447.39	220.29	457.92	5	6.00	23.76	D_{50}= 5cm
39/5	503.42	247.88	1040.24	9	12.15	32.24	50cm< x< 100cm
40/1	258.24	127.18	0	0	0	-	N = 100
40/2	341.37	168.09	185.65	1	3.19	0.08	
40/3	410.52	202.14	447.30	3	6.40	16.19	
40/4	514.50	253.35	1766.83	13	20.18	33.18	

Table 3.4' continued

Column: 1	2	3	4	5	6	7
41/1	232.70	114.58	0	0	0	-	
41/2	334.97	164.94	307.34	2	-	-	S_o = 49.24%
41/3	446.90	220.05	730.54	5	9.61	23.67	$\frac{\rho_s}{\rho}$ = 2.65
41/4	498.67	245.54	868.65	6	10.24	31.60	
41/5	541.57	266.67	1054.65	7	11.45	37.02	D_{50}= 5cm
41/6	588.71	289.88	2320.26	17	23.17	42.06	50cm<x<100cm
42/1	206.05	101.46	0	0	0	-	N = 100
42/2	303.05	149.22	434.18	3	-	-	
42/3	586.13	288.61	1161.00	8	11.64	41.80	
43/1	407.34	200.57	0	0	0	-	
43/2	465.42	229.14	234.02	2	2.95	26.67	
43/3	601.81	296.33	2504.87	18	24.46	43.32	
44/1	272.18	134.01	0	0	0	-	
44/2	342.01	168.40	711.56	4	12.22	0.03	
44/3	514.91	253.54	883.16	5	10.08	33.75	
45/1	406.80	200.30	0	0	0	-	
45/2	464.50	228.72	931.41	6	11.78	26.56	
46/1	258.30	127.19	0	0	0	-	
46/2	235.60	165.26	302.58	2	-	-	
46/3	463.60	228.27	519.20	4	6.57	26.57	
46/4	605.04	297.90	2868.20	20	-	43.62	
47/1	343.30	169.04	0	0	0	-	
47/2	418.90	206.26	734.46	6	10.31	18.56	
47/3	466.35	229.63	917.23	7	11.56	26.86	
47/4	557.72	274.62	1487.08	10	15.67	38.84	
48/1	340.10	167.47	0	0	0	-	
48/2	411.57	202.66	501.46	3	7.16	17.13	
48/3	468.66	230.66	1208.73	8	15.10	27.22	
49/1	462.61	227.78	0	0	0	-	
49/2	513.25	252.71	519.75	5	5.96	33.54	
50/1	255.77	125.94	0	0	0	-	
50/2	334.42	164.62	202.37	2	-	-	
50/3	401.45	197.67	466.12	4	6.8	15.04	
50/4	457.91	224.97	1028.50	8	13.85	25.85	

Table 3.4 continued

Column: 1	2	3	4	5	6	7
51/1	336.90	165.84	0	0	0	-	S_o = 49.24%
51/2	408.93	201.36	1086.13	6	15.62	16.60	$\frac{\rho_s}{\rho}$ = 2.65
51/3	460.74	226.87	1509.58	9	19.25	25.97	
51/4	558.90	275.20	1591.19	10	16.73	38.97	D_{50}= 5cm
51/5	596.75	293.83	-	32	-	-	
52/1	256.61	126.35	0	0	0	-	50cm< x< 100cm
52/2	327.11	161.06	133.35	1	-	-	N = 100
52/3	506.85	249.57	238.55	2	2.76	32.71	
52/4	555.78	273.66	384.58	3	4.07	38.62	
52/5	635.42	312.88	3724.38	23	-	-	
53/1	114.00	18.03	0	0	0	-	S_o = 15.82%
53/2	147.18	23.28	69.50	1	-	-	$\frac{\rho_s}{\rho}$ = 1.48
53/3	215.30	34.06	458.30	5	15.80	26.87	
53/4	273.77	43.31	1437.00	20	-	-	D_{50}= 5cm
54/1	145.70	23.05	0	0	0	-	50cm< x< 100cm
54/2	180.26	28.52	330.40	4	13.62	12.65	N = 100
54/3	237.32	37.54	562.10	6	17.58	33.65	
54/4	340.10	53.80	-	80	-	-	
55/1	152.95	24.19	0	0	0	-	
55/2	181.45	28.71	422.30	5	17.28	13.22	
55/3	203.94	32.26	580.20	7	21.13	22.80	
55/4	254.42	40.32	-	50	-	-	
56/1	152.95	24.19	49.00	1	2.37	-	
56/2	206.05	32.59	127.10	2	4.57	23.58	
56/3	276.91	43.80	-	70	-	-	
57/1	155.76	24.64	0	0	0	-	
57/2	183.82	29.70	414.70	4	16.76	14.34	
57/3	232.71	36.81	-	70	-	-	
58/1	110.00	17.40	0	0	0	-	
58/2	157.14	24.90	184.60	3	8½68	0	
58/3	188.48	29.82	796.30	11	31.37	16.14	
58/4	232.71	36.81	-	60	-	-	

Table 3.4 continued

Column: 1		2	3	4	5	6	7
59/1	110.00	17.40	0	0	0	-	S_o = 15.82%
59/2	157.00	24.84	167.30	3	-	-	$\frac{\rho_s}{\rho}$ = 1.48
59/3	188.00	29.82	228.30	4	10.78	-	
59/4	203.00	32.11	417.60	7	15.28	22.43	D_{50}= 5cm
59/5	245.00	40.18	-	50	-	-	50cm<x<100cm
60/1	106.00	16.76	0	0	0	-	N = 100
60/2	157.00	24.84	330.00	4	-	-	
60/3	188.00	29.74	-	20	-	-	
61/1	157.00	24.84	78.10	1	-	-	
61/2	188.00	29.74	519.60	6	20.51	22.43	
61/3	203.00	32.11	-	25	-	-	
62/1	144.20	12.98	0	0	0	-	
62/2	211.24	19.01	186.60	4	-	-	
62/3	246.28	22.17	505.70	5	28.02	12.07	
62/4	282.34	25.41	1074.50	9	51.93	23.29	
62/5	364.69	32.82	-	15	-	-	
62/6	426.56	38.39	-	50	-	-	
63/1	210.21	18.92	0	0	0	-	
63/2	241.84	21.76	980.90	8	46.06	25.49	
63/3	290.65	26.16	1380.85	11	59.33	31.83	
63/4	371.17	28.59	868.18	17	61.56	47.72	
63/5	414.20	37.28	1868.18	26	-	-	
64/1	161.23	14.51	0	0	0	-	S_o = 9.00%
64/2	191.90	17.27	221.00	4	-	-	$\frac{\rho_s}{\rho}$ = 1.48
64/3	294.36	26.49	660.35	7	30.69	26.43	
64/4	325.13	29.26	812.35	8	34.09	33.39	D_{50}= 5cm
64/5	374.08	33.67	-	28	-	-	50cm<x<100cm
65/1	142.69	12.84	0	0	0	-	N = 100
65/2	180.26	16.22	162.40	3	-	-	
65/3	296.56	26.69	441.80	7	20.33	26.97	
65/4	350.15	31.51	580.20	8	22.69	38.14	
65/5	383.82	35.44	718.90	9	24.92	45.00	
65/6	476.46	42.88	-	30	-	-	

Table 3.4 continued

Column: 1		2	3	4	5	6	7
66/1	176.61	15.90	0	0	0	-	S_o = 9.00%
66/2	212.26	19.10	217.70	4	-	-	
66/3	346.74	30.67	416.40	6	16.68	36.45	$\frac{\rho_s}{\rho}$ = 1.48
66/4	436.60	39.29	946.80	10	-	-	
67/1	158.52	14.27	0	0	0	-	D_{50}= 5cm
67/2	219.20	19.74	118.20	3	-	-	50cm< x< 100cm
67/3	329.10	29.62	377.55	6	15.65	34.20	N = 100
67/4	360.51	32.45	488.65	8	18.48	39.94	
67/5	412.62	37.14	1293.35	18	-	-	
68/1	155.67	-	0	0	0	-	
68/2	218.30	19.65	530.17	4	33.14	0.08	
68/3	256.61	23.10	599.67	5	31.89	15.63	
68/4	294.36	26.49	803.37	7	37.25	26.43	
68/5	322.45	29.02	1525.12	15	64.56	32.84	
69/1	177.84	16.01	0	0	0	-	
69/2	225.14	20.26	385.64	5	23.38	3.80	
69/3	259.13	23.32	576.64	7	30.39	16.42	
69/4	296.28	26.76	698.74	9	32.08	27.16	
69/5	352.00	31.68	743.34	10	28.82	38.47	
69/6	431.61	38.80	872.24	11	27.62	49.77	
70/1	136.49	12.28	0	0	0	-	
70/2	190.76	17.17	48.30	1	-	-	
70/3	218.30	19.65	249.30	3	-	-	
70/4	243.62	21.43	309.70	4	17.74	9.05	
70/5	335.62	30.21	758.85	8	30.87	35.48	
70/6	368.29	33.14	1115.65	13	41.37	41.18	
71/1	83.26	7.49	0	0	0	-	
71/2	136.49	12.28	46.70	1	-	-	
71/3	195.25	17.57	494.00	8	-	-	
71/4	240.04	21.60	-	17	-	-	
72/1	169.09	15.22	0	0	0	-	
72/2	202.87	18.26	339.40	4	-	-	
72/3	286.90	25.82	597.40	7	28.40	24.50	
72/4	315.66	28.41	-	26	-	-	

Table 3.4 continued

Column: 1		2	3	4	5	6	7
73/1	248.03	22.32	471.10	6	25.95	12.67	S_o = 9.00%
73/2	280.80	25.27	704.55	8	34.25	22.87	$\frac{\rho_s}{\rho}$ = 1.48
74/1	351.38	31.62	351.38	9	13.64	38.36	
74/2	500.41	45.09	913.20	11	24.88	56.78	D_{50}= 5 cm
74/3	677.66	60.94	-	75	-	-	50cm<x<100cm
							N = 100

Table 3.5 ; Contains e_o, Ω_{co}, r_o, e_1, Ω_{cl} and r_1 as Defined in Equations 3.7.3 and 3.7.4 and Appendix I

Symbol	S_o	D_{50}	ρ_s/ρ	e_o	Ω_{co}	r_o	e_1	Ω_{cl}	r_1
Dimensions	%	cm	-	-	$\frac{981 \text{ dynes}}{\text{sec-cm}}$	%	-	$\frac{981 \text{ dynes}}{\text{sec-cm}}$	%
	6.8	5	2.65	31.15	55.44	66	4.61	58.45	58
	15.82	5	2.65	106.38	114.71	53	4.97	100.88	64
	23.34	5	2.65	103.09	89.97	72	4.45	77.76	84
	49.24	5	2.65	75.53	167.95	70	5.21	162.93	80
	9.0	5	1.48	256.41	24.91	65	7.94	24.37	83
	15.82	5	1.48	107.53	19.49	65	3.27	13.87	82

Table 3.6 ; Comparison of Ω_c Versus S_o, Based on Data From Different Sources

Source of data	D_{50} cm	ρ_s/ρ	Ω_c $\frac{981 \text{ dynes}}{\text{sec-cm}}$	S_o %
Neill	0.62	2.54	1.41	0.45
(1967)	"	"	2.14	0.55
	"	"	2.62	0.43
	"	"	2.44	0.37
	"	"	2.86	0.40
	"	"	2.22	0.37
	"	"	2.45	0.24
	"	"	2.83	0.24
	"	"	2.03	0.20
	0.85	2.52	3.47	1.70
	"	"	2.49	0.85
	"	"	6.01	0.66
	"	"	5.60	0.41
	2.00	2.52	9.04	2.70
	"	"	10.48	1.97
	"	"	8.56	1.46
	"	"	10.47	1.16
	"	"	13.05	1.07
	"	"	11.16	0.75
	"	"	14.75	0.75

Table 3.6 continued

Source of data	D_{50} cm	ρ_s/ρ	Ω_c $\frac{981 \text{ dynes}}{\text{sec-cm}}$	S_o %
Ashida and Bayazit (1973)	2.25	2.49	22.30	2.00
	"	"	18.50	5.00
	"	"	18.37	7.50
	"	"	22.87	15.00
	"	"	17.00	20.00
	1.20	2.65	6.75	1.00
	"	"	6.25	2.50
	"	"	4.25	10.00
	"	"	4.37	12.50
	0.64	2.50	3.25	1.00
	"	"	3.00	2.50
	"	"	2.12	5.00
Reiteration solution based on Eqs. 1.5 to 1.10	5.00	2.65	96.39	6.80
	"	"	100.33	15.82
	"	"	120.88	23.34
	"	"	161.30	49.24
Present research (1975)	5.00	2.65	55.44	6.80
	"	"	114.71	15.82
	"	"	89.97	23.34
	"	"	167.95	49.24
	"	1.48	19.49	9.00
	"	1.48	24.91	15.82

STAGE II

(includes Chapters 4 and 5)

"Force measurement on a sphere
in a shallow stream and the
initial instability
of a loose sphere."

CHAPTER 4

Hydrodynamic Forces on a Sphere in a Supercritical Rough Flow and their Statistical Analysis

4.1 Purpose

As was mentioned previously, Stage II of the present investigation is an idealization of Stage I. In addition to the complexity of the flow picture over a steep bed of stones, the geometry of the stones themselves and their arrangement together add another set of variables that affects the initial instability of any one stone. Hence, the main idealization proposed is to build a uniform bed of fixed spheres, suspend one sphere in the flow by a steel leaf and measure the instantaneous forces on the sphere induced by the stream. Although the experimental details and results of Stage II are found in Chapter 5, the present chapter will discuss the following theoretical ideas:

1. How to isolate the instantaneous drag, lift and skin friction forces on a sphere in a supercritical stream.
2. What desirable properties should the force transducer possess so as to have a linear response to the input forces of the stream.
3. Having obtained simultaneous records of the instantaneous drag, lift and skin friction forces, what statistical analysis needs to be done and how can the stability of a loose sphere be investigated.

4.2 Isolation of Drag, Lift and Skin Friction Forces

Let a sphere be suspended by a steel leaf in a shallow supercritical stream. Consider the stream to be steady and the bed to have the geometric configurations shown in Figs. 4.1 a and b.

The stream forces acting on the sphere consist of the drag FD, the

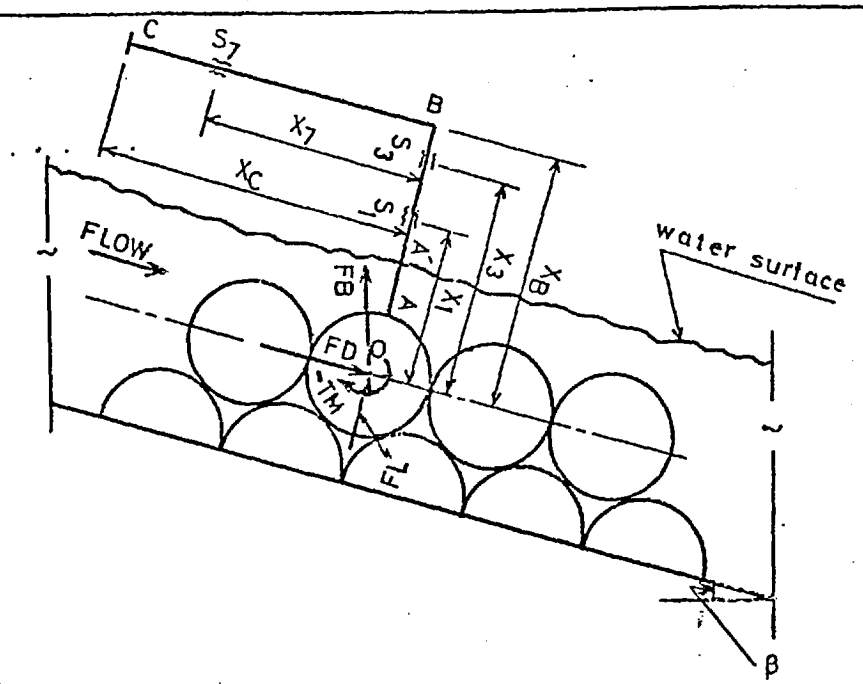


FIG. 4.1a , profile of an ideal bed of spheres and a supercritical flow over it

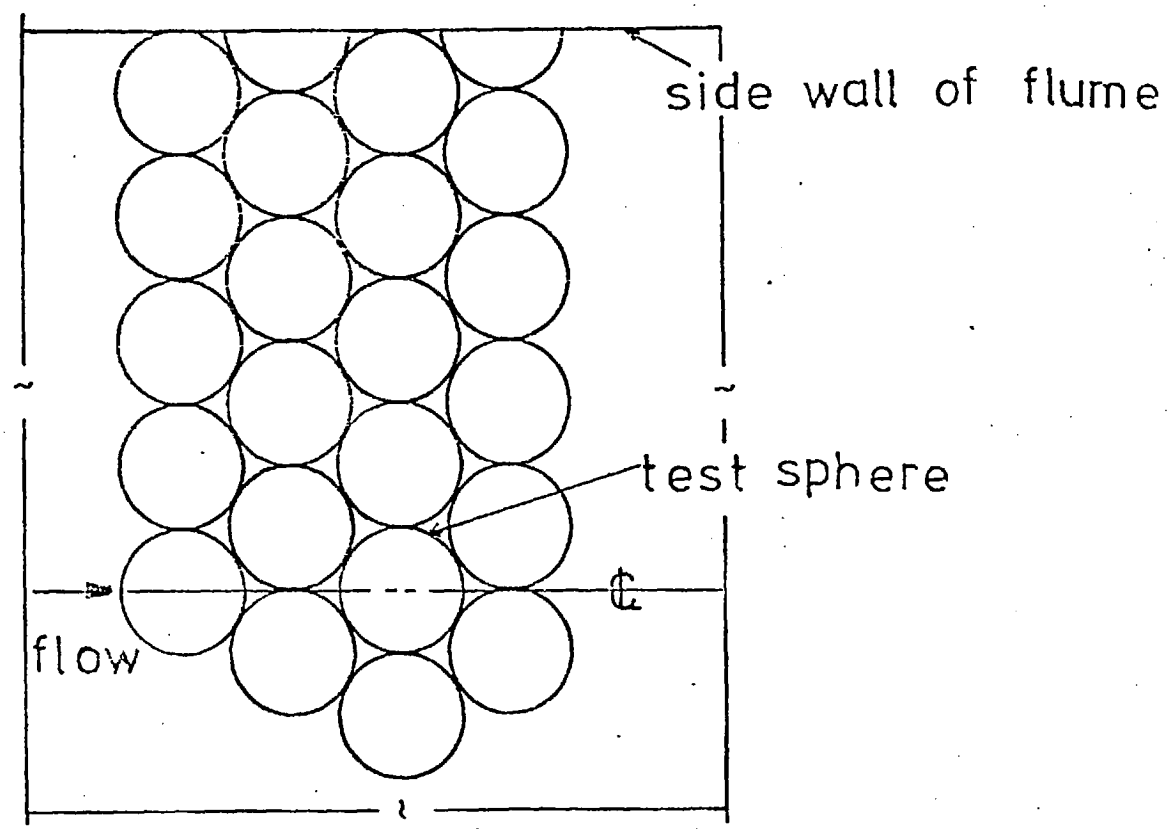


FIG. 4.1b , plan of hexagonal pattern of spheres

lift FL, a torque TM due to the skin friction forces distributed on the surface of the sphere and a buoyancy force F_B. All these forces are represented diagramatically in Fig. 4.1a .

The steel leaf OAA'BC is a cantilever with a 90^o bend at point B. The bending moments set up in the cantilever at one instant of time are shown in Fig. 4.2 .

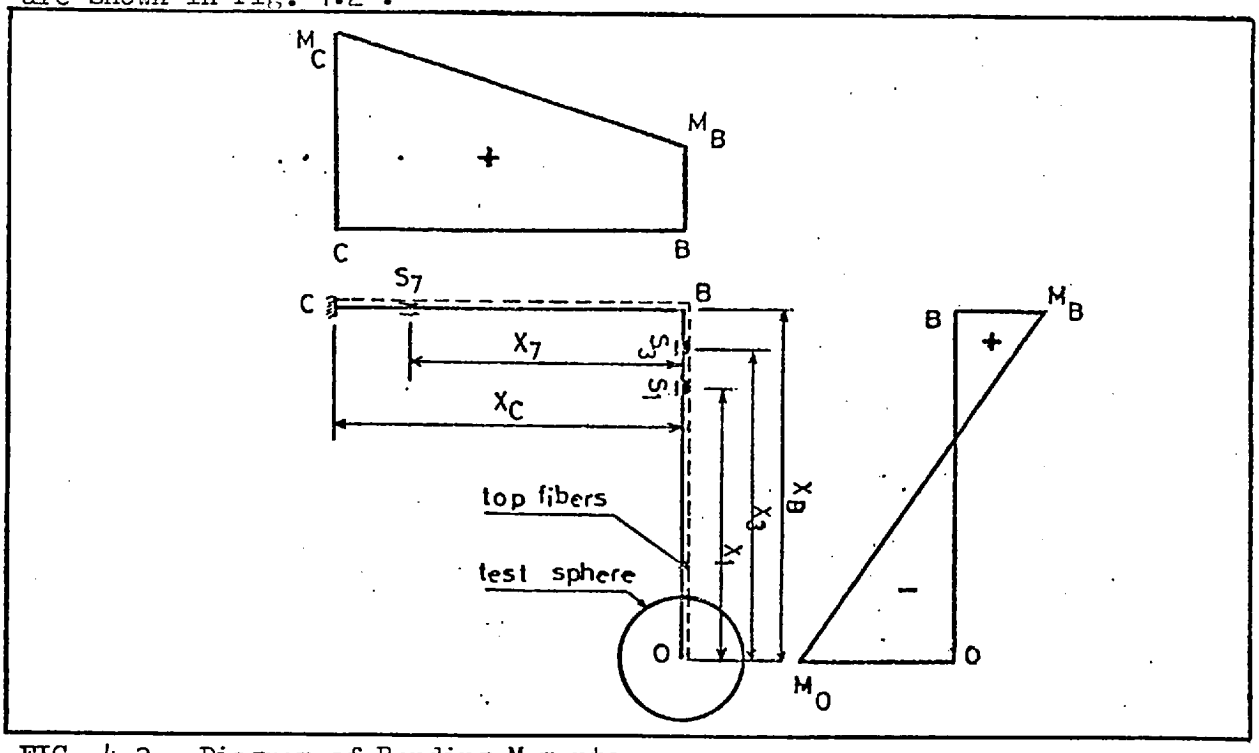


FIG. 4.2 , Diagram of Bending Moments

Positive bending moments are defined as those which produce compression in the top fibres of the cantilever.

The co-ordinates of the bending moment diagram are:

$$M_o = -TM$$

$$M_B = M_o + (F_D - F_B \sin \beta)\ \overline{OB}$$

$$M_C = M_B + (FL + F_B \cos \beta)\ \overline{BC}$$

where $\overline{OB}$ and $\overline{BC}$ are distances shown in Fig 4.2 .

Let the strains at locations S_1, S_3, S_7 (see Fig. 4.1a) be measured by wire resistance strain guages. If the stresses induced in the cantilever are within the elastic limit of steel, then the bending moment at any section in the cantilever will be directly proportional

to the strain measured there. Therefore, the bending moments M_1, M_3 and M_7 could be measured at sections S_1, S_3 and S_7 respectively. Finally, FD,FL and TM are given by the following equations:

$$FD = \frac{M_3 - M_1}{X_3 - X_1} + F_B \sin\beta \quad \text{..... Eq. 4.1}$$

$$TM = M_3 - X_3(FD - F_B \sin\beta) \quad \text{..... Eq. 4.2}$$

$$FL = \frac{1}{X_7}(M_7 - TM - X_B(FD - F_B \sin\beta)) - F_B \cos\beta \quad \text{.....Eq. 4.3}$$

where X_1, X_3, X_7 and X_B are distances shown in Fig 4.1a and Fig 4.2 .

4.3 Desirable Dynamic Properties of the Force Transducer

It would be ideal if there is a linear relationship between the turbulent forces on the sphere (see Fig. 4.1a) and the stresses transmitted to the cantilever. The turbulent forces on the sphere act as an input (or an exciting) source to the cantilver; while the stresses in the cantilever are the response or the output from it.

Bendate and Piersol (1971) in their book about random data analysis, reviewed the frequency-response functions of simple mechanical systems.

Let the force input, F(in), to a mechanical system have a dominant frequency f and the mechanical system itself have a natural frequency f_n and damping characteristics ξ. The force output from the mechanical system would be magnified in magnitude or shifted in phase (relative to a static force input) depending upon the combination of properties of F(in), f, f_n and ξ. Fig. 4.3a shows the variations of the gain factor with f/f_n for different damping ratios ξ, where the gain factor is the ratio of deflections (produced in the mechanical system) caused by an exciting force F(in) with frequency f, to the deflections caused by a static force equal in magnitude to F(in).

Fig. 4.3b is a plot of f/f_n Vs. phase factor for different damping ratios ξ . The phase factor is a measure of lag in time between the output deflections and the exciting force F(in).

The above mentioned discussion about forced vibrations of a mechanical system leads to the following recommendations that must be considered in the structural design of the cantilever.

1. The cantilver and the sphere attached to it should have a high natural frequency both in air and in water.

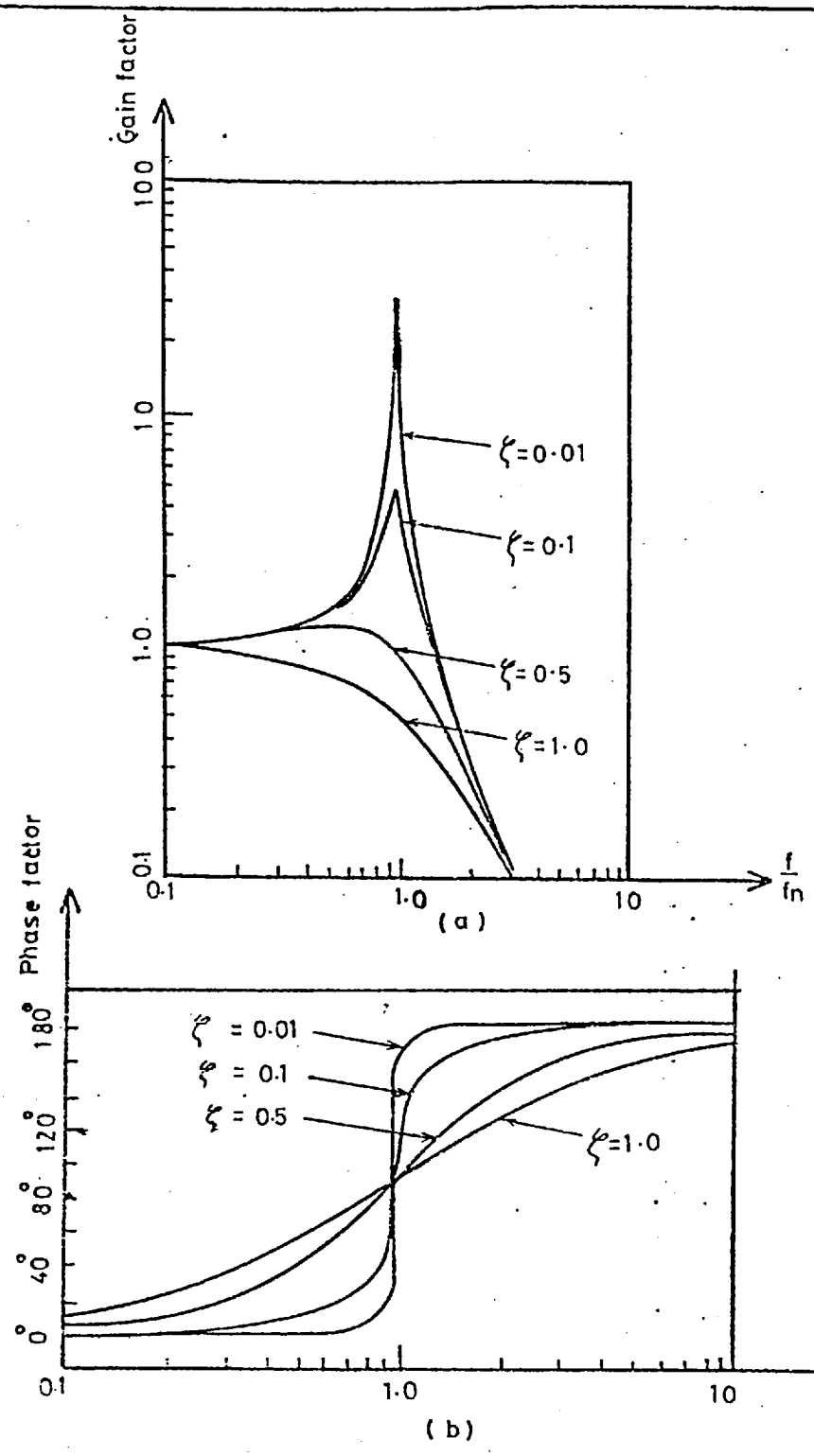
2. Since the turbulent forces on the sphere are expected to have a wide band of frequencies f , the ratio f/f_n should be different from unity, otherwise the response from the cantilver will be radically magnified.

3. Ideally, it would be desirable to have a cantilever with a gain factor of 1 and a phase factor of 0^o for all frequencies encountered.

4.4 Analysis of Random Data

It is now assumed that the cantilever in Fig. 4.1a responds linearly to the turbulent forces of the stream. Since the turbulent forces on the test sphere are expected to be random, it is necessary to describe the nature of their randomness statistically.

The instantaneous stresses at sections S_1, S_3 and S_7 (in the cantilever shown in Fig. 4.1a) could be described by three simultaneous random waves as shown in Fig. 4.4 . Using equations 4.1, 4.2 and 4.3 allows the calculation of the instantaneous and simultaneous values of FD, TM and FL respectively.



FIGS. 4·3a & b , Frequency response functions of a mechanical system with a force input. (a) Gain factor. (b) Phase factor.

(from Bendat (1971))

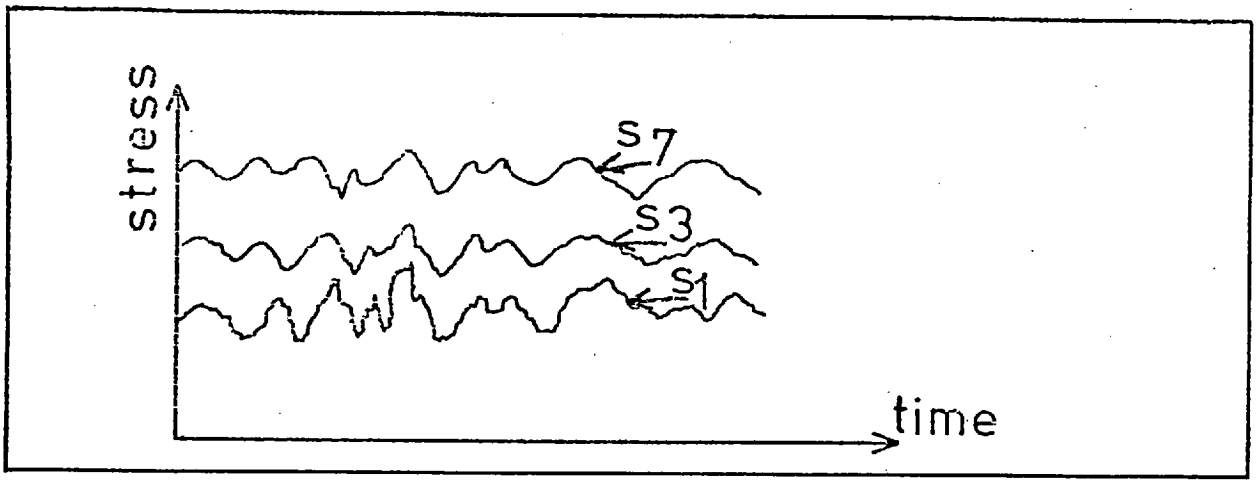


FIG 4.4 , Simultaneous Recrods of Stress at Sections S_1, S_3 and S_7

4.4.1 Basic Descriptive Properties of a Random Wave

Bendate and Piersol (1971) have also outlined the main types of statistical functions necessary to describe the basic properties of a random wave.

It is always necessary to establish whether a random wave is stationary or not. The simplest test for stationarity of a random wave is to see whether the arithmetic mean of the wave amplitudes changes with changing lengths of the record. If the arithmetic mean does not change materially after an optimum length of record, it could be said that there are no increasing or decreasing trends in the wave and the wave is described as stationary.

The mean square value furnishes a rudimentary description of the intensity of the data. It is often desirable to think of a random wave as a static or time invariant mean and a dynamic or fluctuating component superimposed on it. The mean square value is a measure of the fluctuating part.

The probability density function describes the probability that a certain wave amplitude will occur at any instant of time.

The autocorrelation function furnishes a criterion for the dependence

of the values of wave amplitudes at one instant of time on those at another.

The power spectral density function is a measure of the occurrence of dominant frequencies in a random wave.

Joint probability density, autocorrelation and power sprectral density functions for two or more random waves could also be desirable to describe a physical process.

4.4.2 Digital Analysis Procedures of a Random Wave

Let a continuous random record X(t) have a sample length T and be sampled at points Δt apart. See Fig. 4.5 .

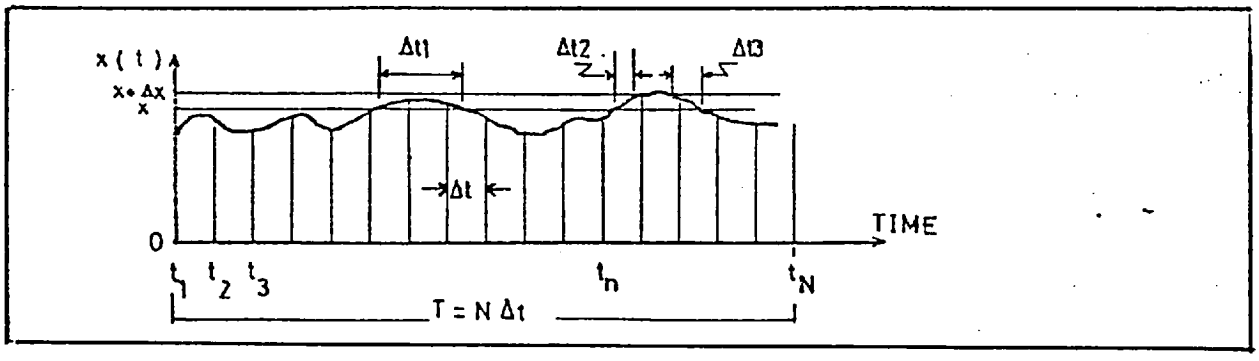


FIG. 4.5 , Sampling of a Continuous Record

The functions that statistically describe a random wave are now defined in a form suitable for digital computers.

1. Arithmetic Quantities

1.a The mean value

The sample mean value is given by:

$$\overline{X} = \frac{1}{N} \sum_{n=1}^{n=N} X_n \qquad \text{.....Eq. 4.4}$$

where n = 1,2,3 ..... N,

N is the number of data points and

X_n is the nth amplitude of the random wave.

1.b The standard deviation and the third moment

The sample standard deviation is given by

$$S_d = \left(\sum_{n=1}^{n=N} \frac{(X_n - \overline{X})^2}{N - 1} \right)^{\frac{1}{2}} \quad \text{..... Eq. 4.5}$$

The third moment of the data about the mean value is

$$\overline{X^3} = \left(\sum_{n=1}^{n=N} \frac{(X_n - \overline{X})^3}{N - 1} \right)^{1/3} \quad \text{..... Eq. 4.6}$$

2. The Probability Distribution Function

Consider the sample record X(t) illustrated in Fig. 4.5 . The probability that X(t) assumes a value within the range X and X + ΔX may be obtained by the ratio $\frac{T_x}{T}$, where Tx is the total amount of time that X(t) falls inside the range (X, X + ΔX) during an observation time T. ΔX is a small increment in X(t).

The ratio $\frac{T_x}{T}$ will approach an exact probability if T approaches infinity. In equation form:

$$\text{prob}(X < X(t) < X+\Delta X) = \lim_{T \to \infty} \frac{T_x}{T} \quad \text{..... Eq. 4.7}$$

The probability density function ρ(X) can be defined as:

$$\rho(X) = \lim_{\Delta X \to 0} \frac{\text{prob}(X < X(t) < X+\Delta X)}{\Delta X} = \lim_{\Delta X \to 0} \frac{1}{\Delta X} \lim_{T \to \infty} \frac{T_x}{T} \quad \text{..... Eq. 4.8}$$

Curves of ρ(X) vs X are called probability density curves while Prob(X < X(t) < X+ΔX) vs X are called cumulative probability distribution curves .

For digital computations, a sorting procedure is needed to assemble the amplitudes of a random wave X(t) in a descending order of magnitude.

The probability that a certain $X(t)$ is exceeded will be equal to the ratio of the rank order of $X(t)$ to the total number of data points.

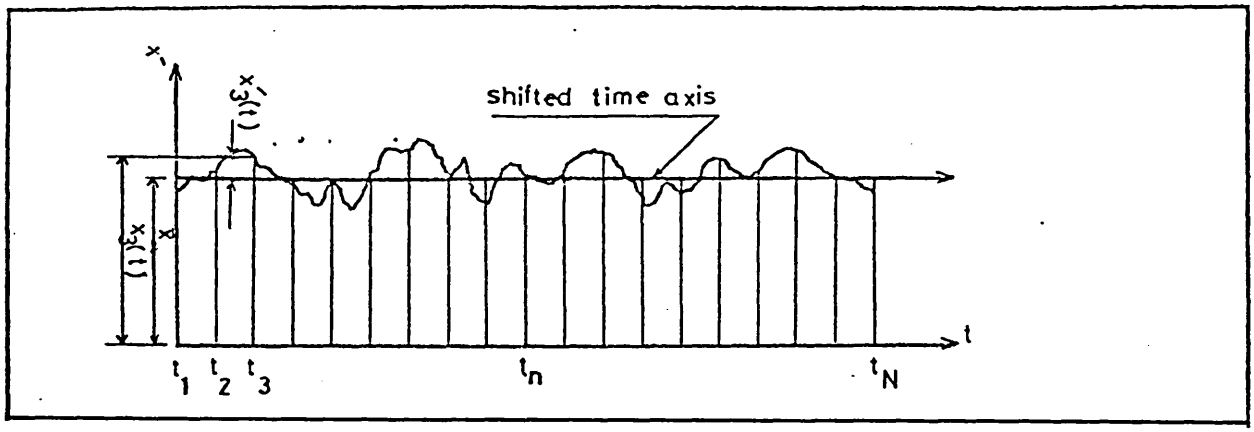


FIG. 4.6 , Sampling of a Stationary Random Record with a Zero Mean

3. The Autocorrelation Function; $R(r\Delta t)$

Take a random wave $X'_n(t)$ which is stationary and the time axis is shifted so as to let the mean value of $X'_n(t)$ equal zero, see Fig. 4.6 .

The autocorrelation function of this transformed wave may be obtained in the following way:

1. Compute the product of $X'_n(t)$ at times t and $t + r\Delta t$, where

   r varies from $0 \rightarrow M$, n varies from $1 \rightarrow N$,

   $r\Delta t$ is called the lag time and

   $M\Delta t$ is the maximum lag time

i.e. Compute $X'_n(t)\, X'_n(t + \Delta t)$, for r = 1

$X'_n(t)\, X'_n(t + 2\Delta t)$, for r = 2

$X'_n(t)\, X'_n(t + M\Delta t)$, for r = M

2. Sum up all N-r products for each lag time $r\Delta t$ and divide by the number of products N-r.

Hence, the autocorrelation function for r = 1 is:

$$R(1\Delta t) = \frac{1}{N-1} \sum_{n=1}^{n=N-1} X'_n\, X'_{n+1}$$

for r = 2:

$$R(2\Delta t) = \frac{1}{N-2} \sum_{n=1}^{n=N-2} X'_n X'_{n+2}$$

and for rth lag rime:

$$R(r\Delta t) = \frac{1}{N-r} \sum_{n=1}^{n=N-r} X'_n X_{n+r} \quad \text{..... Eq. 4.9}$$

where n = 1,2,3 ..... N

r = 0,1,2 ..... M

For zero lag time :

$$R(0) = \frac{1}{N} \sum_{n=1}^{n=N} X'^2_n \quad \text{..... Eq. 4.10}$$

Hence R(0) is equal to the mean square value of the transformed wave and is the maximum value of the autocorrelation function.

The autocorrelation function R(rΔt) could be normalized by dividing R(rΔt) by R(0). Hence ,the ratio $\frac{R(r\Delta t)}{R(0)}$ is called the autocorrelation coefficient and varies according to the following inequality:

$$-1 < \frac{R(r\Delta t)}{R(0)} < +1$$

A plot of rΔt vs $\frac{R(r\Delta t)}{R(0)}$ is called the autocorrelogram and is a measure of the dependence of one set of random wave amplitdues measured at time t on those measured at time t +rΔt.

4. The Power Spectral Density Function; G(f)

Consider the stationary random wave X'(t) which has a zero mean and is shown in Fig . 4.6 . The mean square value of the wave amplitudes in a frequency range f to f + Δf may be obtained by filtering the sample

record $X'(t)$ and computing the averages of the square of the filtered amplitudes. This average square value will approach an exact mean square value as the observation time T approaches infinity. In equation form:

$$\overline{X'^2}\,(f,\Delta f) = \lim_{T \to \infty} \frac{1}{T} \sum_{t=0}^{t=T} (X'^2(t,f,\Delta f)\Delta t$$

where $X'(t,f,\Delta f)$ is the portion of $X'(t)$ in the frequency range f to $f + \Delta f$.

For small Δf, a power spectral density function $G(f)$ may be defined such that:

$$\overline{X'^2}\,(f,\Delta f) = G(f)\Delta f$$

Hence

$$G(f) = \lim_{\Delta f \to 0} \frac{\overline{X'^2}(f,\Delta f)}{\Delta f}$$

$$= \lim_{\substack{\Delta f \to 0 \\ \Delta t \to 0}} \frac{1}{\Delta f} \lim_{T \to \infty} \frac{1}{T} \sum_{t=0}^{t=T} X'^2(t,f,\Delta f)\Delta t$$

An important property of the power spectral density function lies in its relationship to the autocorrelation function. Specifically, for a stationary random wave with a zero mean, the two functions are related by:

$$G(f) = 4 \int_0^{\infty} R(r\Delta t) \cos\{\pi \frac{nr\Delta t}{M\Delta t}\} d(r\Delta t) \quad \ldots\ldots\ldots\ldots \text{Eq. 4.11}$$

For purposes of numerical analysis, using the trapezoidal rule for integration, equation 4.11 can be rewritten (following the procedure of Blackman and Tukey (1959) as:

$$G(f) = 2\Delta t\left(R(0) + 2\sum_{r=1}^{r=M-1} R(r\Delta t)\cos\frac{rn\pi}{M} + R(M\Delta t)\cos n\pi\right) \quad \text{.... Eq. 4.12}$$

where $n = 0,1,2 \ldots\ldots M$

$r = 1,2,3 \ldots\ldots M$

$G(f)$ in equation 4.12 is the raw estimate of the power spectral density function. To obtain a better power spectral estimate at any frequency, a simple smoothing operation is performed. Better power spectral estimate in this context means to account for the inaccuracies of expressing $G(f)$ in terms of discrete values at the corresponding frequencies.

Blackman and Tukey (1959) reported that a smoothing operation could be done in the following way:

$$\begin{aligned} G(0) &= 0.54\ G(0) + 0.46\ G(1) \\ G(f) &= 0.23\ G(f-1) + 0.54\ G(f) + 0.23\ G(f+1) \quad \text{..... Eqs. 4.13} \\ G(M) &= 0.46\ G(M-1) + 0.54\ G(M) \end{aligned}$$

This smoothing operation is referred to as the Hamming procedure.

The maximum frequency (f_{max}) that can be investigated in a random wave is a function of Δt, hence

$f_{max} = \frac{1}{2\Delta t}$, f_{max} is called sometimes the folding frequency.

The lowest frequency obtainable is theoretically:

$$f_{min} = \frac{1}{N\Delta t}$$

But, because only one cycle is measured the estimation of $G(f_{min})$ is not accurate. Probably, a more practicable limit is $\frac{2}{N\Delta t}$.

On the other hand, if frequencies greater than f_{max} are present, the function $G(f)$ for frequencies slightly less or equal to f_{max} would be magnified. This phenomenon is referred to in spectral analysis as "folding".

Therefore, for a 5 sec record, sampled at 0.025 sec intervals, the frequency range that could be reliably detected would probably be:

$$0.8 \text{ HZ} < f < 15 \text{ HZ} .$$

4.5 Stability of a Sphere

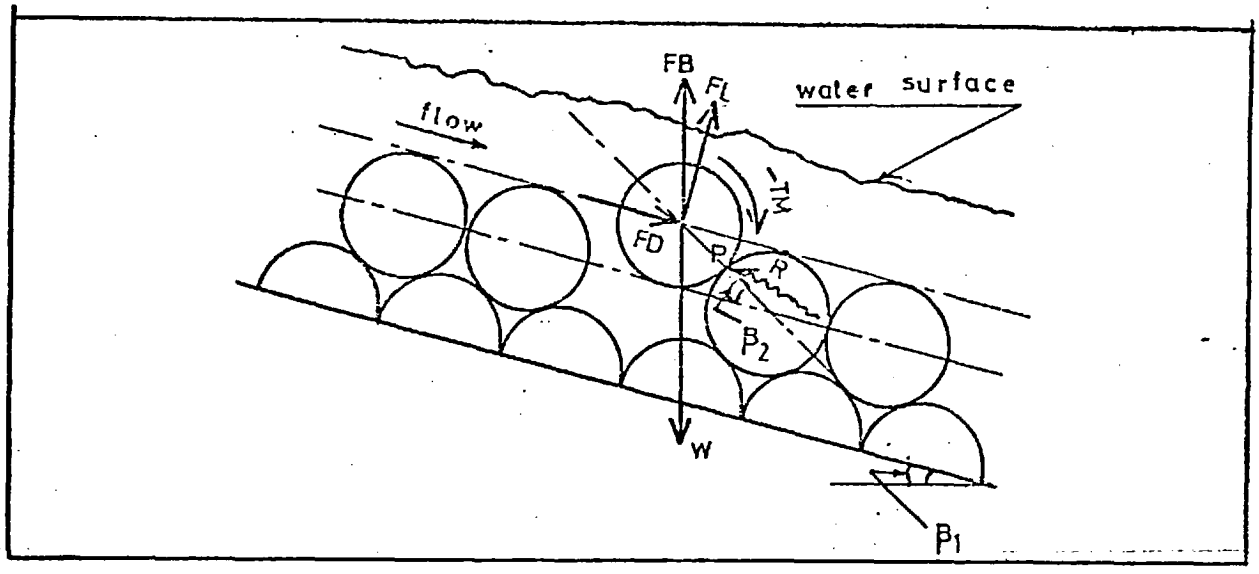


FIG. 4.7 , Forces Acting on a Loose Sphere

Consider a loose sphere of diameter D and mass density ρ_s. The loose sphere is part of a closely packed bed of fixed spheres of the same diameter. See Fig. 4.7 . Let the channel bed make an angle β_1 with the horizontal and the channel be considered wide (say the width of the channel $>$ 10D).

Investigate now the response of the loose sphere to a supercritical stream of water which is steady. The forces acting on the loose sphere are:

FD, FL, TM, W, F_B and R

where $W = g\rho_s \frac{\pi}{6} D^3$

$F_B = g\rho \frac{\pi}{6} D^3$, ρ is the mass density of water

R is an unknown reaction force from the fixed spheres

FD, FL and TM are as previously defined in equations 4.1, 4.3 and 4.2 respectively.

Assume as a result, the loose sphere will roll over the next fixed sphere downstream with an angular acceleration a.

The sum of moments of all the forces about a contact point P is:

$$\frac{D}{2} FD \sin \beta_2 - \frac{(\rho_s-\rho)}{\rho_s} W \frac{D}{2} \cos (\beta_1+\beta_2) + \frac{D}{2} FL \cos \beta_2 - TM$$

where β_2 is the instantaneous angle that the line joining the centres of the loose sphere and the one fixed downstream makes with the original channel bed. See Fig. 4.7 .

The angular momentum of a sphere rolling on another with an angular acceleration a is:

$I\,a + m \frac{D^2}{4} a$, where I is the moment of inertia of a sphere about its diameter.

$I = \frac{2}{5} m \frac{D^2}{4}$, where m is the mass of the sphere.

Hence the angular momentum of the sphere is:

$$\left(\frac{2}{5} m \frac{D^2}{4} + m \frac{D^2}{4} \right) a = \frac{7}{5} m \frac{D^2}{4} a$$

For a sphere accelerating in a stream of water, an extra resistance is encountered due to the need to accelerate some water particles around the sphere. This extra resistance is usually referred to as the added mass.

In an infinitely deep and irrotational flow, Valentine (1969) evaluated the added mass term for a sphere moving with constant speed in an otherwise stationary fluid. For such an ideal flow picture the added mass $m' = \frac{1}{2} M_w$, where M_w is the mass of the water displaced by the sphere.

The presence of a rough bed near the sphere increases m' while the presence of a close free surface decreases it. Hence it was simply assumed for this investigation that $m' = \frac{1}{2} M_w$.

Equating the moment of all forces acting on the sphere to the angular momentum (adjusted for m') one obtains:

$$\frac{D}{2} FD \sin\beta_2 - \frac{\rho_s-\rho}{\rho_s} W \frac{D}{2} \cos(\beta_1+\beta_2) + \frac{D}{2} FL \cos\beta_2 - TM = \frac{7}{5}(m+m') \frac{D^2}{4} a$$

Solving for a:

$$a = \frac{20}{7(m+m')D}\{\tfrac{1}{2}FD \sin\beta_2 + \tfrac{1}{2}FL \cos\beta_2 - (\rho_s-\rho) \frac{g\pi D^3}{12} \cos(\beta_1+\beta_2) - \frac{TM}{D}\}$$

.....Eq. 4.14

The stability of the loose sphere could be statistically described as follows:

1. Compute the instantaneous angular accelerations a of the sphere using equation 4.14 .
2. Compute the cumulative probability distribution function for a.
3. Estimate the stability of the particle as the probability that $a \leqslant 0$.

CHAPTER 5

Experiments and Discussion of Results of Stage II

5.1 Scope of Experiments

The scope of experiments in Stage II of the research consists of the following aspects:

1. Modify the existing flume used for Stage I and build a bed of spheres as was shown in Fig. 4.1 a and b.

2. Design a force transducer and calibrate it.

3. Measure the instantaneous drag, lift and torque on a sphere for 24 different hydraulic conditions including different volumetric discharges, channel slopes and sphere protrusions (see Table 5.1).

4. Determine experimentally the critical stream power that will just dislodge a loose sphere. Four different channel slopes and three sphere protrusions are investigated.

5.2 Modification of Existing Flume

The only modification to the flume described previously in Chapter 3 was to line the flat channel bed with one layer of wooden hemispheres glued in a hexagonal pattern. Another layer of spheres of the same diameter (5.1 cm) and hexagonal packing was glued on top of the layer of hemispheres. See Fig. 4.1 a and b and Plate 4 . Three spaces were left in the top layer of spheres along the centre line of the flume where each space accommodates one sphere of diameter 5.1 cm.

The three spaces left allowed flexibility in changing the longitudinal location of either the instrumented sphere for the purpose of force measurements or the loose sphere for the purpose of the critical stream power measurements.

5.3 Description of Force Transducer

5.3.1 Choice of Dimensions

The force transducer consists of a cantilever beam OAA'BC bent at a 90^{o} angle at point B. See Plate 7. Fig. 5.1 shows the dimensions of the cantilever beam with the locations of the straingauges. The test sphere was glued to the threaded part OA of the circular rod OA''. The test sphere itself was made of a very light material (polystyrene) with mass density of 0.059 gm/cm^{3}.

The following considerations have led to the development of the force transducer.

A. Part A''BC of the cantilver is bent at point B to allow isolation of F_D, TM and FL according to the theory presented in article 4.2. The width of the cantilver beam was chosen to be 1.5 cm and was dictated mainly by the dimensions of the strain gauges. The thickness of the beam and the longitudinal dimensions A''B and BC were a compromise between a transducer with a high natural frequency and that where the stresses induced by the stream are large enough to be measured.

B. The test sphere is suspended from a fixed point C above the water surface. To offer the least resistance to the flow, part OAA'A'' of the cantilver was chosen as a circular rod 5 mm in diameter. Part OA was threaded so as to secure better bond between the polystyrene sphere and the circular rod. An equally important factor that decided what length and diameter the circular rod should be was to maintain a high natural frequency of the force transducer as a whole.

5.3.2 Strain Gauges

A. Specifications

Wire resistance strain gauges were used. They were manufactured

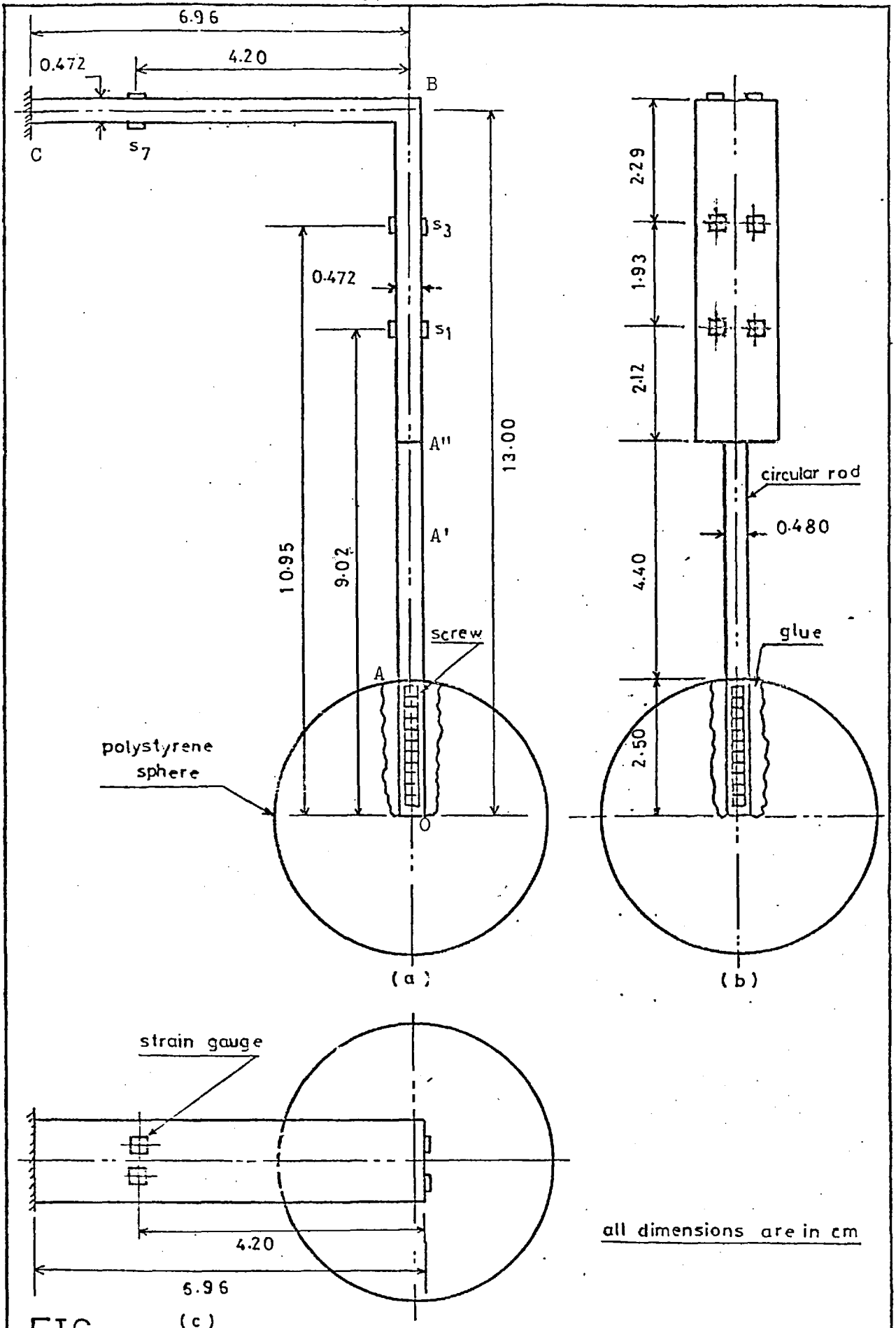


FIG. 5.1 a,b & c. Dimensions of force transducer. (a) Profile. (b) Side view. (c) Plan

by Micro-Measurement, Romlus, Michigan, U.S.A. and their type is EA-06-125MG-120. Each straingauge has a resistance of 120.0 $\pm$ 0.2% ohms, a gauge factor (which is defined as the ratio of the percentage change in resistance to the strain) of 2.085 $\pm$ 0.5%, a strain limit of 5%, a temperature range of -75°C $\rightarrow$ 205°C, a length of 3.2 mm and a fatigue life of 10^8 cycles at $\pm$ 1200 microstrains.

Kock et al (1952) have provided a concise but comprehensive description of the techniques of measuring bending stresses by wire strain gauges. The techniques followed in cementing the strain gauges to the cantilever and water-proofing them are similar to those recommended by Kock et al (1952). Plate 8 is a close view of the force transducer showing the strain gauges glued and water-proofed.

B.Wiring Diagrams

To measure the stress at a point in a simple cantilever due to a load p (see Fig. 5.2a), a straingauge T could be glued to the top fibres of the cantilver and the increase in resistance in the gauge will be proportional to the strain induced by the load. If the material of the cantilever is not stressed beyond the elastic limit, the strain will be directly proportional to the stress there. The change in resistance in the gauge will be proportional to the potential difference ΔE_1 measured in the circuit shown in Fig. 5.2b . Where R ,R are two equal and unstressed resistances, T is the stressed straingauge and R_s is a dummy gauge of equal resistance to T but is glued to an unstressed piece of the same metal as that of the cantilever.

The circuit shown in Fig. 5.2c gives a potential difference $\Delta E_2 = 4\Delta E_1$. Where T and C represent straingauges in equal tension and compression respectively.

Three circuits like that shown in Fig. 5.2c were wired up to measure

the stress at three different cross-sections S_1, S_3 and S_7 in the cantilever beam. See Figures 5.1a, b and c and Plates 7 and 8.

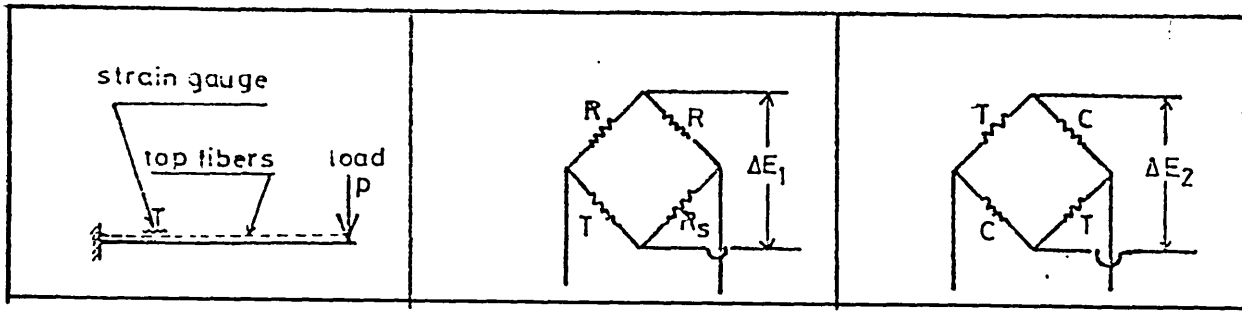


FIG. 5.2a Loading Diagram

FIG. 5.2b One-armed Bridge

FIG. 5.2c Four-armed Bridge

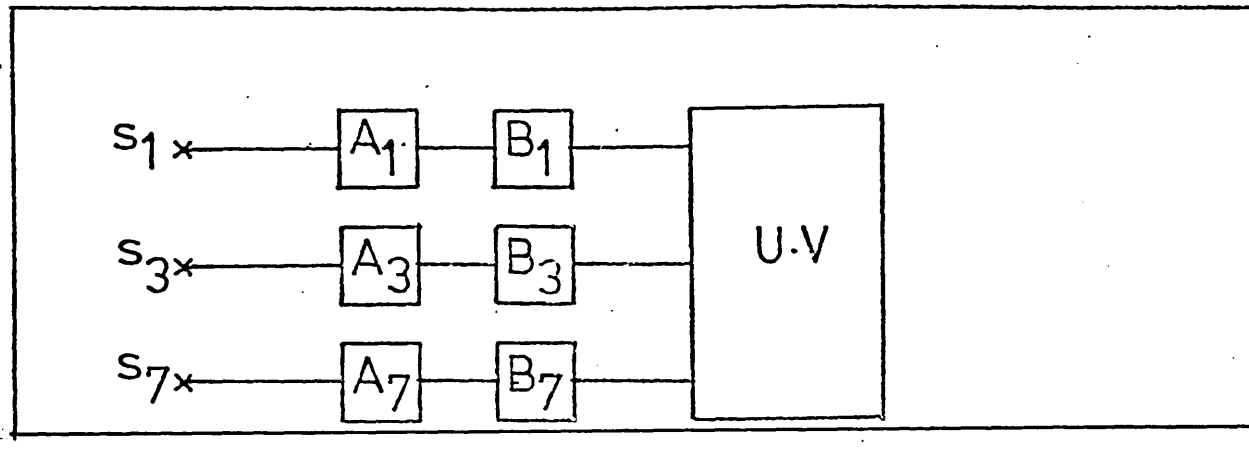


FIG. 5.3 , Block diagram of electronic set-up

5.3.3 Block Diagram of Electronic Set-Up

Fig. 5.3. is a block diagram of the electronic set up used to measure the stresses simultaneously at cross-sections S_1, S_3 and S_7 in the cantilever shown in Figs.5.1a, b and c. In Fig. 5.3 , A_1 is a San Gamo amplifier (manufactured by West Control Ltd., England), while A_3 and A_7 are identical and synchronized 581 DNH amplifiers (manufactured by Automation Industries, Holland). B_1, B_3 and B_7 are 3 independent buffer circuits of resistors connected upstream of a multi-channel ultra violet recorder (type 1185, manufactured by New Electronic Products, England).

A simultaneous record of S_1, S_3 and S_7 was obtained by selecting an optimum range of amplifier sensitivity for each of the three signals. A paper speed of 10 cm/sec was selected so as to obtain clear records with peaks and troughs that can be identified visually.

5.3.4 Natural Frequency

The natural frequency of vibrations of the force transducer shown in Fig.5.1a, b and c and Plate 7 was measured both in air and water in the following way:

In air, a small impulsive force was applied to the sphere which is an integral part of the force transducer. The variation of stress at a cross-section (say S_1) in the cantilver was measured by a U.V. recorder and a typical record of the decay of free vibrations in air is shown in Fig. 5.4a . Since the speed of the paper in the U.V. recorder was 10 cm/sec and the number of peaks counted in each cm is 16, then the natural frequency of the transducer is 160 cycles/sec.

Similarly, the natural frequency of the transducer when the sphere was wholly immersed in still water was also measured and a typical record is shown in Fig. 5.4b . Although the decay of vibrations is not as smooth as in the case of air (this is due to the reflections of water from the side walls of a 30 cm x 30 cm x 30 cm container), the natural frequency in still water is observed to drop to 70 cycles/sec.

5.3.5 Static Calibration of Force Transducer

Each four-armed bridge of cross-sections S_1, S_3 and S_7 (see Fig.5.1a, b and c) was statically calibrated in the following way:

The force transducer was clamped by a vice in the position shown in Fig. 5.5a . A mass of 200 gm was suspended by a light string at a distance L_1 from the centre line of the circular rod and the bending

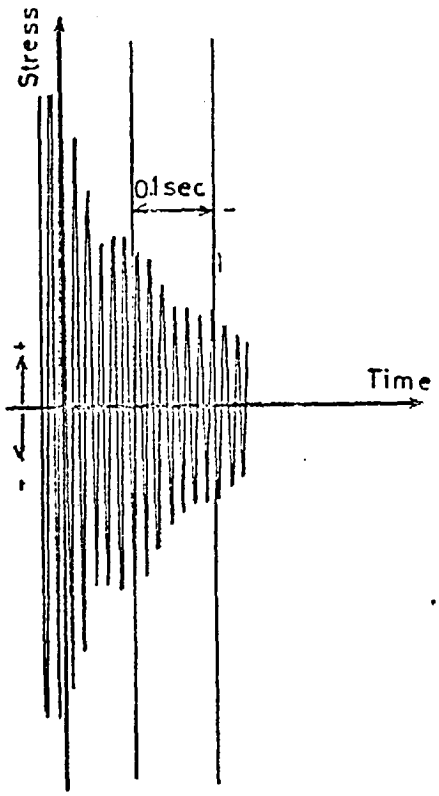


FIG. 5.4b,
Free vibrations of force transducer in water; f_n=70 HZ

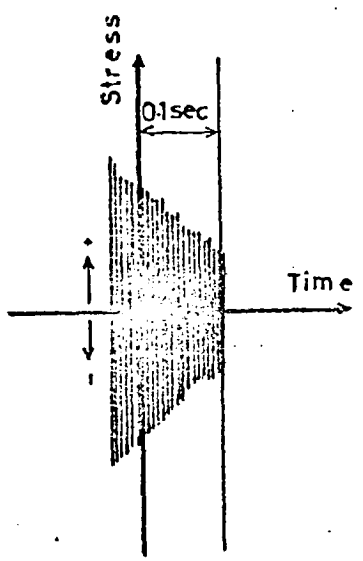
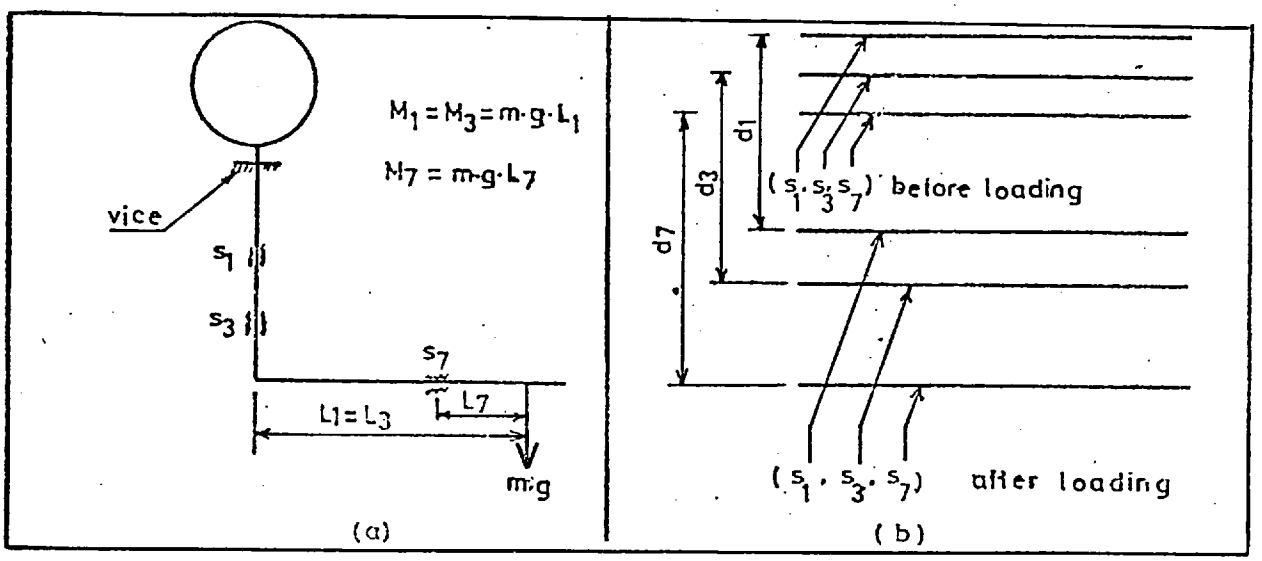


FIG. 5.4a , Free vibrations of force transducer in air; f_n=160 HZ.

moment at each point S_1, S_3 and S_7 was calculated. The three amplifiers A_1, A_3, A_7 and the ultra violet recorder were switched on and a short record of the stress at points S_1, S_3 and S_7 was recorded before and after the 200 gm mass was suspended (see Fig. 5.5b). The deflections d_1, d_3 and d_7 of the signals S_1, S_3 and S_7 on the U.V. recorder paper were related to the bending moments M_1, M_3 and M_7 respectively. The same experiment was repeated for different masses suspended and the calibration constant for each four-armed bridge was found practically constant. Sample calibration constants for signals S_1, S_3 and S_7 are shown in Fig. 5.6 .



FIGS. 5.5a & b , Static calibration of force transducer
(a) Loading diagram
(b) Deflections of signals S_1, S_3 & S_7 after loading

5.4 Experimental Procedure

5.4.1 Simultaneous Records

After the four-armed bridges at cross-sections S_1, S_3 and S_7 (see Fig.5.1) were statically calibrated, the force transducer was positioned so that the polystyrene sphere was suspended in positions A', B' and C' in Fig.5.12 . Hence, the polystyrene sphere was not touching any of the fixed spheres around it. The protrusion of the polystyrene sphere above the bed was measured as the normal distances from the centre of the

polystyrene sphere in positions A', B' and C' in Fig. 5.12 to the line joining the centres of fixed spheres.

Before any water was allowed to flow in the flume, the datum lines of signals S_1, S_3 and S_7 were recorded on the U.V. recorder paper. A steady volumetric discharge was then maintained in the flume and the three signals S_1, S_3 and S_7 were simultaneously recorded. The speed of the U.V. recorder paper was always kept at 10 cm /sec. If the three signals intersected one another or any of them occurred outside the 30 cm wide recording paper, the sensitivity of the signals was adjusted by choosing a coarser micro-strain range on the amplifiers.

Fig. 5.6 shows a typical simultaneous record of the stresses (hence the bending moments) at sections S_1, S_3 and S_7 for the hydraulic conditions of record number 16, Table 5.1.

The length and number of records was dictated by the following factors:

1. To expose the polystyrene sphere to a sufficient number of hydraulic conditions so as to include different discharges, channel slopes and sphere protrusions.

2. Not to consume a prohibitive amount of recording paper (in the U.V. recorder), computer time and computer cards.

3. To record for long enough, so that the statistical functions (such as mean values, standard deviations etc.) computed from such records would not be much different (within 1 to 2% difference) from those obtained from very long records. Preliminary calculations performed on data obtained from record number 6 , showed that the statistical functions discussed in Chapter 4 of the variables FD , FL and TM, varied only 1% or less when the length of the record varied from 10 seconds to 5 seconds. The sampling time interval was kept always as 0.025 seconds. Hence it was decided that 200 sampling points at 0.025 second intervals are sufficient for the statistical analysis of the data.

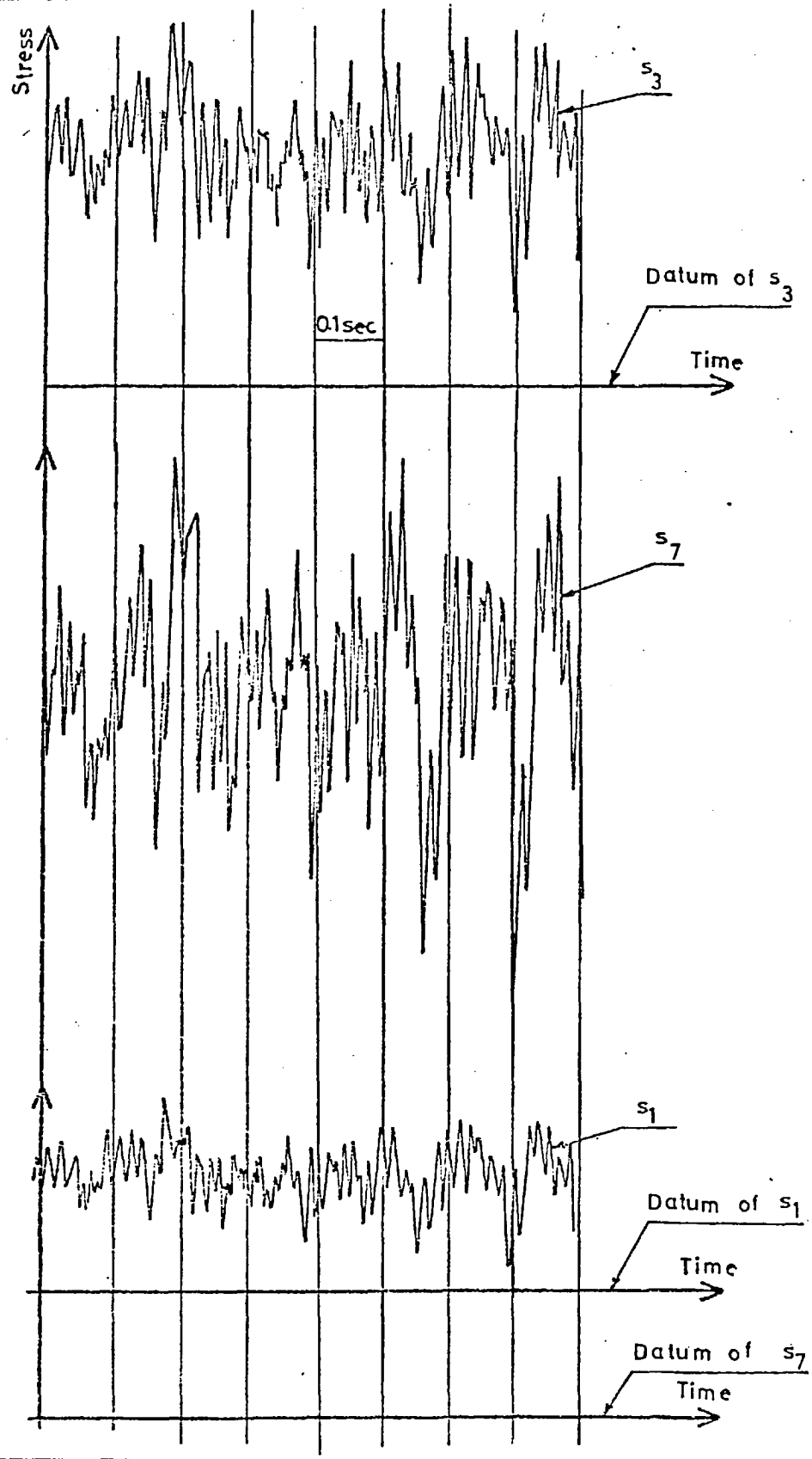


FIG. 5.6 , Simultaneous records of s_1, s_3 & s_7

Vertical scales

1 cm of s_1 = 223 x 981 dynes-cm

1 cm of s_3 = 143 x 981 dynes-cm

1 cm of s_7 = 84 x 981 dynes-cm

Finally, it should be mentioned that preliminary records (not included in this thesis) similar to those shown in Fig. 5.6 were taken when the polystyrene sphere was removed from the force transducer. Such measurements demonstrated that the hydrodynamic forces on the 0.5 cm diameter, 6.9 cm long circular rod (see Fig. 5.1) are negligible compared to those acting on the 5.1 cm diameter test sphere.

5.4.2 Digitization and Filtering of Simultaneous Records

An x-y digital reading equipment (type Z.A.E.I.B., manufactured by P.C.D. Limited, England) was used to puch on cards the simultaneous amplitudes of the three records S_1, S_3 and S_7. A constant sampling time step of 0.025 sec was dictated by the minimum horizontal step of 2.5 mm that the x-y reader could digitize. The length of each record was 5 seconds, hence 200 time steps were digitized for each signal.

Visual inspection of the simultaneous records shows the following features:

(i) The thickness of the datum lines in Fig. 5.6 is originally in the order of 0.2 to 0.3 cm and the frequency of the datum line signal varies between 40-50 cycles/sec superimposed on a very dense signal. A straight horizontal line was drawn in the middle of this thick signal and was considered to be the line of zero stress for the signal under consideration.

(ii) The simultaneous records S_1, S_3 and S_7 contain a predominant frequency of 40-50 cycles/sec. This feature was thought to be due to the following factors:

1. Electronic noise is superimposed on the true response of the force transducer.
2. Vibrations from the laboratory pumps and the tumbling water in the laboratory sumps may be picked up by the

force transducer.

3. There could have existed some high frequency components in the stream turbulent forces (acting on the test sphere) that are well tuned to the natural frequency of the force transducer to produce some amplification in the recorded stress signals.

Based on the above mentioned observations and discussion, it was decided to adopt a digital filtering technique to remove the above mentioned 40-50 cycles/sec amplifications in the raw records. When digitizing a record, a line midway between the high frequency peaks and troughs was followed with data punched on cards at 0.025 sec intervals as shown in Fig. 5.7 .

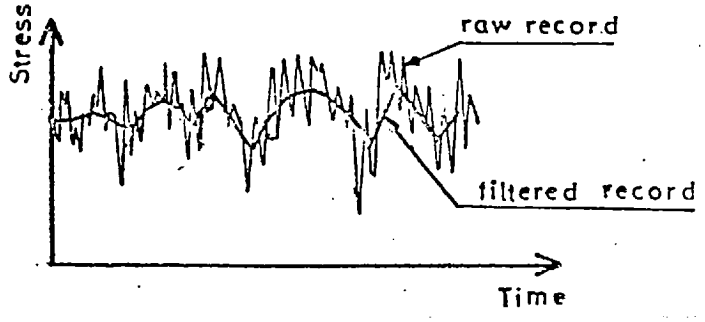


FIG. 5.7 , Digital filtering of a record

5.4.3 Experiments on the Initial Instability of a Loose Sphere

The force-measurement programme of tests was supplemented by a series of experiments to determine the critical stream power that will just dislodge a loose sphere of mass density 2.65 gm/cm^3 and diameter 5.1 cm. The loose sphere was placed in one of the test holes left in the top layer of fixed spheres (see Fig 4.1 a and b). The test holes were located along the centre line of the flume and at distances 66.25,

110.42 and 154.58 cm respectively downstream of the leading edge of the flume. The protrusion of the sphere was varied by placing 4 cm by 4 cm square steel plates on the bottom of the test hole. The thickness of each plate was 0.6 cm , hence, by placing one, two or three square plates on top of each other the loose sphere was exposed 0.6, 1.2 and 1.8 cm respectively.

The critical stream power was determined experimentally in the following way:

1. The channel slope was set in turn at 6.8%, 15.82%, 23.32% and 35.0%.

2. For each channel slope, the test sphere was placed in the test hole with a known exposure and the volumetric discharge was gradually increased (increments of 1000 cm^3/sec within a period of 1 minute) until the loose sphere was first dislodged by the stream. The discharge was decreased again 3 → 5 litres/sec below the lowest one that dislodged the sphere in 1 minute. Finally, smaller increments (500 cm^3/sec) of the discharge for a period of 10 minutes were maintained until the sphere was dislodged for a particular discharge called the critical discharge. The critical stream power was then calculated according to equation 2.1 .

Similar experiments were conducted for each of the channel slopes, sphere protrusions and longitudinal locations of the test holes above.

5.5 Experimental Results and Discussion

5.5.1 Force Measurements

Three computer programs (see Appendix II) were written to compute and plot the following statistics of the drag (FD), turning Moment (TM) and lift (FL) acting on the instrumented sphere.

1. The instantaneous values according to equations 4.1, 4.2 and 4.3 respectively; the mean value according to equation 4.4 and the standard deviation according to equation 4.5 .

2. The cumulative probability distribution according to equation 4.7 and the skewness of distribution according to equation 5.1 .

3. The autocorrelation and power spectral density functions according to equations 4.9 and 4.13 respectively.

The hydraulic parameters under which the experiments were conducted are summarized in Table 5.1.

It should be mentioned that Figs.5.8,5.14,5.15 and 5.16 in the following articles correspond to the hydraulic conditions of record No.16.

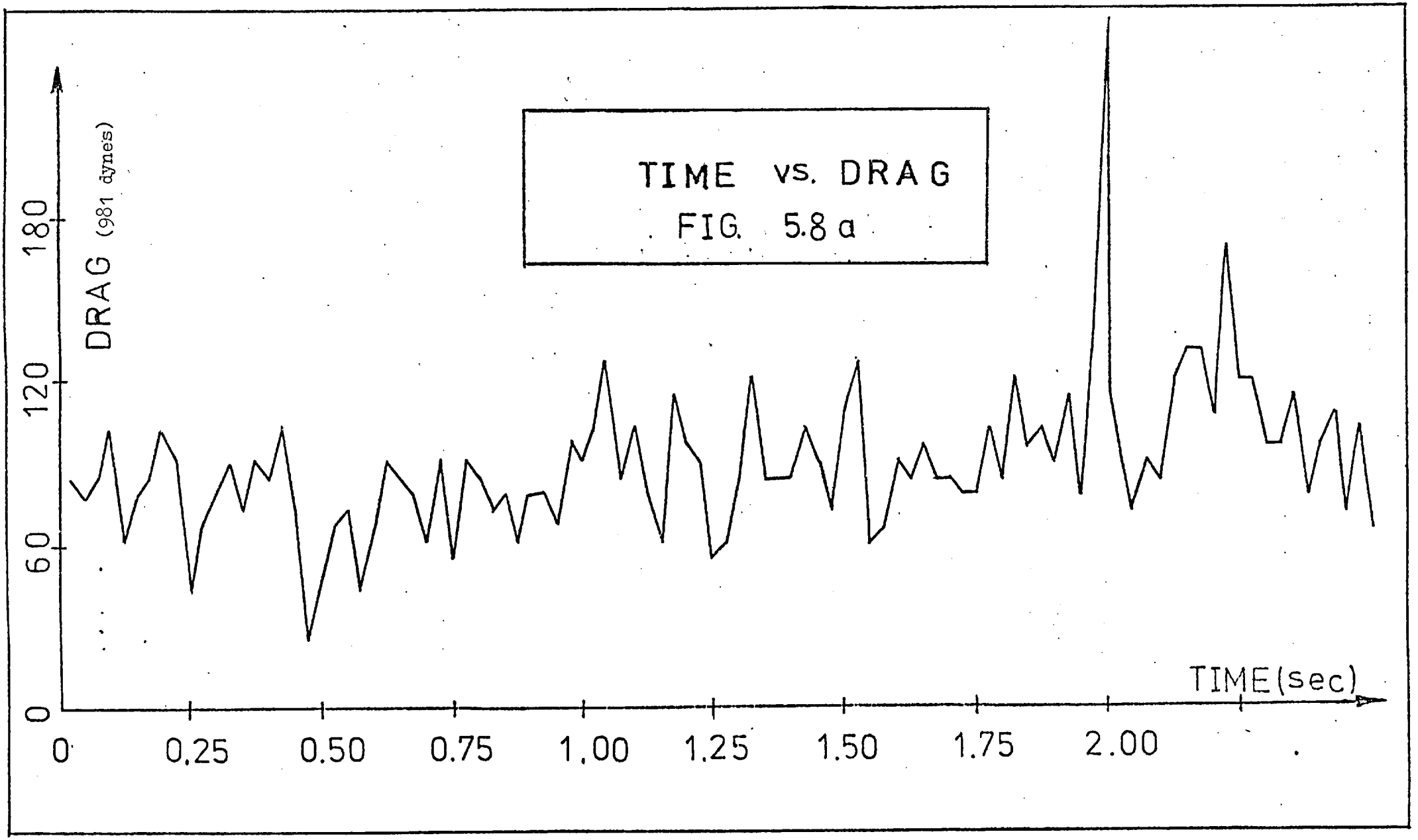
5.5.1.1 Instantaneous Values of FD, FL and TM

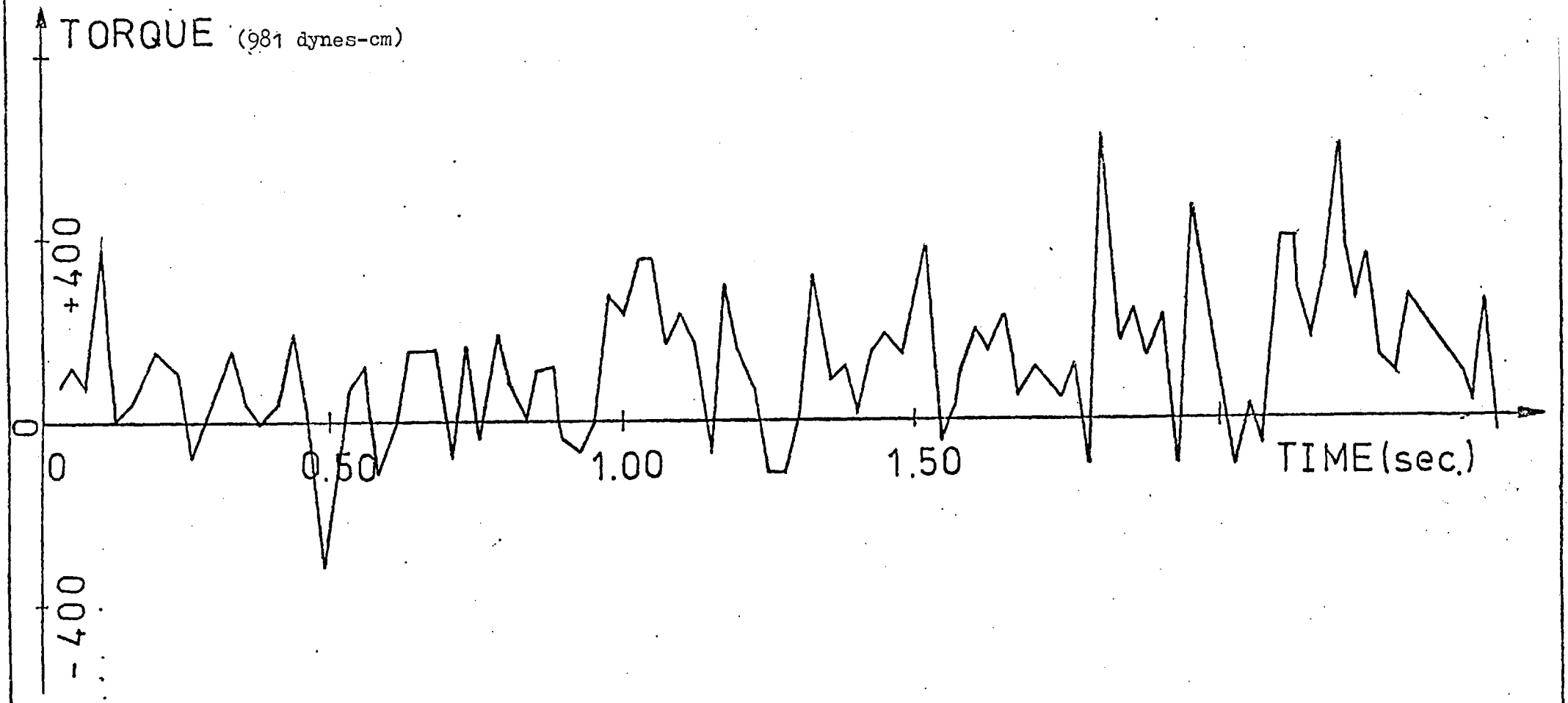
Figures 5.8a,b and c show sample plots of the instantaneous and simultaneous values of FD, TM and FL respectively. A distinct feature common to all these plots is that the instantaneous fluctuations are large as compared to the mean value. An average frequency of fluctuation of 13 cycles/sec is also common. The peaks and troughs in each of Figs. 5.8a, b and c show some correspondence to those in the other two. This feature cannot be generalized, however, as a dominant characteristic of all instantaneous force plots for the rest of the records in Table 5.1, and hence no conclusion may be drawn about the correlation between the fluctuations in drag, lift and moment.

5.5.1.2 Mean Values and Standard Deviations

5.5.1.2.1 Drag

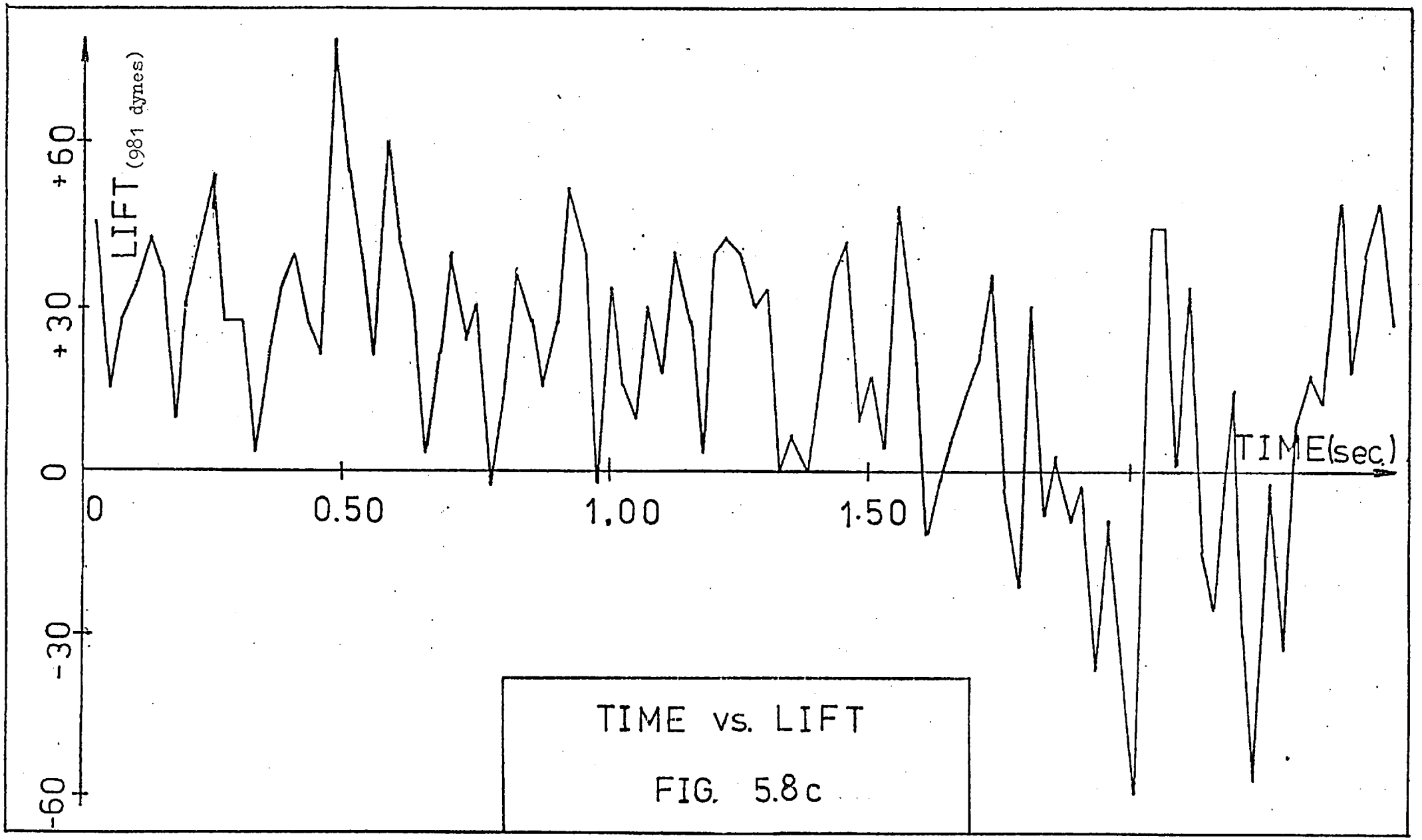
Figures 5.9a,b and c are plots of the mean drag force ($\overline{FD}$) as ordinates and the stream power per unit area of channel bed Ω as abscissa. The sphere protrusions for the three figures are 2.84, 3.84 and 4.84 cm respectively. One standard deviation above and one


TIME vs. DRAG
FIG. 5.8 a
DRAG (981 dynes)
180
120
60
0
TIME(sec)
0
0.25
0.50
0.75
1.00
1.25
1.50
1.75
2.00



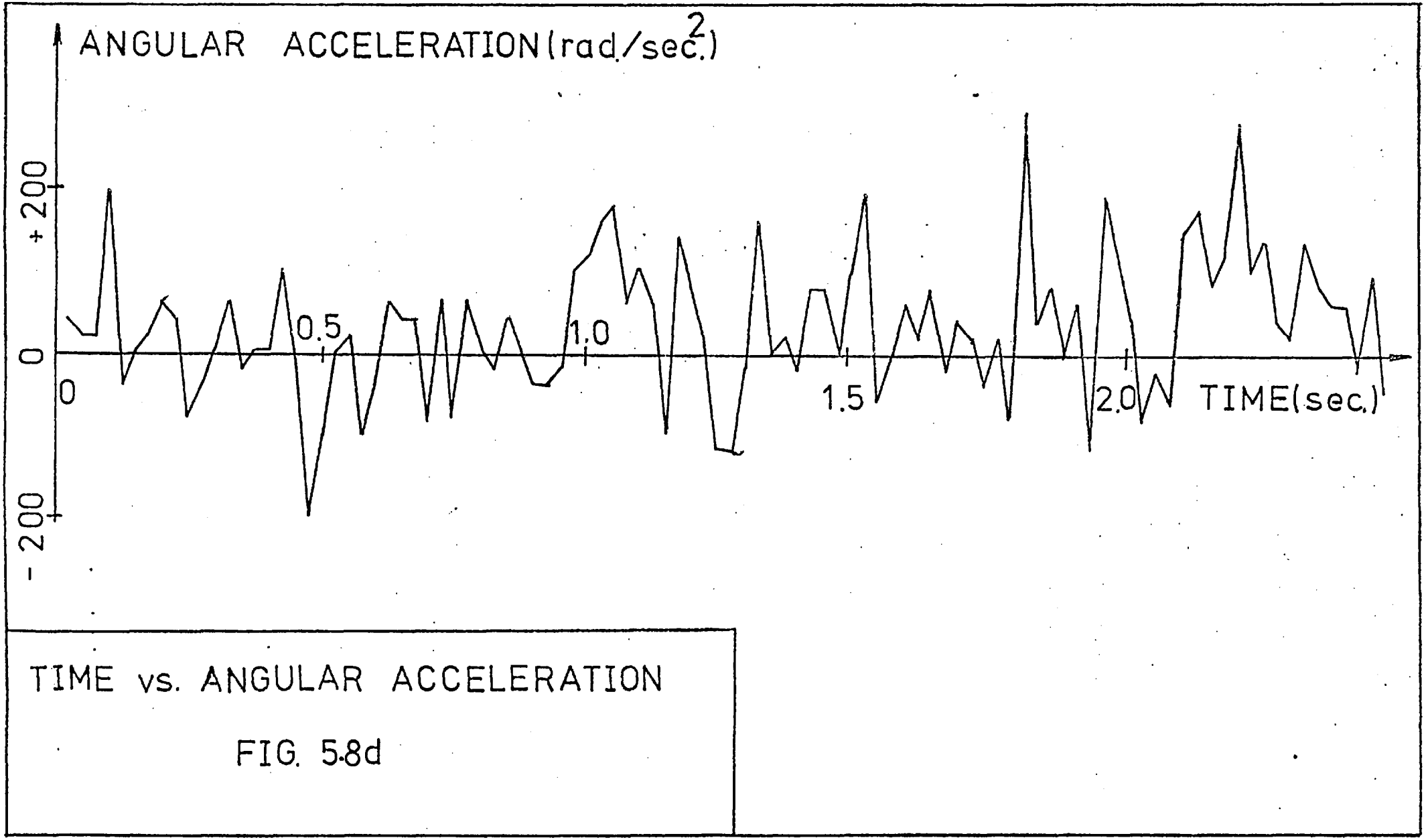
TIME vs. TORQUE

FIG. 5.8 b



TIME vs. LIFT

FIG. 5.8c



TIME vs. ANGULAR ACCELERATION

FIG. 5.8d

below the mean values are also shown for each experimental run.

Figures 5.9a,b and c show the following features:

1. The mean drag force on a sphere in a supercritical shallow stream increases with stream power. Such a trend could be attributed to the following reason:

Part of the supercritical stream acts as an impact jet on the test sphere. The impact force is equal to the rate of change of momentum in the jet. Since greater stream powers are associated with greater mass flow rates of water and greater stream velocities, the trend of $\overline{FD}$ increasing with Ω becomes supported by classical physical reasoning.

2. It is noticed that the increase in $\overline{FD}$ due to increasing Ω values is not a smooth one. The scatter in the $\overline{FD}$ - Ω figures could be attributed to the mean value being unrepresentative of a long time average. On the other hand, the reason for so much scatter could be due to the presence of a randomly distorted water surface (see Plate 6) that is near enough to affect the pressure distribution on the surface of the sphere. The formation of a turbulent wake with pockets of air entrained into it from the atmosphere, adds yet another factor that increases the scatter of a mean drag force for increasing stream powers. Another reason - and perhaps a likely one - is that there may be instrumental and measurement errors that are systematic in a particular run (giving a general upward or downward bias in that run) but which vary from one run to the next (see section 5.5.2).

3. The ratio of the standard deviation of the drag force $(Sd)_{FD}$ to the mean value $\overline{FD}$ varies from 0.21 to 0.55 for 21 out of 24 experimental runs (see Table 5.1). Only records number 9, 10 and 11 have $\frac{(Sd)_{FD}}{\overline{FD}}$ equal to 2.02, 0.945 and 1.414 respectively.

4. Comparison of Fig. 5.9c with Figs. 5.9a and b shows that greater protrusions of the polystyrene sphere weakly decreases the mean drag force. This feature could be attributed to the reduction in form

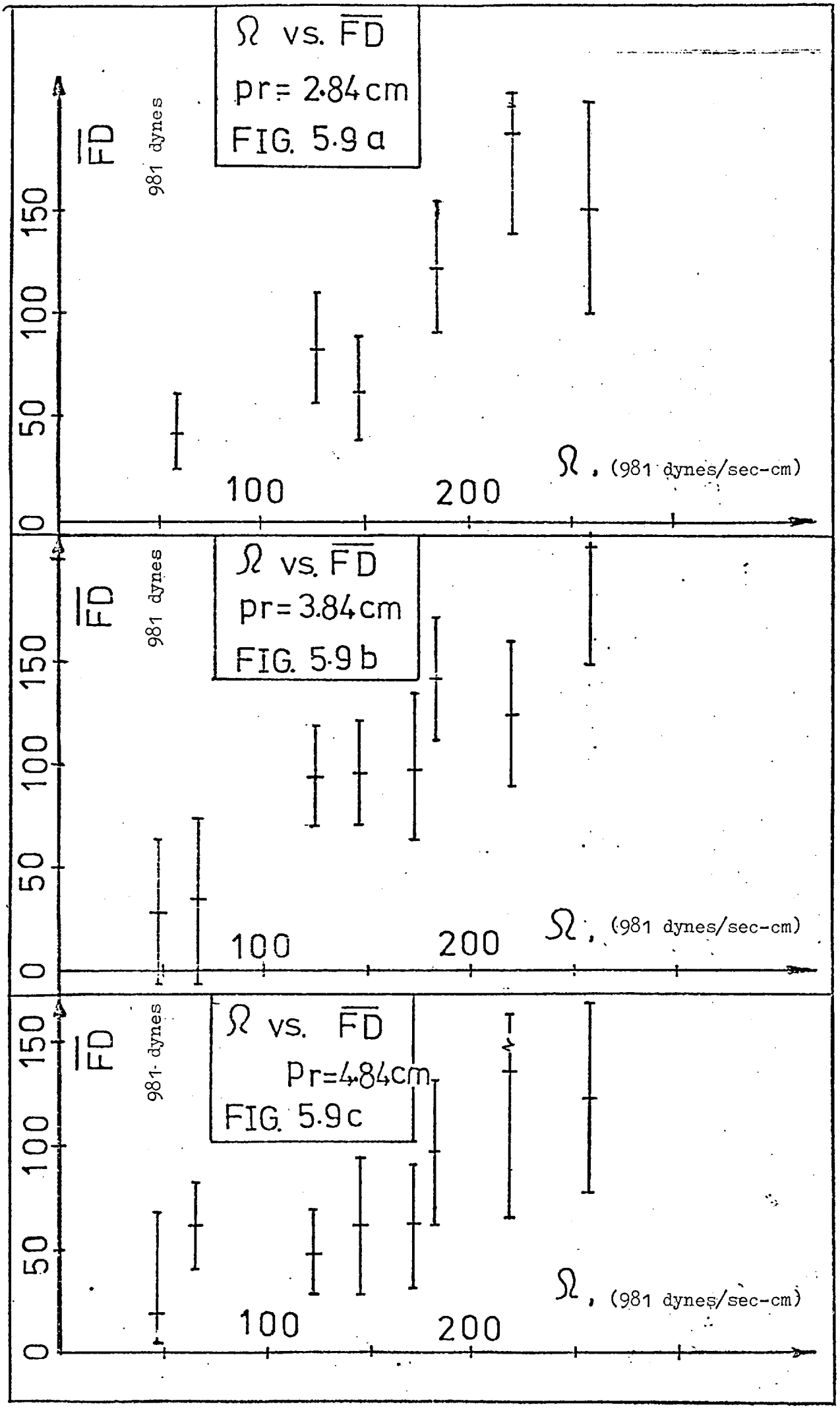
drag as a result of pressure build up in the wake of a sphere placed in shallower and shallower streams. In other words, as the sphere is more and more exposed to the stream, there will be thinner and thinner sheets of water flowing over the downstream half surface of the sphere. But, such thin sheets of water are moving slower than the fast coming water hitting the test sphere. Probably, the result is that a region of high pressure is created on the downstream half surface of the sphere relative to a low pressure region on the upstream half surface.

5.5.1.2.2 Lift

The mean hydrodynamic lift force $\overline{FL}$ (after deducting the buoyancy force according to equation 4.3) varies with Ω in a completely different way as compared to $\overline{FD}$. For a sphere protrusion of 2.84 cm , Fig. 5.10a shown a predominant positive $\overline{FL}$ with increasing Ω. There is no obvious trend that $\overline{FL}$ increases with increasing Ω.

When the test sphere is exposed 3.84 and 4.84 cm respectively, Figs. 5.10 ,b and c show a distinctly negative $\overline{FL}$ with increasing Ω. A mean lift force is created by the pressure difference between the distributions of pressures below axis x-x' and above it of the sphere shown in Fig. 1.3. For small sphere protrusions, the mean lift force is approximately constant with increasing Ω,because there are two counter balancing effects: (i) the prevalence of high velocities above axis x-x' tend to create higher lift on the upper surface of the sphere; for greater channel slopes (hence, greater Ω for the same discharge), the flow becomes shallower and a greater proportion of the flow finds its way between the voids of the bed of spheres and hemispheres, tending to create a lower pressure on the lower surface.

For greater sphere protrusions, a large portion of the flow passes underneath the exposed sphere at a high velocity; while the water that passes over it is shallow, piling up to form a hump and hence creating


Ω vs. $\overline{FD}$
pr = 2.84 cm
FIG. 5.9 a
$\overline{FD}$
981 dynes
0
50
100
150
100
200
Ω, (981 dynes/sec-cm)
Ω vs. $\overline{FD}$
pr = 3.84 cm
FIG. 5.9 b
$\overline{FD}$
981 dynes
0
50
100
150
100
200
Ω, (981 dynes/sec-cm)
Ω vs. $\overline{FD}$
Pr = 4.84 cm
FIG. 5.9 c
$\overline{FD}$
981 dynes
0
50
100
150
100
200
Ω, (981 dynes/sec-cm)

a high pressure region above the sphere. The net effect is a predominantly negative lift.

It could be anticipated that a saltating solid in a shallow and supercritical stream would perform short and fast saltations, because at the moment a solid is lifted from the bed, a predominant negative lift force would act to bring the particle back to the bed. The impact force created, together with the predominant positive $\overline{FL}$ would assist to maintain another cycle of saltations.

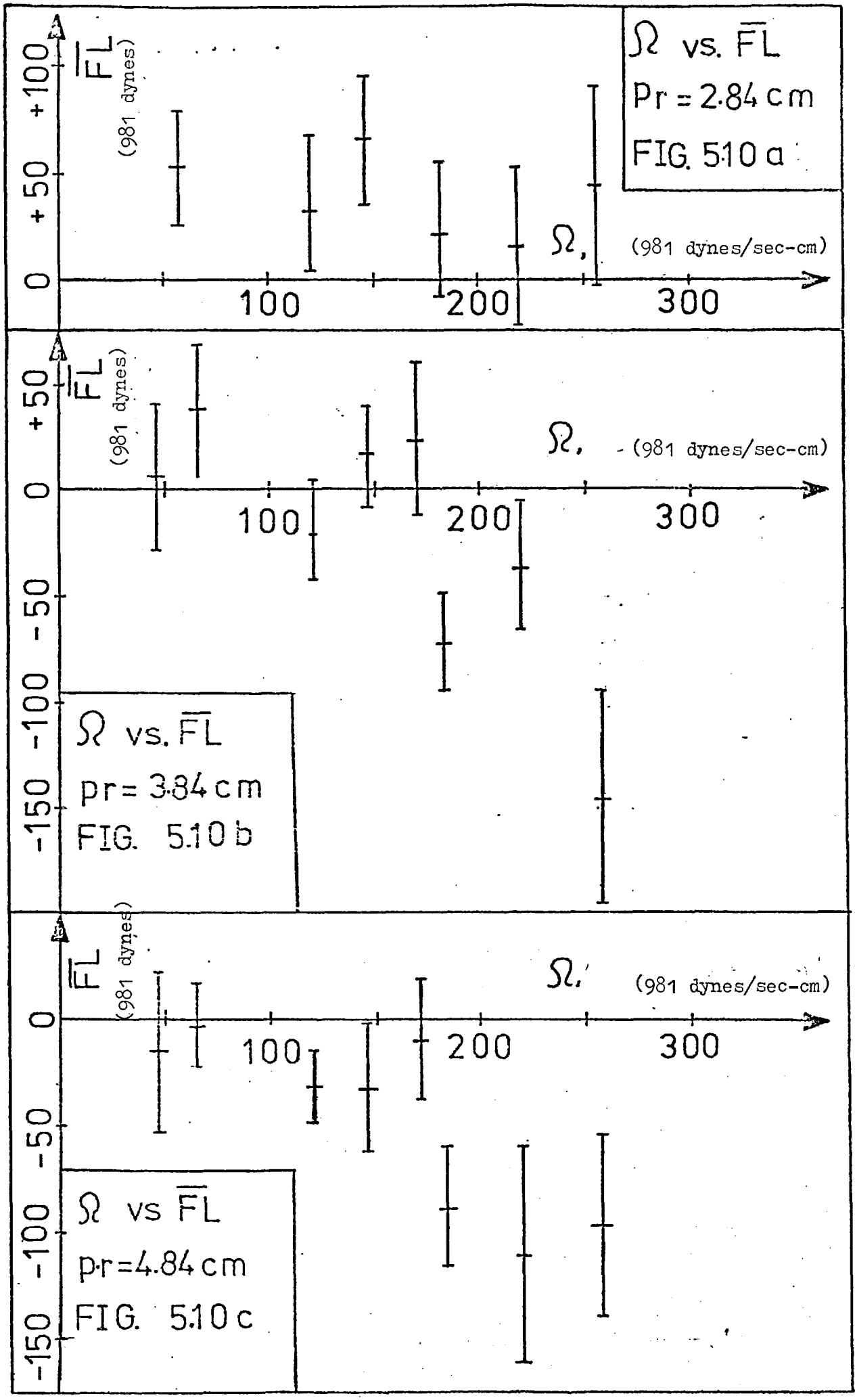
It is interesting to compare the relative magnitudes of $\overline{FL}$ to $\overline{FD}$ irrespective of the direction of each force. It is observed that for the majority of test points shown in Figures 5.9a,b&c and 5.10a,b and c, $\overline{FL}/\overline{FD}$ is in the range of 0.3 → 1.0.

On the other hand, the standard deviations from the mean lift force in Figures 5.10a,b and c varies between 30% to 100% for 13 records (see Table 5.1), 100% to 150% for 5 records and from 150% to 497% for 6 records.

5.5.1.2.3 Skin Friction Drag

One of the surprising findings that emerged from the instantaneous force measurements is the demonstration that skin friction stresses distributed on the surface of the sphere are appreciable in comparison with drag and lift. It is thought that these skin friction stresses are due to the collapse of small eddies on the surface of the sphere. Although the force transducer (described previously) cannot detect the distribution of the skin friction stresses on the sphere surface, the overall effect of them is recorded as an overall torque TM that affects the stability of a loose sphere.

Figures 5.11a, b and c are plots of the mean torque $\overline{TM}$ for increasing values of Ω for three sphere protrusions 2.84, 3.84 and 4.84 cm


Ω vs. FL
Pr = 2.84 cm
FIG. 5.10 a
FL (981 dynes)
Ω, (981 dynes/sec-cm)
+100
+50
0
100
200
300
Ω vs. FL
pr = 3.84 cm
FIG. 5.10 b
+50
0
-50
-100
-150
Ω vs FL
p·r = 4.84 cm
FIG. 5.10 c

respectively. The mean torque $\overline{TM}$ is shown to increase with Ω in a manner similar to that revealed by $\overline{FD}$. But, more scatter and inconsistency prevails in Figs. 5.11a,b and c relative to the scatter in Figs. 5.9a,b and c. The standard deviation of the fluctuating TM values varies in the range of 44% to 150% of $\overline{TM}$ for 13 test runs, and from 150% to 460% for 11 runs (see Table 5.1 again). It must be mentioned that contrary to equation 4.2, TM is considered to be positive when acting in a clockwise direction in Figs. 5.8b,5.11a,b and c, 5.14c and in Table 5.1.

5.5.1.2.4 Angular Acceleration

The instantaneous angular acceleration, a, was computed using equation 4.14, for a loose sphere with a mass density of ρ_s=2.65gm/cm^3, diameter = 5.1 cm and resting at intermediate positions A, B and C as shown in Fig. 5.12. Fig. 5.8d shows a sample plot of the instantaneous angular acceleration a versus time.

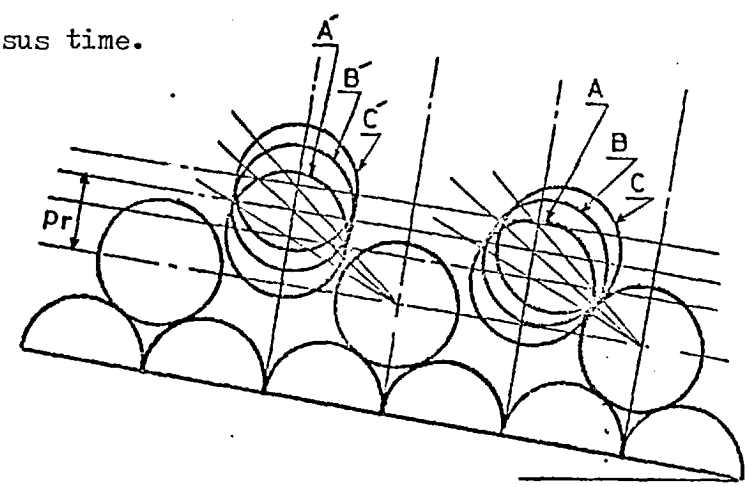
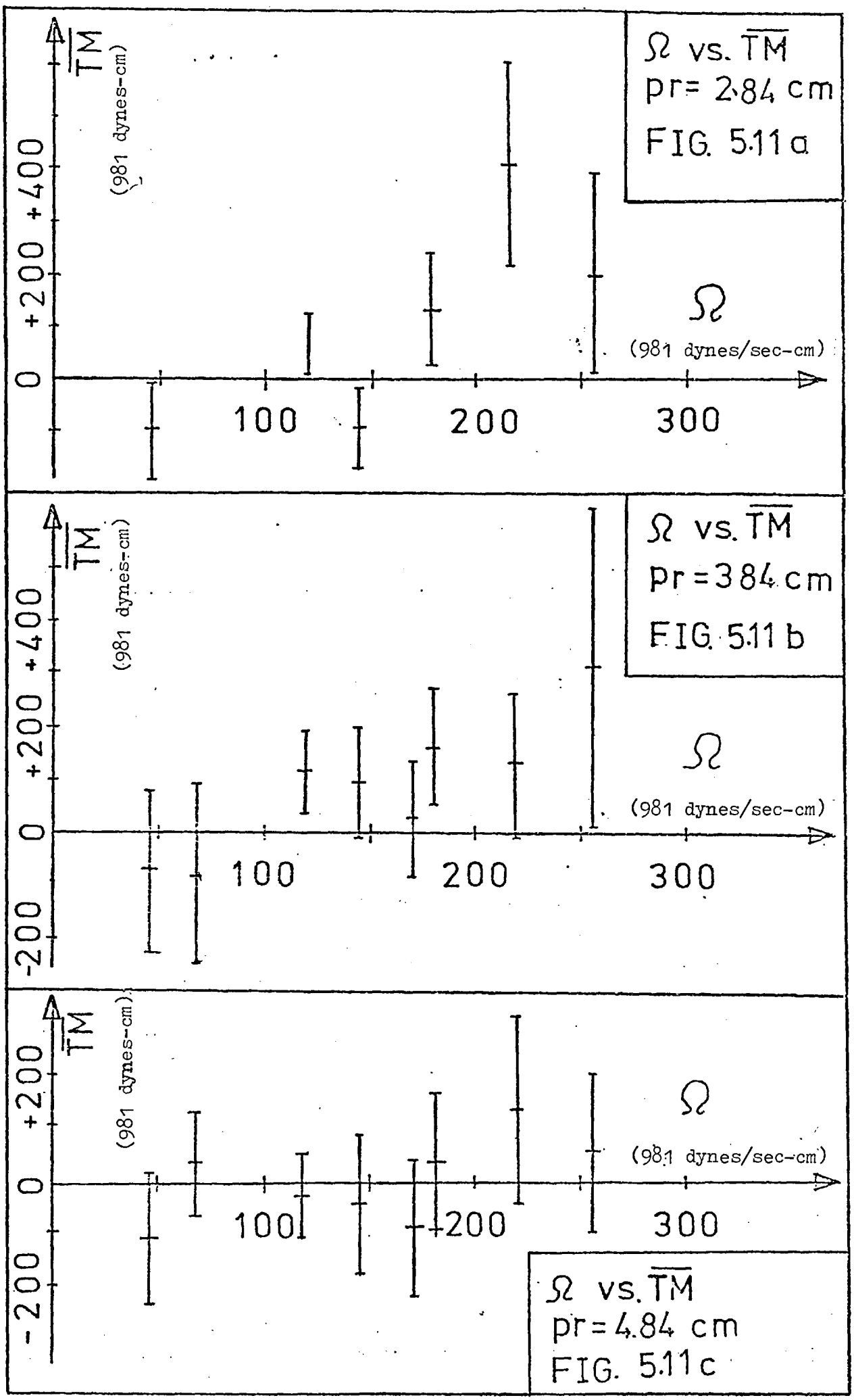


FIG 5.12 . Actual and assumed suspension locations of the test sphere.

It must be mentioned that, in the force measurements, the test sphere was suspended in positions A', B' and C' respectively (see Fig. 5.12 again). This assumption was made because FD, FL and TM can only be measured if the test sphere is completely unrestrained by any of the fixed spheres.

Figures 5.13a,b and c show the variation of $\overline{a}$ for increasing Ω,


$\overline{TM}$
(981 dynes-cm)
0
+200
+400
100
200
300
Ω
(981 dynes/sec-cm)
Ω vs. $\overline{TM}$
pr= 2.84 cm
FIG. 5.11 a
$\overline{TM}$
(981 dynes-cm)
-200
0
+200
+400
100
200
300
Ω
(981 dynes/sec-cm)
Ω vs. $\overline{TM}$
pr = 3.84 cm
FIG. 5.11 b
$\overline{TM}$
(981 dynes-cm)
-200
0
+200
100
200
300
Ω
(981 dynes/sec-cm)
Ω vs. $\overline{TM}$
pr = 4.84 cm
FIG. 5.11 c

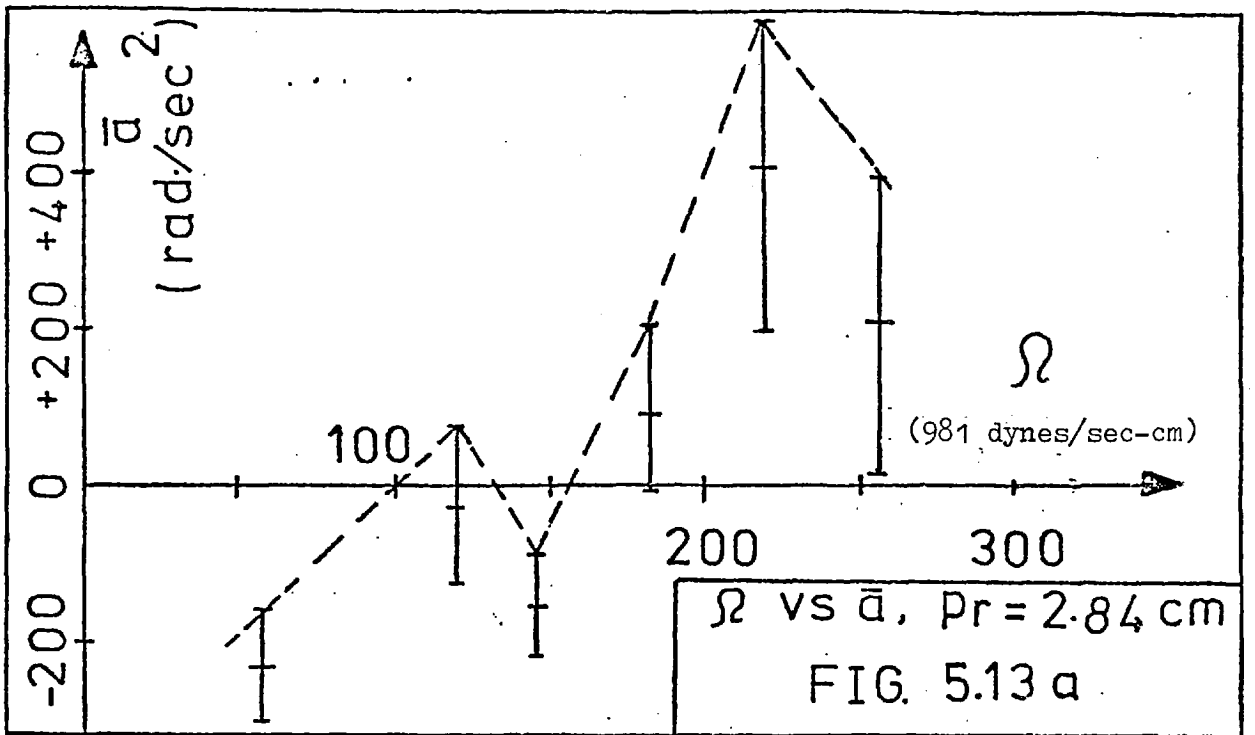
where the sphere protrusion varies from 2.84, 3.84 to 4.84 cm respectively. A positive $\overline{a}$ indicates that the moment of the fluid driving forces about the point of contact P (Fig. 4.7) exceeds that of the immersed weight of the loose sphere. Hence, whenever $\overline{a} \leq 0$, the loose sphere could be thought of as stable and whenever $\overline{a} > 0$, the loose sphere could be considered unstable and conseuently might roll or saltate along the bed downstream.

Comparison of the variation of $\overline{TM}$ with Ω (see Figs.5.11a, b and c) with the variation of $\overline{a}$ with Ω (see, Figs.5.13a, b and c) shows that there is a similarity between the variations of both variable $\overline{TM}$ and $\overline{a}$ with Ω. Even the standard deviations of both TM and a from the mean values $\overline{TM}$ and $\overline{a}$ respectively look similar.

It could be reasoned that the increase of $\overline{a}$ with Ω at small sphere protrusions is produced more or less equally by the torque due to skin friction, the form drag and the lift. Although $\overline{FL}$ becomes increasingly negative for larger Ω values, $\overline{a}$ still persists to be positive. It could be anticipated consequently that at large protrusions, a loose sphere would still roll downstream, but it would be brought down to the bed due to the increasingly negative lift force on it.

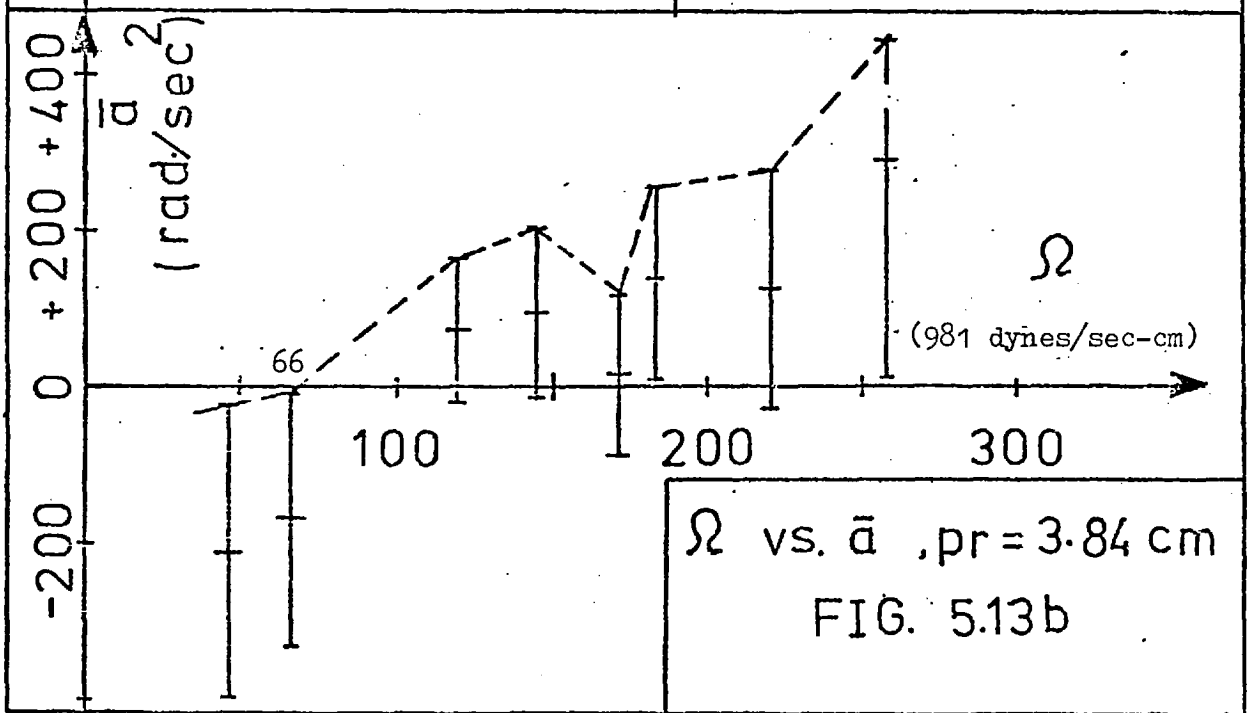
The standard deviations of a are in the range of 44% to 150% for 15 runs, except where $\overline{a}$ is very close to the zero value. In such a case, the standard deviations become several times greater than the mean values.

Upper envelope curves could be drawn by joining the ordinates of $\overline{a}$ + one standard deviation (see Figs. 5.13 a, b and c). It could be seen that the upper envelope curves intercept the Ω -axis at greater Ω_c values for smaller and smaller sphere protrusions, where Ω_c=100x981, 66x981 and 37x981 dynes/cm-sec for the sphere protrusions of 2.84, 3.84 and 4.84 cm respectively. Such a trend implies that a loose sphere



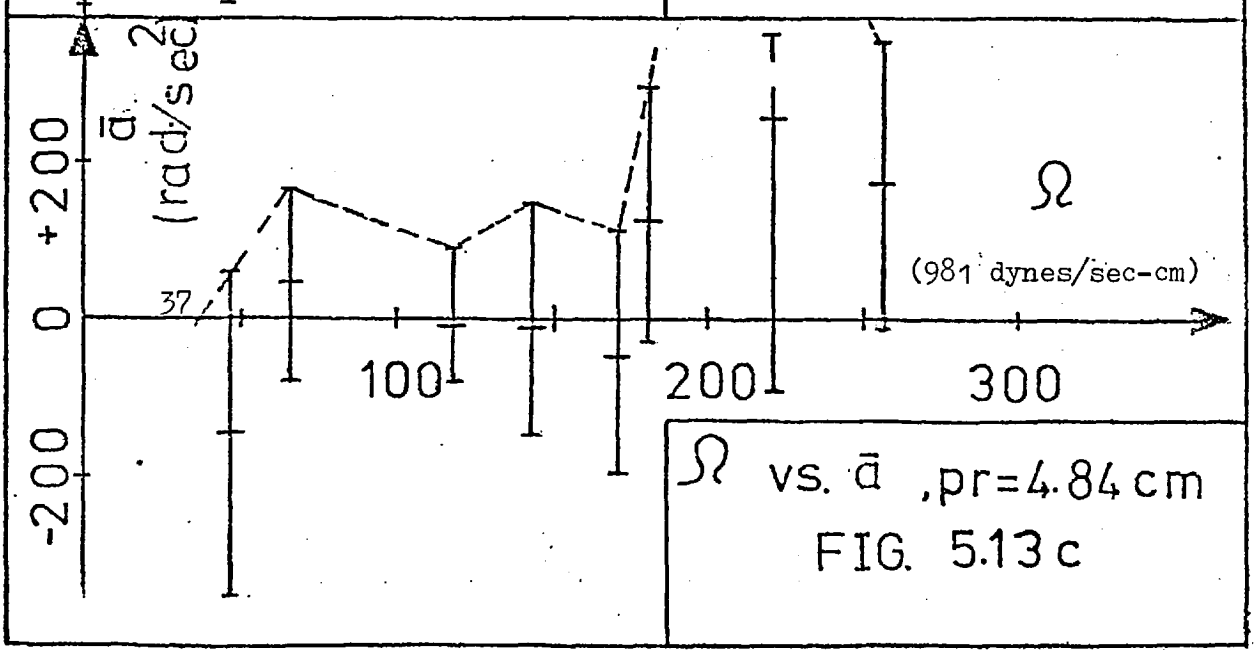
Ω vs ā, pr = 2.84 cm

FIG. 5.13 a



Ω vs. ā, pr = 3.84 cm

FIG. 5.13b



Ω vs. ā, pr = 4.84 cm

FIG. 5.13 c

becomes more unstable for greater sphere protrusions and for the same stream power.

Due to the high fluctuations of the fluid driving forces on a sphere (as could be judged from the high values of the standard deviations of FD,FL and TM), it is suggested for design purposes, that the mean value plus one standard deviation above the mean of FD, FL and TM might be considered when deciding whether a loose sphere is stable or not.

5.5.1.3 Probability Distribution

Sample cumulative probability distribution curves of FD, FL, TM and a are shown in Figs. 5.14a,b,c and d respectively. All these curves show a distinct S shape. Such a feature implies that the cumulative probability distributions of the above mentioned variables are either normal or somewhat skewed normal distributions. The skewness Sk from the normal distribution of a variable X could be calculated by the following equation:

$$Sk = \frac{\overline{X^3} - 3\overline{X}\,\overline{X^2} + 2(\overline{X})^2}{(\overline{X^2} - (\overline{X})^2)^{3/2}} \qquad \text{..... Eq. 5.1}$$

For a normal distribution with zero mean, Sk = 0. Variation of Sk for FD, FL, TM and a are shown in Table 5.1, where Sk varies in the following ranges:

-2.56 → 4.02 for FD

-4.07 → 3.64 for FL

-4.95 → 2.31 for TM

and -3.69 → 5.06 for a .

There is no consistent trend that the skewness of distributions increases or decreases with Ω or sphere protrusion.

For the sake of brevity, not all probability distribution curves of the angular acceleration a are included in this thesis.

However, the stability of a loose sphere based on probability considerations is investigated in the following way.

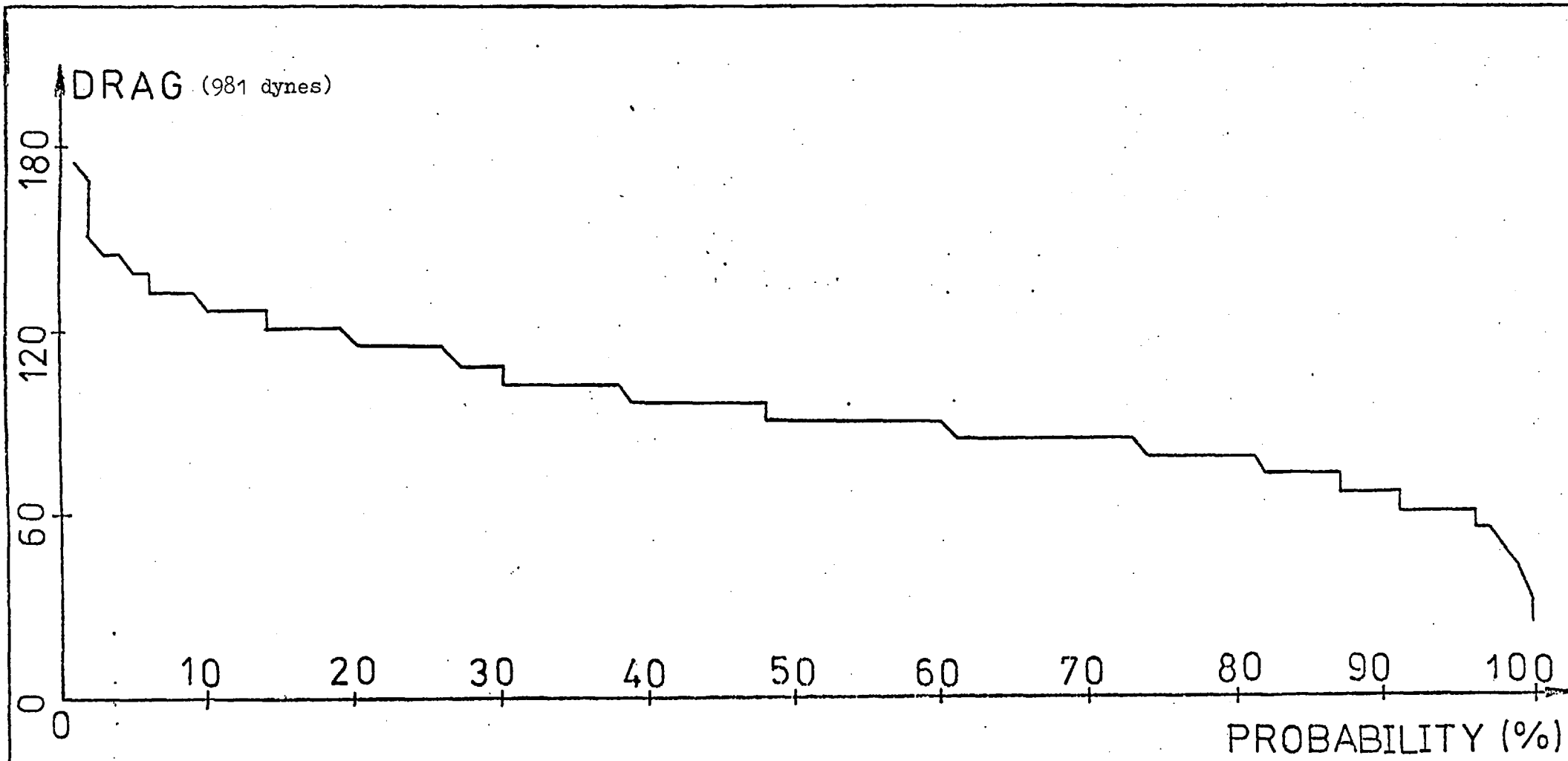
For each hydraulic condition tested, the probability that the angular acceleration $a \leq 0$ may be read from the probability distribution curve and is defined as the percentage stability. Figs.5.14e, f and g show percentage stability versus Ω for the three sphere protrusions 2.84, 3.84 and 4.84 cm respectively, where the following characteristics are deduced:

1. Percentage stability decreases with increasing Ω.

2. Percentage stability reaches a high value 85% for a critical stream power Ω_c. The 85% stability is chosen because in a normal probability distribution the mean value of fluctuations of a variable + one standard deviation are not exceeded 85% of the time. Consequently the critical stream powers obtained from Figs 5.13a,b and c could be compared with those which can be obtained from Figs.5.14e, f and g as will be mentioned subsequently.

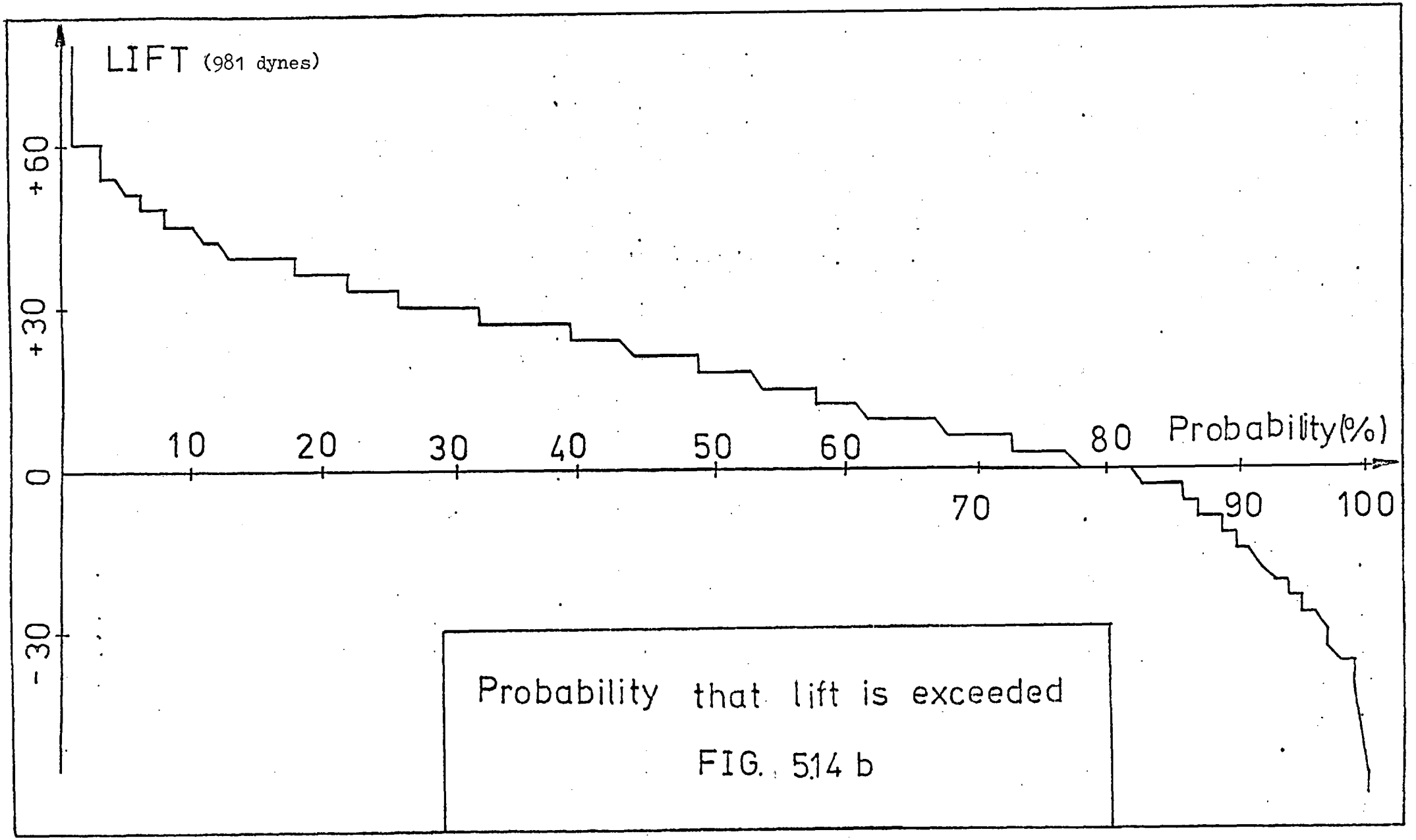
3. The critical stream power Ω_c based on probability considerations weakly decreases with increasing protrusion of the test sphere, where Ω_c = 77.5 x 981, 74 x 981 and 40 x 981 dynes/sec-cm for the sphere protrusions of 2.84, 3.84 and 4.84 cm respectively. It should be mentioned that a similar trend was revealed from Figs. 5.13a, b and c.

4. It will be remembered (see section 3.2.2.5.3) that the experiment with loose stones showed an increase in Ω_c with increasing S_o values according to equation 3.8. However, results from the force measurements in Stage II do not show a similar trend because the number of volumetric discharges tested for each sphere protrusion pr and channel slope S_o is not sufficient to isolate the effect of S_o on Ω_c.



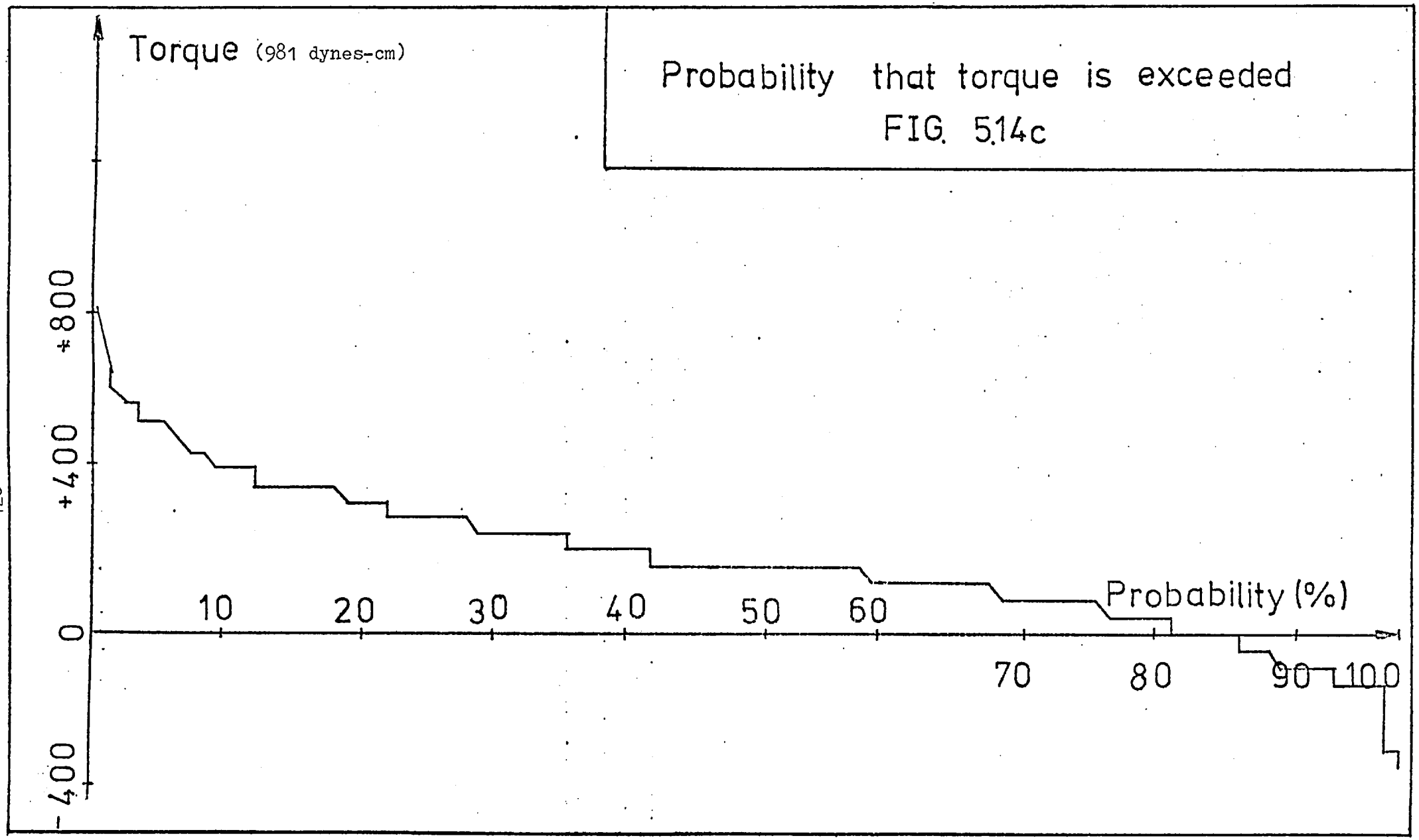
PROBABILITY that drag is exceeded

FIG. 5.14 a



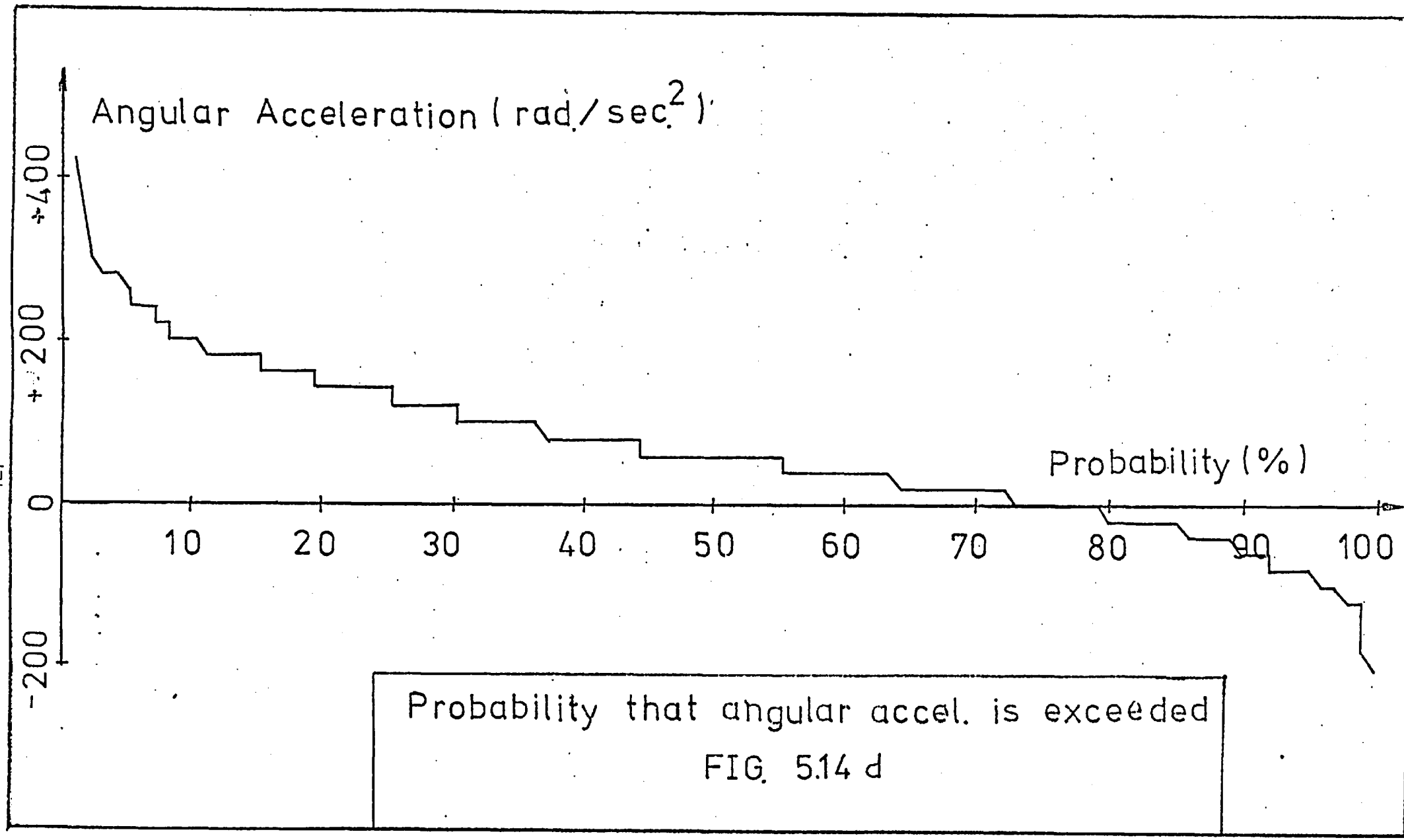
Probability that lift is exceeded

FIG. 5.14 b



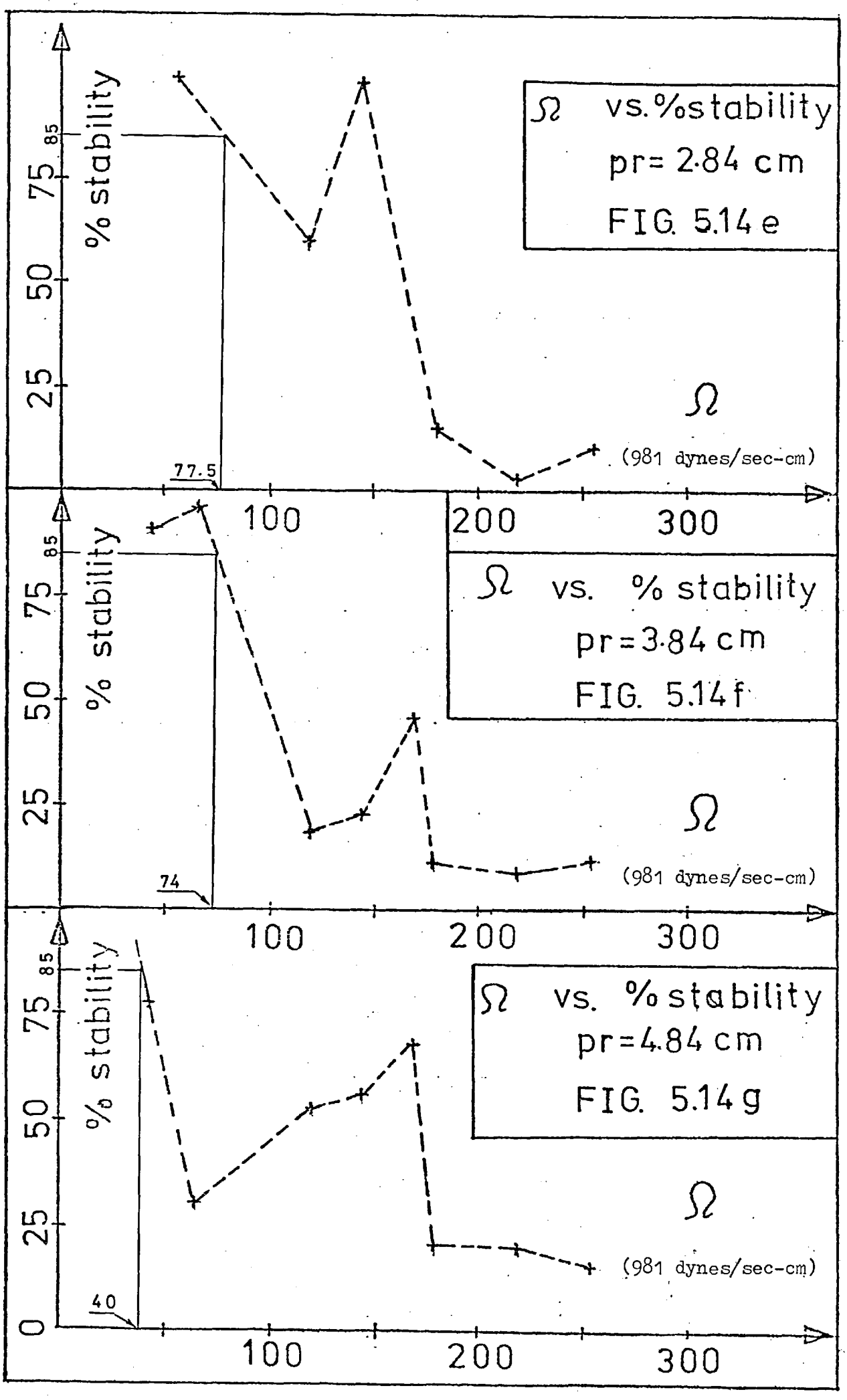
Probability that torque is exceeded

FIG. 5.14c



Probability that angular accel. is exceeded

FIG. 5.14 d


% stability
85
75
50
25
77.5
100
200
300
Ω
(981 dynes/sec-cm)
Ω vs. % stability
pr = 2.84 cm
FIG. 5.14 e
% stability
85
75
50
25
74
100
200
300
Ω
(981 dynes/sec-cm)
Ω vs. % stability
pr = 3.84 cm
FIG. 5.14 f
% stability
85
75
50
25
0
40
100
200
300
Ω
(981 dynes/sec-cm)
Ω vs. % stability
pr = 4.84 cm
FIG. 5.14 g

5.5.1.4 Auto Correlation Functions

The autocorrelation coefficient $\frac{R(r\Delta t)}{R(o)}$ is plotted as ordinate and the lag time ($r\Delta t$) as abscissa for the three variables FD, FL and TM. Sample plots of ($r\Delta t$) versus $\frac{R(r\Delta t)}{R(o)}$ are shown in Figs.5.15a, b and c respectively. The maximum lag time in all aforementioned figures is 100 time steps, where each step is 0.025 sec. Comparison of the shapes of the autocorrelation curves for all the test runs and for the three variables FD, FL and TM show a rapid decay of the auto correlation coefficient immediately after several time steps only. Such a trend is characteristic of stationary, random variables with a wide band of frequencies. The rapid decay of $\frac{R(r\Delta t)}{R(o)}$ also implies that there is practically no dependence of one set of values of FD, FL and TM measured at one instant of time upon another set of values measured at earlier or subsequent instants of time.

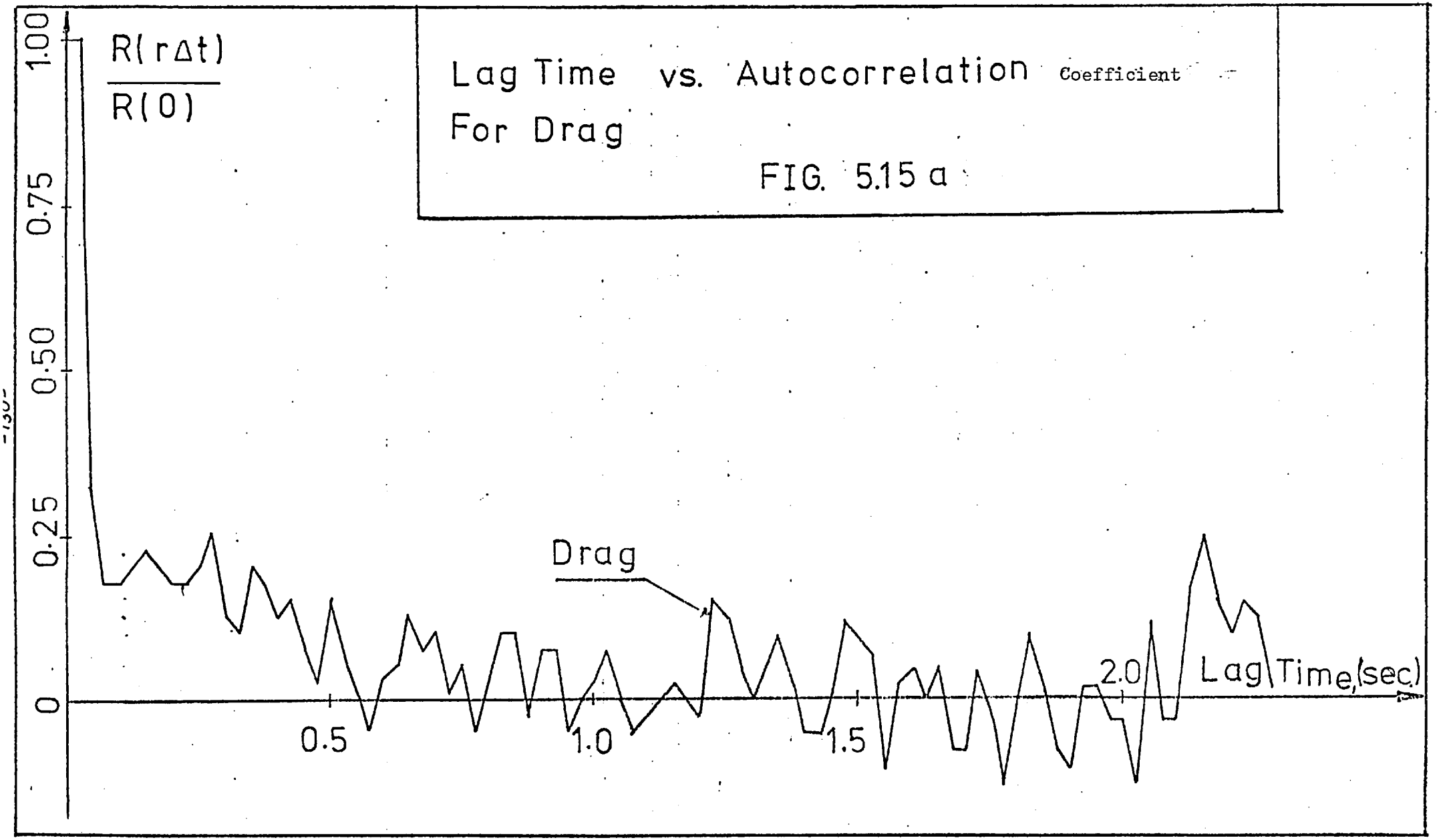
There is no clear indication from all the autocorrelation curves plotted that the stream power or the protrusion of the test sphere affect the rapid decay of $\frac{R(r\Delta t)}{R(o)}$.

5.5.1.5 Spectral Density Functions

For one test run, sample graphs of the power spectral density function G(f) as ordinates and the frequency f as abscissa are presented in Figs.5.16a, b and c for the variables FD, FL and TM respectively.

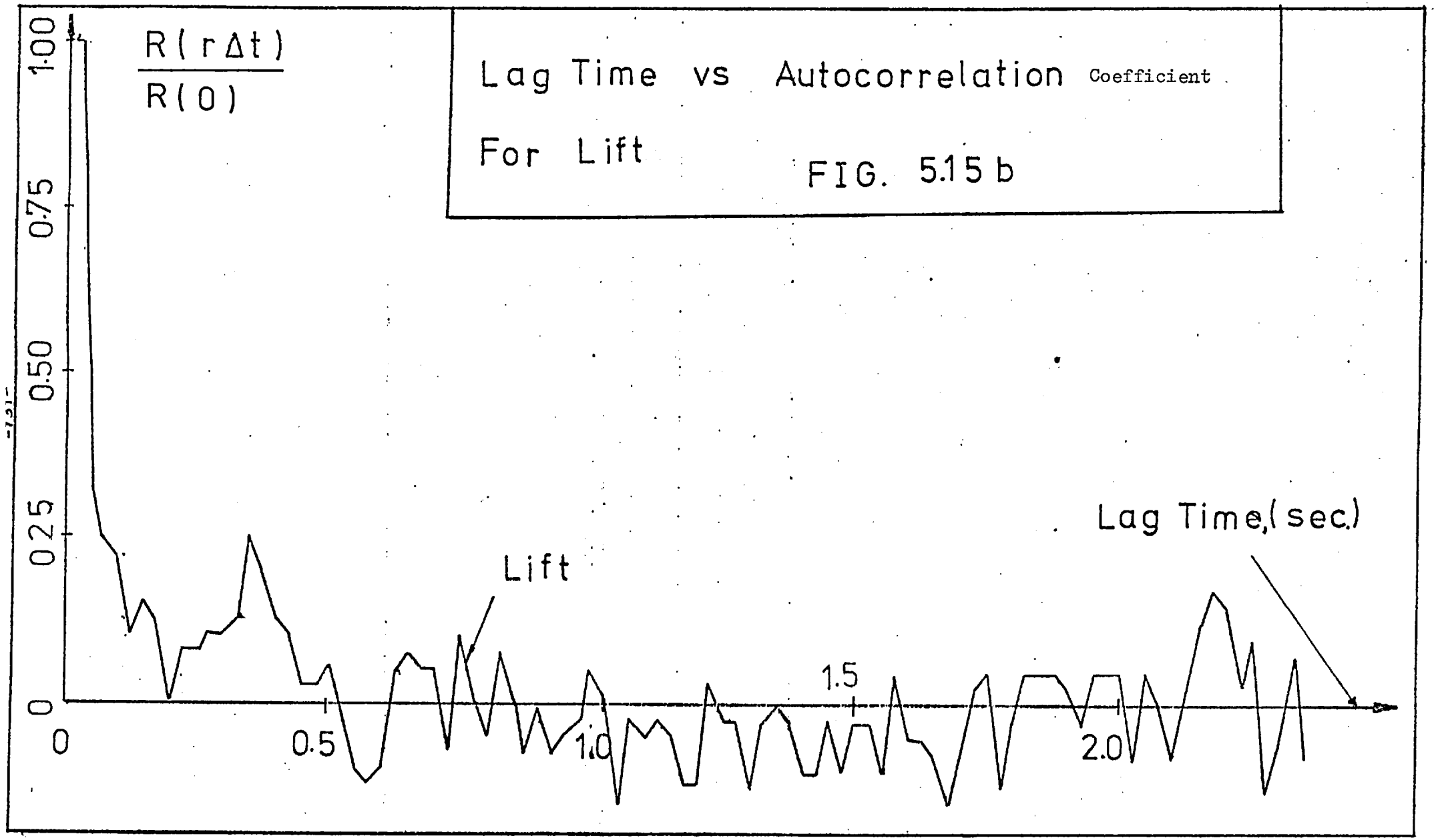
There is one feature dominating all spectral density graphs obtained in this investigation, namely: all of them have many peaks and troughs in a wide band of frequencies ranging from 0.8 Hz to 15 Hz.

Apperley (1968) has done a similar spectral analysis as in this investigation, but found that the graphs of frequency f as abscissa and G(f) as ordinate for drag and lift on a sphere in one subcritical flow are smooth concave curves. He also found that the function G(f)



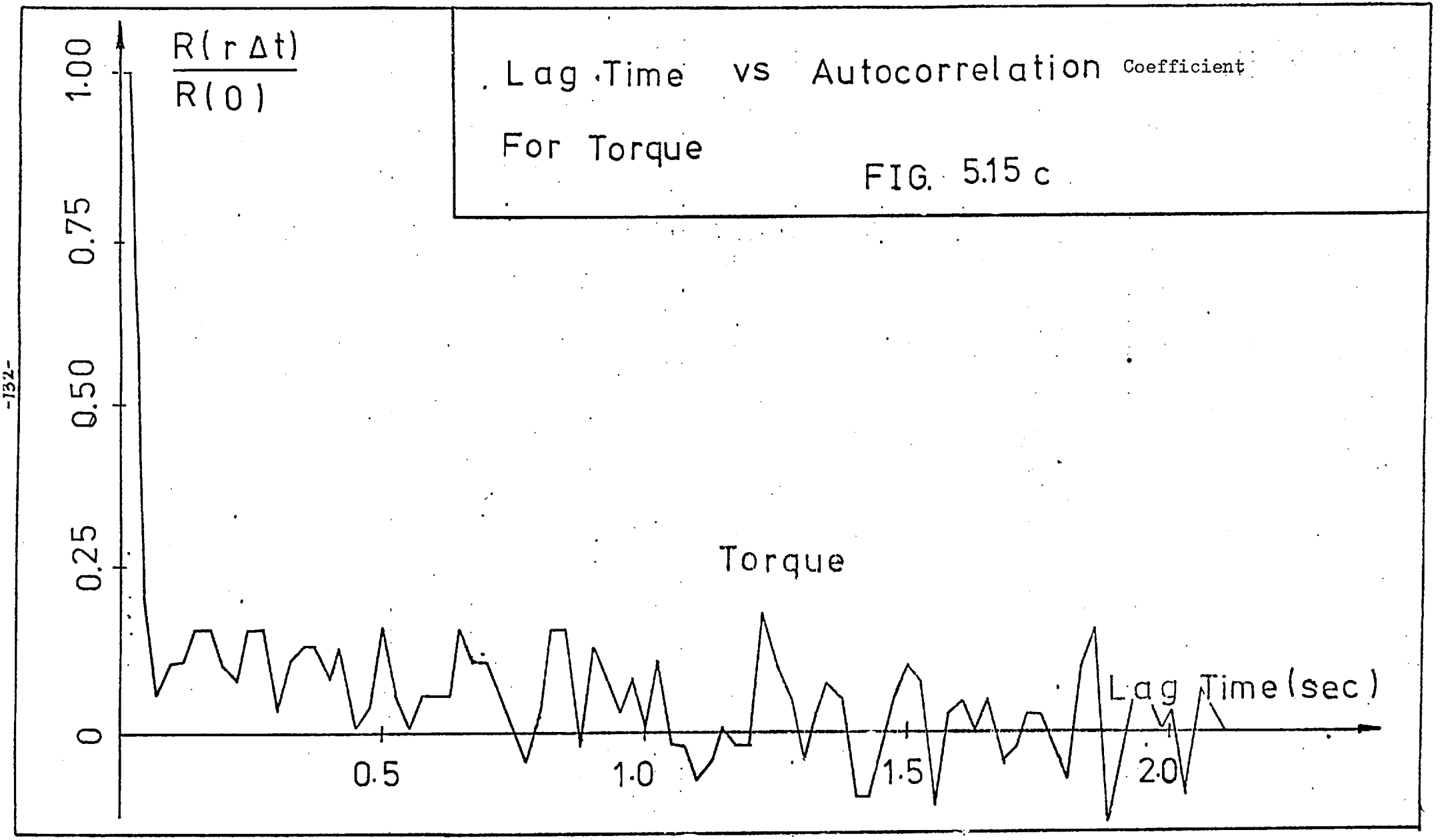
Lag Time vs. Autocorrelation Coefficient For Drag

FIG. 5.15 a



Lag Time vs Autocorrelation Coefficient For Lift

FIG. 5.15 b


Lag Time vs Autocorrelation Coefficient
For Torque
FIG. 5.15 c
R(r Δt) / R(0)
1.00
0.75
0.50
0.25
0
Torque
0.5
1.0
1.5
2.0
Lag Time (sec)

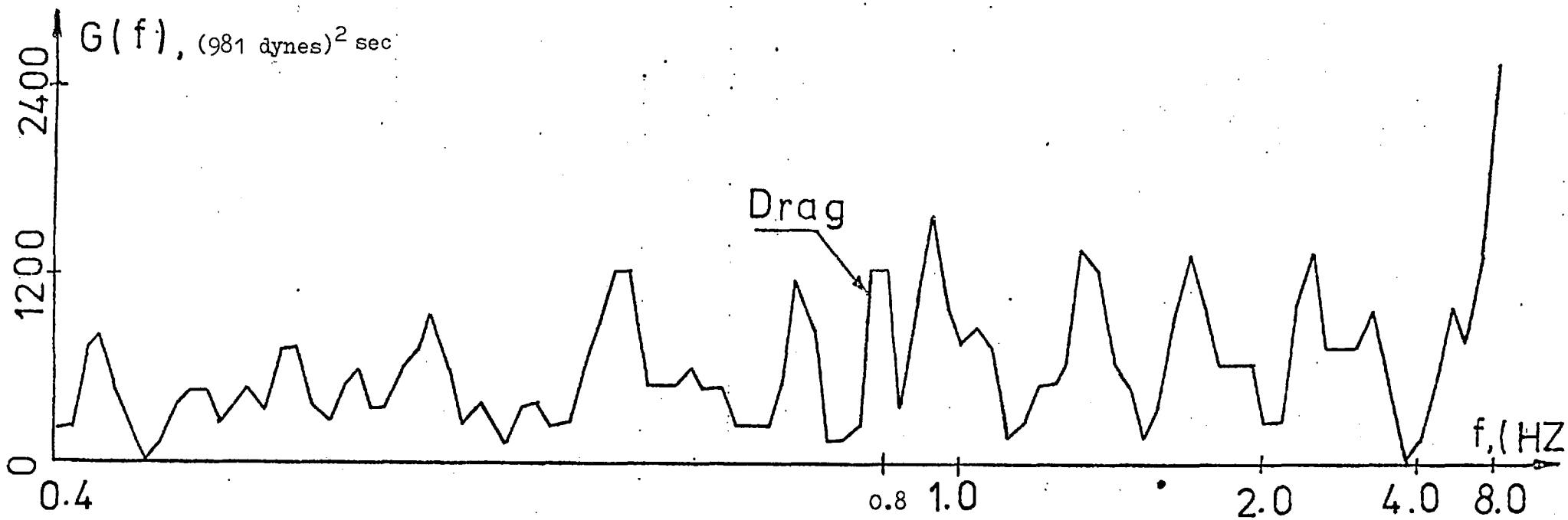
is at a maximum at low frequencies of 0.1 Hz and decreases smoothly with increasing fequencies approaching 20 Hz.

The distinct difference between Apperley's (1968) results and those shown in Figs. 5.16a, b and c could be attributed to the contrast between the eddy structure in turbulent subcritical streams and the eddy structure in turbulent supercritical ones. It may be anticipated in the latter case, that the distorted water surface (see Plates 3 and 6) and the turbulent wakes behind individual solid particles of a rough steep bed constitute a main source of creating eddies of low frequency and of a size which may be not much smaller than the size of each solid. The fast moving thin layer of fluid in the non separation zone (as the one shown in Fig.1.4) constitutes a source of very small eddy size (relative to the diameter of the sphere) and of a high frequency.

The interaction of all this complex set up of eddy structure produces a set of turbulent forces on individual solids.

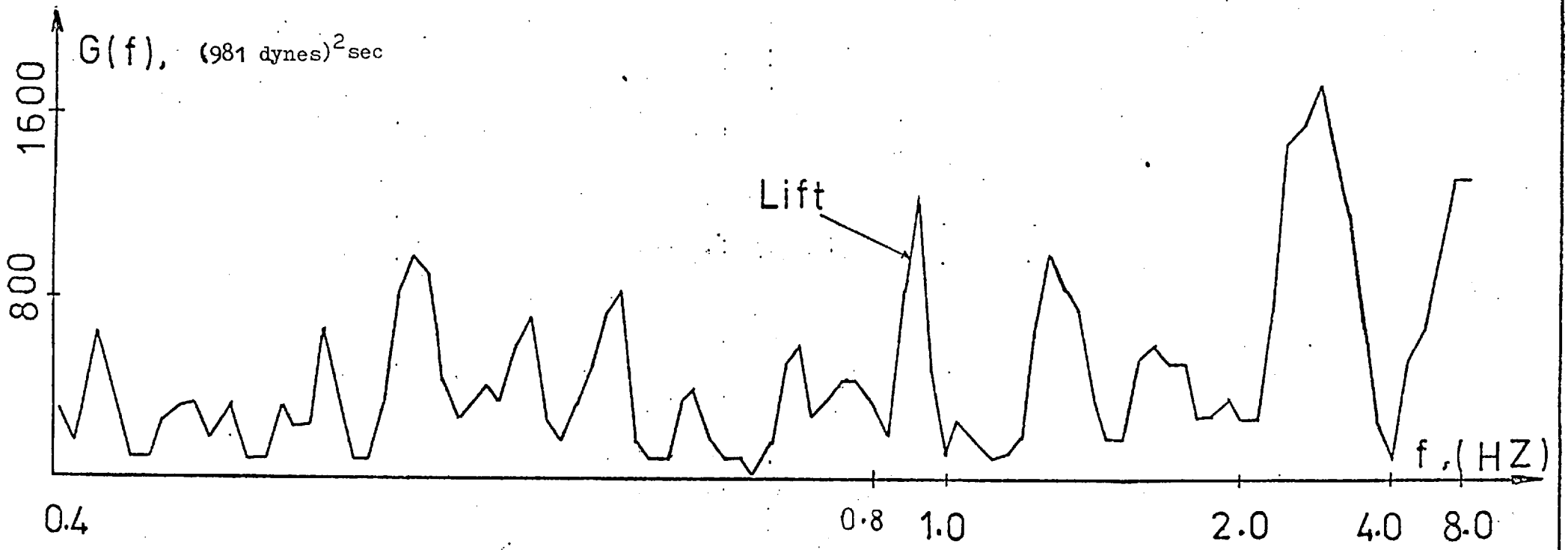
The above mentioned anticipation may be supported by the shapes of the spectral density plots in the following way:

Based on the mean velocity distributions conducted in Stage I (see Figs.2.1 and 2.2) it may be assumed that the mean water velocities around the test sphere in record No. 16 range from 250 cm/sec in the non separation zones (see Fig. 1.4) to -25 cm/sec in the turbulent wakes of the test sphere. The approximate frequencies of the eddies may be obtained by dividing the local water speeds by the diameter of the test sphere. Consequently, the frequencies of the eddies would range from 50Hz to 0. Although the spectral analysis done in this investigation is valid for frequencies between 0.8 and 15 Hz, the multi-peak shapes of the spectral density plots supports the idea that turbulent eddies of a range of frequencies of at least 0.8 to 15 Hz are existant in a tumbling steep stream.



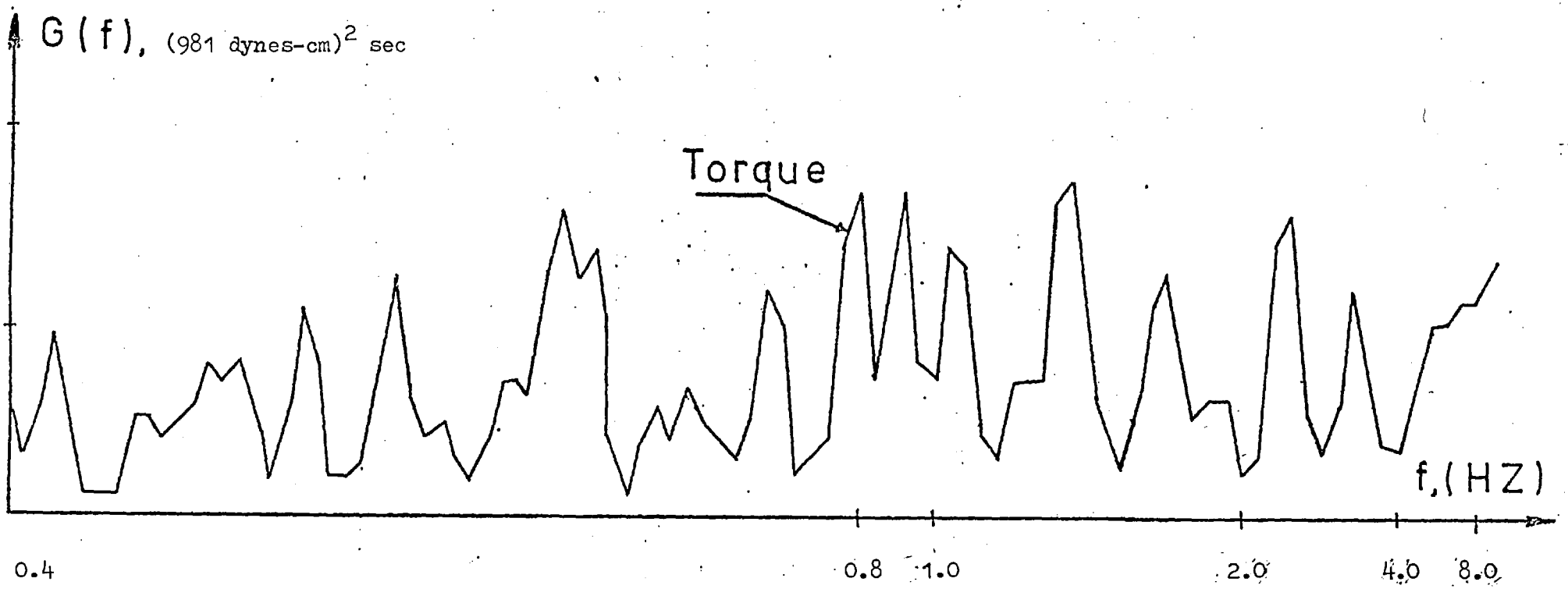
Frequency vs. Power Spectral Density Function For Drag

FIG. 5.16 a



Frequency vs. Power Spectral Density Function For Lift

FIG. 5.16 b



Frequency vs. Power Spectral Density Function For Torque

FIG. 5.16 c

5.5.2 Sources and Relative Magnitudes of Error in Force Measurements

The main sources of error in the instantaneous force measurements of Stage II could be classified under two main categories.

(i) Systematic Errors

1. Signals S_1, S_3 and S_7 could have been magnified due to resonance occurring as a result of the high frequencies of turbulent forces and/or the natural frequencies of the electronic instruments being not much less than the natural frequency of the force transducer in water.

2. Errors in static calibration of the force transducer produce systematic errors in the variables FD, FL and TM. It should be mentioned that static calibration was checked before and after taking groups of three records of the 24 ones taken in Stage II.

(ii) Accidental Errors

1. Digital filtering of the raw records, S_1, S_3 and S_7, could be in error due to the tedious process of identifying the midway between peaks and troughs of the raw records.

2. The x-y reader which was employed to digitize signals S_1, S_3 and S_7 could accidently mis-punch numbers (corresponding to the amplitudes of the signals) in spite of the constant care to prevent this possibilty from occurring.

Consider now the percentage error produced in the computed values of FD, TM and FL due to a +1% error in the bending moments M_1, M_3 and M_7 measured at sections S_1, S_3 and S_7 respectively.

The partial derivatives of the variables, FD, TM and FL (given by equations 4.1, 4.2 and 4.3 respectively) with respect to M_1, M_3 and M_7 are given, respectively, by the following sets of equations.

$$\frac{\partial FD}{\partial M_1} = \frac{-1}{X_3 - X_1}, \quad \frac{\partial FD}{\partial M_3} = \frac{1}{X_3 - X_1}, \quad \frac{\partial FD}{\partial M_7} = 0 \quad \text{.....Eq. 5.2}$$

$$\frac{\partial TM}{\partial M_1} = \frac{+X_3}{X_3 - X_1}, \quad \frac{\partial T_M}{\partial M_3} = \frac{-X_3}{X_3 - X_1} + 1, \quad \frac{\partial T_M}{\partial M_7} = 0 \quad \text{..... Eq. 5.3}$$

$$\frac{\partial FL}{\partial M_1} = \frac{X_B - X_3}{X_7(X_3 - X_1)}, \quad \frac{\partial FL}{\partial M_3} = \frac{-1}{X_7} - \frac{X_B - X_3}{X_7(X_3 - X_1)}, \quad \frac{\partial FL}{\partial M_7} = \frac{1}{X_7}$$

..... Eq. 5.4

The percentages of error in estimated FD, TM and FL values due to +1% error in each of M_1, M_3 and M_7 are given by the following equations:

$$\frac{dFD}{FD} = \frac{\partial FD}{\partial M_1}\frac{M_1}{FD} + \frac{\partial FD}{\partial M_3}\frac{M_3}{FD} + 0 \quad \text{..... Eq. 5.5}$$

$$\frac{dTM}{TM} = \frac{\partial TM}{\partial M_1}\frac{M_1}{TM} + \frac{\partial TM}{\partial M_3}\frac{M_3}{TM} + 0 \quad \text{..... Eq. 5.6}$$

$$\frac{dFL}{FL} = \frac{\partial FL}{\partial M_1}\frac{M_1}{FL} + \frac{\partial FL}{\partial M_3}\frac{M_3}{FL} + \frac{\partial FL}{\partial M_7}\frac{M_7}{FL} \quad \text{..... Eq. 5.7}$$

Substituting equation 5.2 in equation 5.5 , equation 5.3 in equation 5.6 and equation 5.4 in equation 5.7 , one gets:

$$\frac{dFD}{FD} = \frac{M_3 - M_1}{FD(X_3 - X_1)} \quad \text{..... Eq. 5.8}$$

$$\frac{dTM}{TM} = \frac{M_3}{TM} - \frac{X_3(M_3 - M_1)}{TM(X_3 - X_1)} \quad \text{..... Eq. 5.9}$$

and $$\frac{dFL}{FL} = \frac{M_1(X_B - X_3)}{X_7(X_3 - X_1)FL} - \frac{M_3}{FL}\left(\frac{1}{X_7} + \frac{X_B - X_3}{X_7(X_3 - X_1)}\right) + \frac{M_7}{X_7 FL} \quad \text{... Eq. 5.10}$$

A sample solution of equations 5.8, 5.9 and 5.10 for one set of

simultaneous values of M_1, M_3 and M_7 (taken from record number 16), gave the following answers:

For $M_1 = 435 \times 981$ dyne-cm, $M_3 = 544 \times 981$ dyne-cm and $M_7 = 940 \times 981$ dyne-cm and

$$\frac{dM_1}{M_1} = \frac{dM_3}{M_3} = \frac{dM_7}{M_7} = 1\%$$

Then:

$$\frac{dTM}{TM} = -1\% \quad , \quad \frac{dFL}{FL} = -4\% \quad \text{and} \quad \frac{dFD}{FD} = 1\%$$

The above mentioned sample calculations show that the errors produced in TM are of the same order of magnitude as those produced in FD but in an opposite direction; while the errors produced in FL are 4 times higher than those produced in TM and in the same direction.

It should be mentioned that eqations 5.8, 5.9 and 5.10 could be easily modified to consider the effect of i_1, i_3 and i_7 percentages of error in M_1, M_3 and M_7 respectively. Where i_1, i_3 and i_7 assume a reasonable range of values (say between 0 and $\pm$ 10).

Equations 5.8, 5.9 and 5.10 or their modified forms could have been included in the computer programs to work out the percentage of error in ED, TM and FL at each sampled point of the 48000 data points digitized in Stage II. But, the computing time needed would be expensive.

5.5.3 The Critical Stream Power in the Case of a Loose Sphere

Measurements of the critical stream power associated with the initial instability of a loose sphere was described in article 5.4.3. Table 5.2 summarizes the experimental results and Figs. 5.17a, b and c are plots of Ω_c as ordinate and the channel slope S_o as abscissa.

It is clearly revealed from the aforementioned figures that for one protrusion of a loose sphere, Ω_c increases with S_o. Such a trend could be attributed to the greater stream power consumption associated with greater water surface disturbances, more air entrainment and highly turbulent wakes in the downstream side of individual spheres. It is also revealed that for one channel slope, the greater is the protrusion of a loose sphere, the less is the stream power needed to dislodge it from its recess. Such a trend was also revealed from the instantaneous force measurement and particularly in Figs.5.13a, b and c and 5.14e, f and g.

Comparison of Figs.5.17a, b and c with each other show that for one protrusion of a loose sphere, the greater is the distance x (x is the distance measured along the channel slope, from the leading edge of the flume to the position of the loose sphere, see Fig.3.1), the greater is the critical stream power. Hence it could be anticipated that loose stones near the leading edge of a steep rough channel are more vulnerable to be dislodged than those(of the same size and mass density) located further downstream. This is a weak trend. It may be partly attributed to a reduction in shear stress at the bed with distance in the region of boundary layer development close to the inlet, and partly to the progressive consumption of stream power to increase the air concentration with distance in the region of development of a fully-established air-concentration profile.

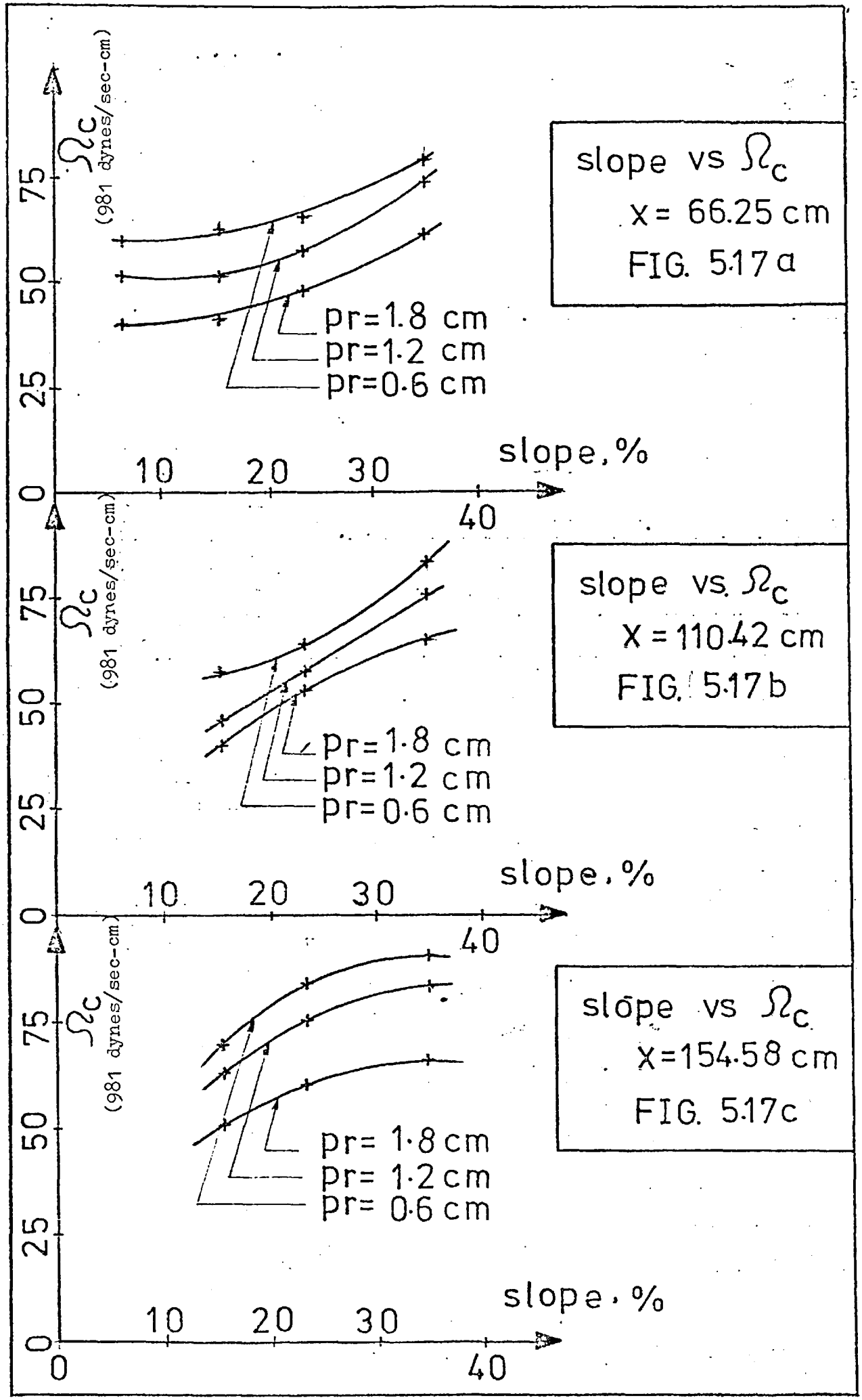

Ω_c (981 dynes/sec-cm)
75
50
25
0
10
20
30
40
slope, %
pr=1.8 cm
pr=1.2 cm
pr=0.6 cm
slope vs Ω_c
X = 66.25 cm
FIG. 5.17 a
Ω_c (981 dynes/sec-cm)
slope, %
pr=1.8 cm
pr=1.2 cm
pr=0.6 cm
slope vs Ω_c
X = 110.42 cm
FIG. 5.17 b
Ω_c (981 dynes/sec-cm)
slope, %
pr= 1.8 cm
pr= 1.2 cm
pr= 0.6 cm
slope vs Ω_c
X = 154.58 cm
FIG. 5.17 c

Table 5.1 Summary of Instantaneous Force Measurements

Record No	S_o %	Ω $\frac{981 \text{ dynes}}{\text{sec cm}}$	pr (cm)	$\overline{FD}$ (981 dynes)	$(Sd)_{FD}$ (981 dynes)	$\frac{(Sd)_{FD}}{\overline{FD}}$	Sk
4	9.0	65.69	1.66	99.98	30.56	0.306	0.908
5		56.19	1.66	94.55	43.14	0.456	1.94
6		56.19	2.66	42.65	15.65	0.367	0.43
8		65.69	4.84	62.95	20.90	0.333	4.02
9		46.27	4.84	19.83	40.47	2.020	-0.74
10		65.69	3.84	38.90	36.79	0.945	-3.68
11		46.27	3.84	28.67	40.62	1.415	-2.56
12	23.34	119.98	2.84	84.07	28.85	0.344	-0.35
13		145.74	2.84	61.65	21.82	0.354	0.02
15		119.98	3.84	94.44	25.39	0.269	-0.94
16		145.74	3.84	95.06	26.92	0.281	1.16
17		170.37	3.84	98.52	34.98	0.355	-0.18
18		119.98	4.84	49.52	19.92	0.402	1.23
19		145.74	4.84	60.65	33.04	0.545	0.79
20		170.37	4.84	60.18	30.44	0.506	-0.30
21	35.00	180.02	4.84	96.94	36.66	0.378	0.43
22		218.67	4.84	135.83	73.23	0.540	3.47
23		255.63	4.84	124.55	44.69	0.359	0.23
24		180.02	3.84	140.05	29.05	0.210	-0.23
25		218.67	3.84	122.86	35.15	0.287	-0.45
26		255.63	3.84	205.74	59.58	0.290	-0.20
27		180.02	2.84	123.64	30.91	0.250	-0.46
28		218.67	2.84	188.62	48.40	0.256	-1.93
29		255.63	2.84	151.04	50.27	0.332	-0.45

Table 5.1 continued

Record No	S_o %	Ω $\frac{981 \text{ dynes}}{\text{sec cm}}$	pr (cm)	$\overline{FL}$ (981 dynes)	$(Sd)_{FL}$ (981 dynes)	$\frac{(Sd)_{FL}}{\overline{FL}}$	Sk
4	9.0	65.69	1.66	39.73	27.11	0.683	-0.80
5		56.19	1.66	-11.71	40.67	-3.465	-1.49
6		56.19	2.66	52.07	23.37	0.442	-4.07
8		65.69	4.84	-3.64	18.08	-4.970	-0.29
9		46.27		-15.74	36.62	-2.330	0.46
10		65.69	3.84	37.04	31.68	0.846	3.64
11		46.27		7.23	33.82	4.690	2.50
12	23.34	119.98	2.84	37.75	31.10	0.825	-1.36
13		145.74		76.41	33.28	0.436	-3.10
15		119.98	3.84	-21.09	22.39	-1.080	-0.51
16		145.74		16.27	22.86	1.405	-0.50
17		170.37		24.84	36.94	1.480	-0.71
18		119.98	4.84	-33.55	17.00	-0.507	-1.58
19		145.74		-32.74	32.12	-0.982	-1.17
20		170.37		-10.78	27.81	-2.590	0.07
21	35.00	180.02		-90.56	27.34	-0.301	-0.50
22		218.67		-112.59	50.30	-0.446	-2.00
23		255.63		-98.94	43.37	-0.437	-0.72
24		180.02	3.84	-73.02	22.25	-0.304	-0.12
25		218.67		-36.23	32.10	-0.885	0.91
26		255.63		-146.30	50.22	-0.343	0.11
27		180.02	2.84	24.26	30.78	1.270	-0.15
28		218.67	2.84	13.18	42.96	3.260	1.26
29		255.63	2.84	42.99	45.97	1.070	0.26

Table 5.1 continued

Record No	S_o %	Ω $\frac{981 \text{ dynes}}{\text{sec cm}}$	pr (cm)	$\overline{TM}$ 981 dynes cm	$(Sd)_{\overline{TM}}$ 981 dynes. cm	$\frac{(Sd)_{TM}}{\overline{TM}}$	Sk
4	9.0	65.69	1.66	+394.12	276.96	0.703	-0.97
5		56.19	1.66	+327.20	393.39	1.202	-2.50
6		56.19	2.66	-191.42	133.43	-0.696	-4.06
8		68.69	4.84	-71.96	202.07	2.808	-4.95
9		46.27		-218.50	343.23	1.571	0.78
10		65.69	3.84	-164.42	306.78	1.866	3.84
11		46.27		-156.80	348.94	2.225	2.31
12	23.34	119.98	2.84	+124.92	-126.66	1.014	0.27
13		145.74		-191.15	155.81	0.815	-0.31
15		119.98	3.84	+321.56	161.71	0.698	1.12
16		145.74		+181.70	200.09	1.101	-1.41
17		170.37	4.84	+48.85	224.81	4.602	0.38
18		119.98		-47.93	138.15	2.882	-0.19
19		145.74		-88.38	252.46	2.857	-0.54
20		170.37		-175.18	253.32	1.446	0.44
21	35.00	180.02		-171.26	251.73	3.533	-0.95
22		218.67		+262.70	577.85	2.200	5.23
23		255.63		+104.76	287.53	2.744	-0.33
24		180.02	3.84	+326.28	224.87	0.689	0.69
25		218.67		+265.90	275.21	1.035	0.03
26		255.63		+618.49	508.95	0.823	0.35
27		180.02	2.84	+260.45	221.85	0.852	0.47
28		218.67		+820.96	362.74	0.442	2.30
29		255.63		+398.77	382.70	0.960	0.64

Table 5.1 continued

Record No	S_o %	Ω $\frac{981 \text{ dynes}}{\text{sec cm}}$	pr cm	$\bar{a}$ rad/sec^2	$(Sd)_a$ rad/sec^2	$\frac{(Sd)_a}{\bar{a}}$	Sk	Prob. ($a \leq 0$) %
4	9.0	65.69	1.66	33.84	127.64	3.772	0.79	44
5		56.19	1.66	64.24	173.85	2.706	1.99	75
6		56.19	2.66	-234.50	70.07	0.299	-0.31	99
8		65.69	4.84	44.10	120.75	2.740	5.06	30
9		46.27		-159.1	206.38	1.297	-0.79	77
10		65.69	3.84	-122.08	165.61	1.357	-3.69	96
11		46.27		-208.00	191.30	0.920	-2.17	91
12	23.34	119.98	2.84	-25.88	98.68	3.813	-0.46	60
13		145.74		-159.70	80.31	0.503	0.47	97
15		119.98	3.84	60.54	90.43	1.492	-1.39	18
16		145.74		67.54	111.59	1.652	1.55	23
17		170.37		11.26	123.41	10.960	-0.44	46
18		119.98	4.84	-5.40	88.02	16.300	0.20	52
19		145.74		-11.98	154.51	12.900	0.55	56
20		170.37		-47.03	153.89	3.272	-0.42	67
21	35.00	180.02		121.76	158.79	1.304	0.91	20
22		218.67		255.78	359.04	1.404	4.94	17
23		255.63		168.43	179.84	1.070	0.35	15
24		180.02	3.84	139.22	126.86	0.911	-0.57	12
25		218.67		123.28	152.21	1.235	0.16	9
26		255.63		287.54	282.53	0.983	-0.35	12
27		180.02	2.84	93.31	113.28	1.214	-0.30	15
28		218.67		409.60	181.83	0.444	-2.11	2
29		255.63		202.22	190.13	0.940	-0.60	10

Table 5.2 Summary of Initiation of Motion Experimental Results on a Loose Sphere, D = 5.1 cm, ρ_s = 2.65 gm/cm^3

Ω_c $\frac{981 \text{ dynes}}{\text{sec cm}}$	q_c (cm^3/sec cm)	x cm	Slope %	pr cm
79.80	228.00	66.25	35.00	0.6
73.93	211.24			1.2
60.95	174.14			1.8
46.07	131.64			2.4
83.00	237.32	110.42		0.6
76.41	218.30			1.2
65.16	186.17			1.8
90.70	259.13	154.58		0.6
83.00	237.32			1.2
65.16	186.11			1.8
63.34	271.38	66.25	23.34	0.6
57.48	246.28			1.2
50.95	218.30			1.8
68.70	294.36	110.42		0.6
59.50	254.92			1.2
55.39	237.32			1.8
84.00	360.00	154.58		0.6
75.26	322.45			1.2
59.50	254.92			1.8
60.71	383.70	66.25	15.82	0.6
51.01	322.45			1.2
41.65	263.28			1.8
57.03	360.51	110.42		0.6
46.57	294.36			1.2
40.33	254.92			1.8
69.85	441.53	154.58		0.6
64.19	405.71			1.2
49.93	315.66			1.8
58.36	858.18	66.25	6.80	0.6
52.96	778.79			1.2
40.28	592.38			1.8

CHAPTER 6

Conclusions

6.1 Stage I

1. To describe the geometrical and physical properties of a coarse solid mixture, it is thought that the following information should be gathered:

   (i) A weight distribution curve, like Fig. 3.1 , is more accurate and practical to determine than the classical size distribution curve obtained by sieve analysis.

   (ii) A shape factor distribution curve, like Fig. 3.2 , gives a fair idea about the flatness of the solids.

   (iii) The mass density of the mixture could be measured by measuring the mass density of individual stones as was mentioned in article 3.2.1.1.

2. Initiation of motion of coarse stones by a shallow supercritical stream constitutes a special problem that has been overlooked in literature. Only recently, few investigators have just touched upon the analysis of this problem.

3. The idea of the stream power, as introduced to sediment transport by R.A. Bagnold, could be adopted and modified to fit the special flow conditions of a shallow supercritical stream. It is thought that the critical stream power as was defined in article 3.2.2.5.1 could be statistically determined for one solid mixture and different channel slopes.

4. The increase of Ω_c with increasing channel slopes S_o is attributed to the extra stream power consumption needed to maintain higher degrees of turbulence and more air entrainment in steeper streams.

5. Prediction of Ω_c for coarser solid mixtures (but of a similar shape and of the same ρ_s as the granite mixture tested in this investigation) subjected to prototype tumbling streams could be based on a Froude model similarity criteria, as was explained in article 3.2.2.5.4. Assuming that air entrainment in the model is less than that in the prototype, this will introduce a scale effect.

6. Comparison of Ω_c as determined in this investigation, with those based on data obtained from different sources shows that the present experiments could be considered exploratory.

7. Solids dislodged by stream powers greater than the critical one are very poorly predicted by equations 3.9 and 3.14. The low degree of correlation in the aforementioned equations is mainly due to the following factors:

1. The crude assumption that the speed of dislodged solids $\overline{U} = \overline{V}g$ (the fall velocity of a solid whose size is equal to D_{50} of the solid mixture).
2. The random shape and orientations of solids.
3. The random nature of the fluid driving forces which will be discussed in the conclusions of Stage II.

6.2 Stage II

1. By designing a force transducer as described in section 5.3, it is possible to isolate and measure the instantaneous and simultaneous values of drag, lift, and torque on a sphere subjected to a supercritical stream. The design of the force transducer should be a compromise between one with a high natural frequency of vibration (in air and water), and one which is not so stiff as to make the stresses induced by the stream too small to measure. The reason why a force transducer should have a high natural frequency is mainly to prevent resonance occurring as a result of the coincidence of the frequency of the turbulent forces on the sphere with the natural frequency of the force transducer. However, since the natural frequency in still water of the force transducer designed for this investigation, is only 70 Hz and electronic noise may have been superimposed on the stress signals, digital filtering was applied to the output stress signals for the reasons mentioned in section 5.4.

2. Statistical analysis of the simultaneous and instantaneous records of FD, FL, TM and a (see Figs. 5.8a, b, c and d) revealed the following features.

6.2.1 Mean Values and Standard Deviations

6.2.1.1 Drag

The mean value of the drag $\overline{FD}$ increases with the stream power as shown in Figs 9.9a, b and c. Increasing the sphere protrusion weakly decreases the mean drag.

The ratio of the standard deviation to the mean value of the drag force $\frac{(Sd)_{FD}}{\overline{FD}}$ varies in the following ranges:

0.2 to 0.55 for 21 test records

and 0.945, 1.415 and 2.02 for records number 10, 11 and 9 respectively (see Table 5.1).

6.2.1.2 Lift

For a sphere protrusion of 2.84 cm, $\overline{FL}$ is virtually constant and positive for increasing values of Ω (see Fig.5.10a); while for greater sphere protrusions of 3.84 and 4.84 cm , $\overline{FL}$ becomes increasingly negative with increasing Ω (see Figs.5.10b and c). The ratio of the standard deviation to the mean value of the lift force $\frac{(Sd)_{FL}}{\overline{FL}}$ varies in the following ranges:

0.3 to 1 for 13 test records

1.0 to 1.5 for 5 test records

and 1.5 to 4.95 for 6 test records

(see Table 5.1).

6.2.1.3 Torque Due to Skin Friction

Surprisingly, TM emerged from this investigation to be an equal contributor to dislodge a loose sphere as drag and lift. $\overline{TM}$ increases with Ω (see Fig.5.11a, b and c), but the degree of scatter is greater than both cases of drag and lift. The ratio of the standard deviation to the mean value of the torque $\frac{(Sd)_{TM}}{\overline{TM}}$ varies in the following ranges:

0.44 to 1.50 for 13 test records

and 1.50 to 4.60 for 11 test runs

as can be seen in Table 5.1.

6.2.1.4 Angular Acceleration

The angular acceleration a of a loose sphere is a measure of

whether the fluid driving forces (FD, FL and TM) overcome the submerged weight of the sphere and hence cause the loose sphere to roll or be ejected from its recess downstream.

The relation between $\bar{a}$ and Ω (see Fig 5.13a, b and c) looks much the same as that between $\overline{TM}$ and Ω. A loose sphere could be considered stable if a critical stream power Ω_c would just make the mean angular acceleration plus one standard deviation above the mean equal to zero. The critical stream power thus defined decreases weakly with increasing protrusion of the test sphere.

The standard deviations of a are in the range of 44% to 150% of $\bar{a}$ for most test runs, except where $\bar{a}$ is close to zero. In such case the standard deviation becomes equal to several times the mean value.

6.2.2 Probability Distributions

Sample probability distribution curves of the variables FD, FL and TM (see Figs. 5.14a, b and c) show a distinct S shape. Such a feature implies that the fluid driving forces are statistically distributed according to a somewhat skewed normal error law. The skewness for each of the aforementioned variables is tabulated in Table 5.1 for all test runs.

The percentage stability of a loose particle is defined as the probability that the angular acceleration is equal to zero. It was shown in Figs. 5.14e, f and g that % stability reaches a high value of 85% for a critical stream power Ω_c. The critical stream power based on probability considerations weakly decreases with increasing protrusion of the test sphere.

6.2.3 Auto Correlation Functions

The shapes of the autocorrelation curves, for all the test runs

and for the three variables FD, FL and TM show a rapid decay of the autocorrelation coefficient $\frac{R(r\Delta t)}{R(o)}$ with increasing lag time ($r\Delta t$). $\frac{R(r\Delta t)}{R(o)}$ reaches a zero value immediately after several time steps (each time step is 0.025 seconds) and then oscillates between positive and negative values indefinitely (see Figs.5.15a, b and c). This shape of autocorrelation curves implies that the fluid driving forces FD, FL and TM are random and have a wide band of frequencies. It could also be concluded that there is practically no dependence of one set of values of FD, FL and TM measured at one instant of time, upon another set of values measured at earlier or subsequent instants of time.

6.2.4 Spectral Density Functions

There is one feature dominating all spectral density curves, namely: all of them have many peaks and troughs in a wide band of frequencies ranging from 0.8 to 15 Hz. Consequently, it may be anticipated that, a steep rough stream is dominated by a complex eddy structure where a wide range of eddy sizes and frequencies may be present.

6.3 The Critical Stream Power in the Case of a Loose Sphere

The variation of Ω_c (associated with the initial instability of a loose sphere) with increasing channel slopes S_o are shown in Figs. 5.17a, b and c, where the following conclusions could be drawn:

(i) For one sphere protrusion, Ω_c increases with S_o.

(ii) For one channel slope, the greater is the sphere protrusion, the less is the critical stream power.

(iii) Keeping the channel slope and the sphere protrusion constant, the critical stream power weakly increases with increasing x (where x is the longitudinal distance from the leading edge of the test flume to the position of the loose sphere).

6.4 The Link Between Stages I and II

Stages I and II of this investigation are linked through the following common grounds:

6.4.1 Link in Geometry and Hydraulic Parameters

In Stage I, the granite stone mixture (which was used to line the channel bed) has a D_{50} = 5 cms and ρ_s = 2.65 gm/cm^3; while in Stage II, the spheres lining the channel bed have a diameter D = 5.1 cms. The mass density of the loose sphere in Stage II was also 2.65 gm/cm^3.

The range of channel slopes covered in both stages varied between 6.8% to 49% in Stage I and from 6.8% to 35% in Stage II. In both stages the flow was shallow and tumbling and the only hydraulic parameters that could be practically measured were the discharge Q and the channel slope S_o. The stream power per unit area Ω was adopted to be the only practical hydraulic parameter to which the initial instability of a loose particle is related.

6.4.2 Link in Results

(i) There is a striking similarity between the trend of increasing Ω_c with increasing S_o in the case of a loose sphere (Stage II, article 5.5.3) and that of a granite stone mixture (Stage I, article 3.2.2.5.2). The only difference between the two trends is that the rate of increase of Ω_c with increasing S_o is much higher in the case of the granite stone mixture (compare Table 3.6 with Table 5.2). Consequently, if both angular and rounded stone mixtures were available to line a steep open channel, the angular mixture is preferred to the rounded one because the former is more stable than the latter under similar hydraulic conditions (it is assumed that the size distribution and the mass density are the same in both angular and rounded stone mixtures).

(ii) It was established in Stage II that the standard deviations of FD, FL and TM (acting on a sphere in a steep rough channel) from their corresponding mean values fluctuate in ranges mentioned in articles 6.2.1.1, 6.2.1.2, 6.2.1.3 and 6.2.1.4.

Consequently, it could be anticipated that the hydrodynamic forces acting on an irregular particle are at least as random as those acting on a smooth sphere, if not more. Hence, the low degree of correlation of equation 3.9 (established in Stage I between the rate of scour and the stream power) could be partly attributed to the wide ranges of fluctuations of the fluid driving forces.

(iii) In Stage I, equation 3.9 shows an increase in scour rate with increasing stream power. Such a trend has a parallel in Stage II, where the mean angular acceleration $\bar{a}$, increases with increasing Ω and % stability decreases with increasing Ω (see Figs.5.13a, b and c and 5.14e, f and g).

(iv) In Stage II, statistical analysis of FD, FL and TM acting on a sphere showed that the aforementioned variables belong to a stationary random category with a wide band of dominant frequencies. Consequently, the initial instability of a loose particle (whether being a sphere or irregular in shape) is a random process that could be investigated via one or both of the following two approaches:

1. Regression analysis to extrapolate Ω_c from scour experiments on real stone mixtures as was done in Stage I.
2. Force measurements on individual geometrical solids (a sphere) and their statistical analysis to shed more light on the nature of forces responsible for the initial dislodgement of a loose particle. Therefore, Stages I and II are thought to complement one another.

(v) The Froude Model similarity criteria could be applied to the results obtained from both Stages I and II to predict the stability of prototype solids subjected to prototype tumbling streams.

6.5 An Outlook for Future Research

It is suggested that future research on the problem of the initial instability of stones in steep shallow streams be along the following lines:

(i) Scour experiments like those in Stage I, but conducted in longer and wider flumes (suggested length 200 times D_{50} and width 10 times D_{50} of the stone mixture tested). D_{50} of the stone mixtures should vary from 10, 20 to 30 cm . The time of observation under which very low rates of scour occur should be increased to perhaps one day for each experimental run. Regression analysis should be employed to determine the critical stream power.

(ii) Force measurements on idealized particles and their statistical analysis, as in Stage II, should include the following.

1. Design a force transducer whose natural frequency in still water is as high as 200 Hz. Such a requirement would entail the use of semi-conductor strainguages to detect the small stresses induced in the force transducer.
2. Investigate the effect of the surface roughness of the ideal particle itself on its initial instability.
3. In order to cover a wide range of slopes, discharges, sphere protrusions, surface roughnesses of the ideal particle itself and different size combinations of spheres in a reasonable time, an improved method of recording the stresses induced in the force transducer and of analysing them

directly is required, by employing sophisticated data analog facilities.

4. Force measurements on other idealized particles such as cubes, pyramids or flat parallelograms could prove helpful in improving the understanding of the initial instability of irregular particles.

5. Initiation of motion experiments on loose cubes, pyramids or flat flakes could be of a considerable value in checking on the force measurements suggested in part 4 above.

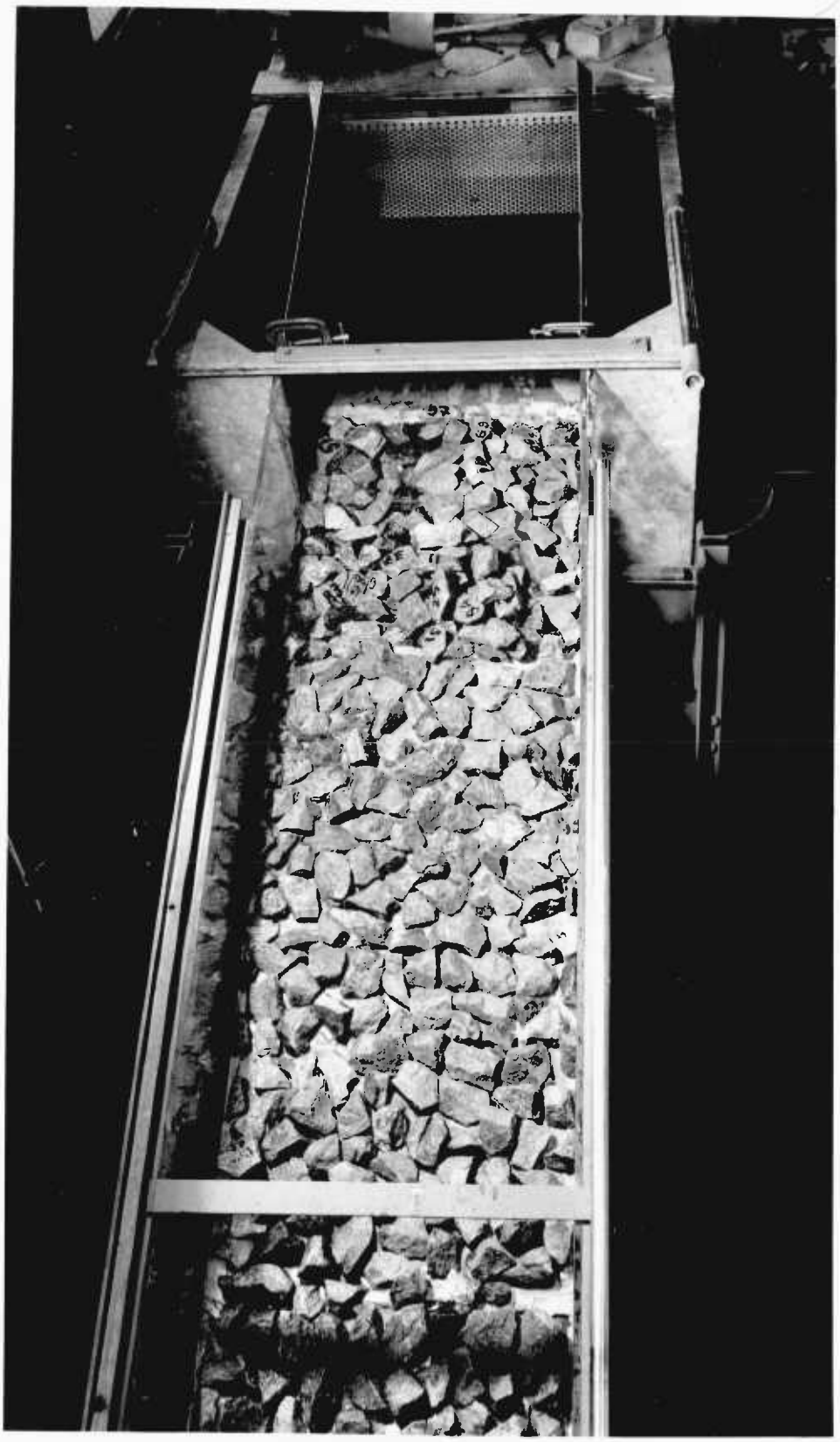


Plate 1. Top view of flume (looking upstream) showing the bed roughened with granite stones. Scale indicator: width of flume = 50 cm.



Plate 2. Top view of flume (looking up-stream showing the shallowness of the stream and the roughness of the water surface. Scale indicator: width of flume = 50 cm.

Q = 24.63 litres/sec, Slope = 30%.

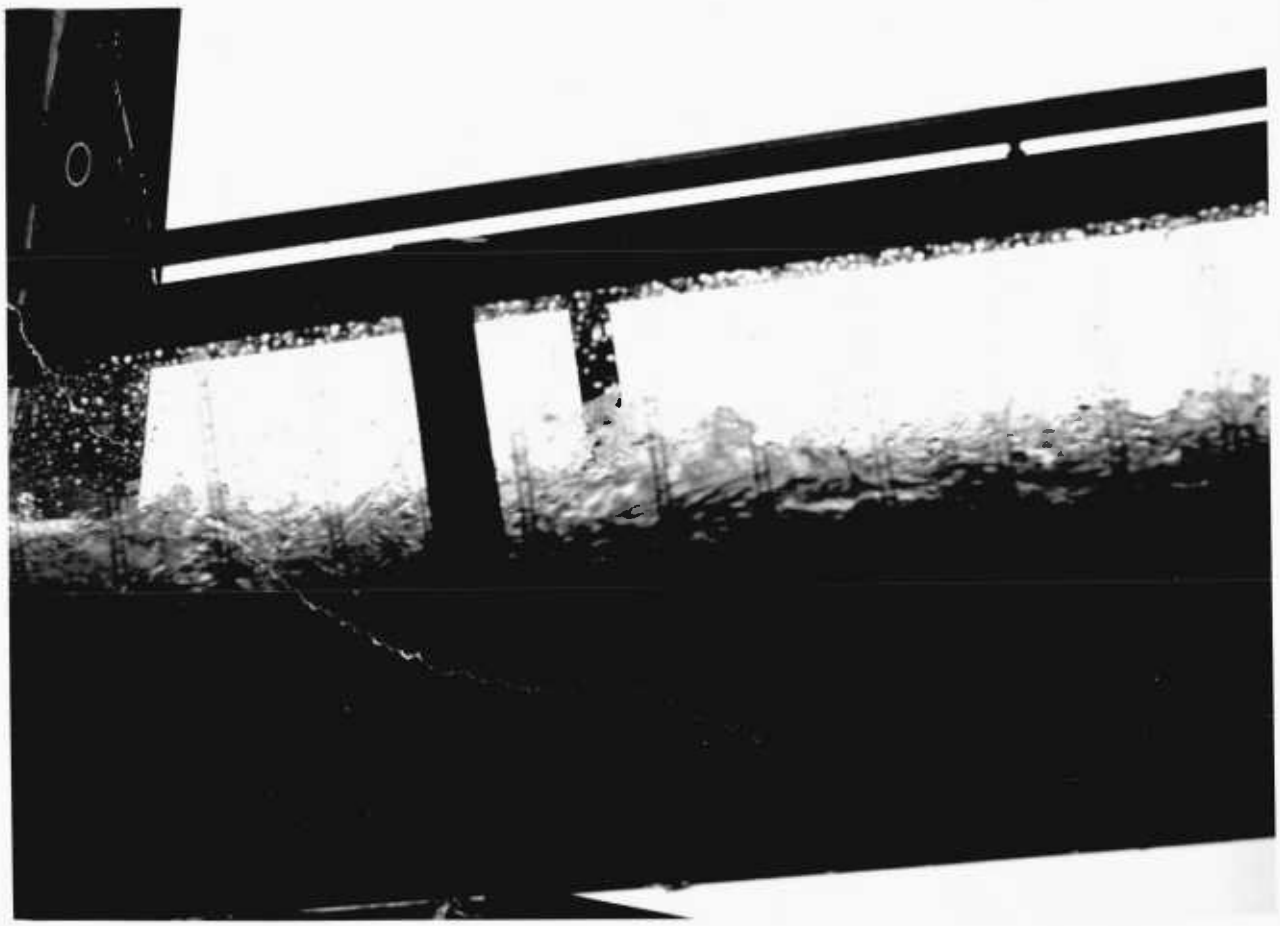


Plate 3. Profile of flow (direction of flow is from right to left) showing a distorted water surface. Scale indicator: Depth of flow is in the order of 6 to 8cm.
Q = 24.63 litres/sec, Slope = 30%.

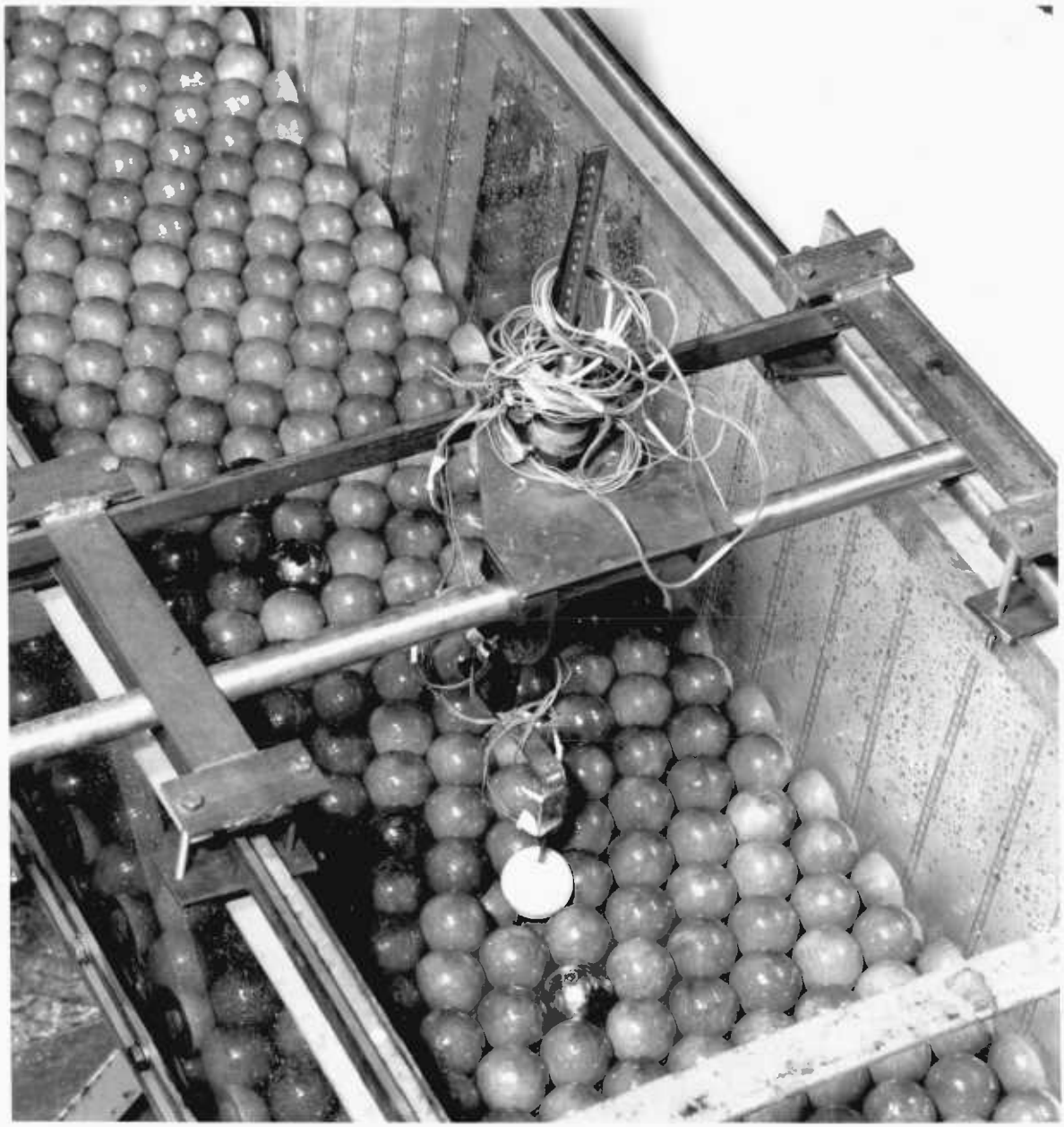


Plate 4. Top view of flume (looking up-stream) showing the force transducer, the idealized bed of spheres and the hexagonal packing. Scale indicator: diameter of each sphere = 5.1 cm.

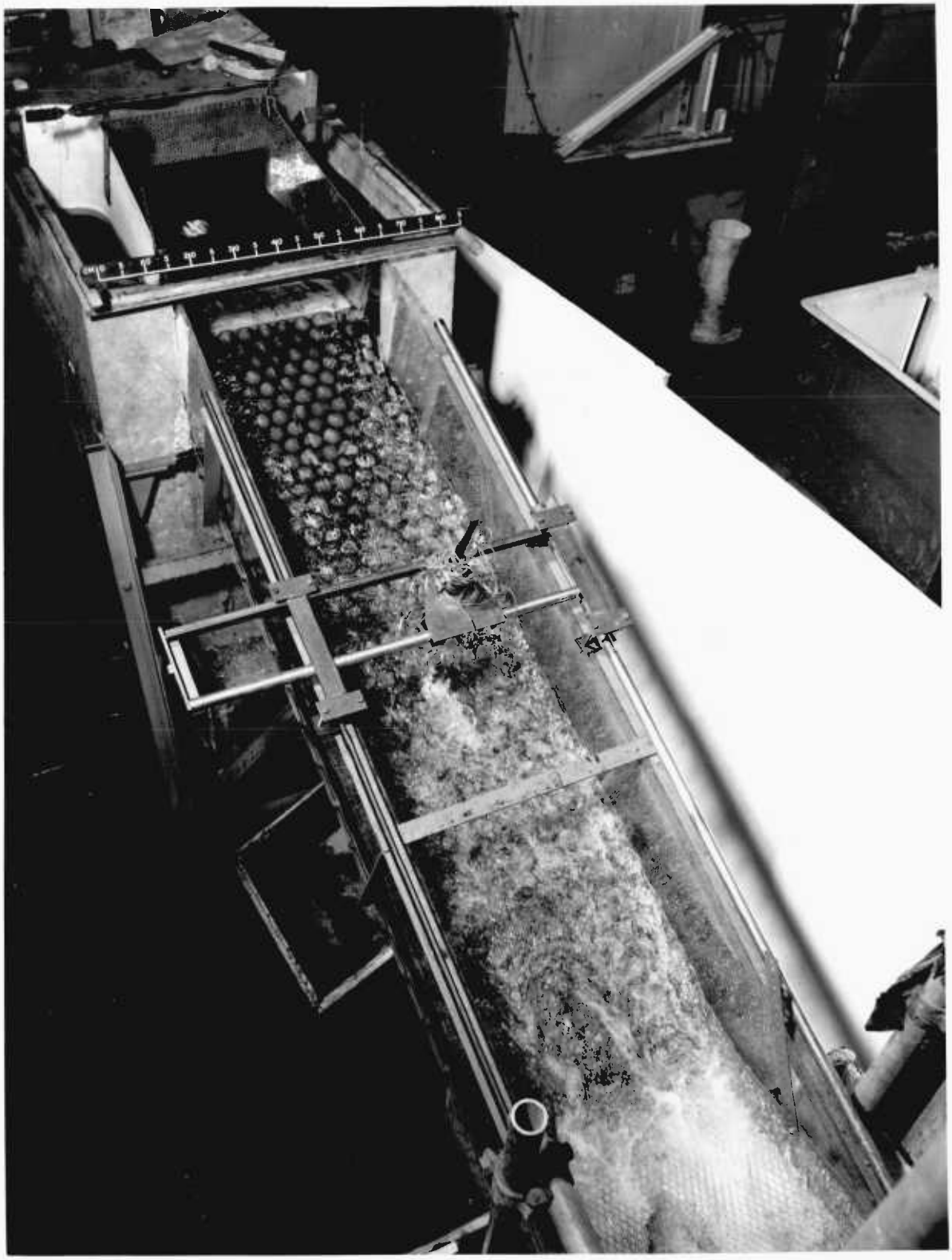


Plate 5. Top view of flume (looking up-stream) showing the force transducer mounted in position and a rough, shallow and supercritical stream over the idealized bed of spheres. Air entrainment is clearly indicated by the white spots on the water surface.

Q = 24.63 litres/sec, Slope = 20.8%.



Plate 6. Profile of a shallow super critical stream over a steep bed of spheres. Scale indicator: diameter of sphere = 5.1 cm.
Q = 24.63 litres/sec. Slope = 20.8%



Plate 7. Profile of force transducer showing the mounting arrangement and the point gauge. Scale indicator: diameter of sphere = 5.1 cm.



Plate 8. A close view of force transducer showing the strain gauges glued and water-proofed. Scale indicator: diameter of sphere = 5.1 cm.

List of Symbols

A	Projected area of a sphere on a plane normal to the mean flow direction. $A = \frac{\pi}{4} D^2$.
A_f	Area of a circular orifice.
A_1	A constant.
a_1, a_2, a_3	Dimensions of an irregular particle measured in three perpendicular directions passing through its centre of gravity, a_1 is the smallest dimension.
$a, \bar{a}$	Angular acceleration (rad/sec^2), mean angular acceleration.
b	A cross-sectional area of a circular cylinder.
$c; c_o, c_1$	A roughness factor; constants of integration.
$\bar{C}$	Mean concentration of air defined as the ratio of the volume of air to the volume of the air-water mixture.
C_1	A non-dimensional constant of integration, calibration constant.
C_3, C_7	Calibration constants.
c_d	A coefficient of discharge of an orifice plate.
C_D	Coefficient of drag of a sphere or of an irregular particle.
C_L	Coefficient of lift of a sphere or of an irregular particle.
cm	Centimetre, 1/100 of a metre. mm = 1/10 of a cm.
D	Diameter of a sphere.
$D_n, (D_n)_d$	Nominal diameter of an irregular solid, $D_n = (\frac{6}{\pi}$ volume of solid$)^{1/3}$, size distribution of a stone mixture.
D_{50}	The nominal diameter of a solid in a solid mixture where 50% by weight of that mixture is finer than that size.
%dg	Percentage damage.
^oC	Degree Centigrade.
d	Depth of flow measured from a theoretical bed level to the water surface.

List of Symbols Continued

d_1, d_3, d_7	Deflections of signals S_1, S_3 and S_7 during static loading.
d_m	An imaginary depth of flow in a rough steep channel.
E	Efficiency of a stream in transporting solids.
$\Delta E_1, \Delta E_2$	Potential difference.
e_o, e_1	Constants.
F_1	A tangential force necessary to pull a solid along a rough inclined bed with a constant speed $\overline{U}$.
F(in)	Force input to a mechanical system.
Fr	The Froude Number defined as $Fr = \overline{V}/(gd)^{\frac{1}{2}}$.
F_B	Buoyancy force.
F.T	The fluid thrust.
f	Frequency of vibrations.
f(...)	A function of ...
f_n	Natural frequency of vibrations of a structure.
FD; $\overline{FD}$	Form drag force; mean drag force.
FL; $\overline{FL}$	Lift force; mean lift force.
ft	Foot, a unit of length.
G	Immersed weight of a solid.
G(f)	Power spectral density function.
g	Acceleration due to gravity.
gm	Gram mass.
H	Head difference between two tapping points in a pipe, measured in cm of water.
Hz	Hertz, one cycle/sec.
I	Hydrodynamic impact force on a solid.
K,k	Empirical constants.
K_m	Mean roughness size of a solid mixture lining a steep channel bed. $K_m = (D_{50}/3)$.

List of Symbols Continued

ℓ	Mean size of a square eddy.
m;m'	Mass of a sphere; added mass of a sphere.
L	Scale ratio of linear dimensions in a Froude Model.
M_B, M_C, M_O M_1, M_3, M_7	Bending moments.
$M\Delta t$	Maximum lag time.
mm	Millimetre.
min	Minute.
N	The total number of solids per layer placed in a mobile section of a known area, or number of data points in a record.
N_L	The number of layers in a mobile section.
N_O	Number of orientations of loose solids.
N_r	A normal contact force.
P.F1, P.F2	Packing factors.
P	Stream power per unit length of a channel.
Δp	Mean pressure difference.
pr	Protrusion of a sphere.
Q	Volumetric discharge of water in a channel or a pipe.
$q; q_c$	Volumetric discharge per unit width of a wide rectangular channel; critical volumetric discharge per unit width.
R	A resistance friction force, or unknown reaction force.
$R(r\Delta t)$	Autocorrelation function.
Re	Reynolds number defined as $\overline{V}D/\nu$.
Re_*	The boundary roughness Resynolds number, defined as $D_n V_{*c}/\nu$.
$r\Delta t$	Lag time.
r_o, r_1	Coefficients of correlation.

List of Symbols Continued

S	The striking area of one solid = $\frac{\pi}{8} D_n^2$.
S_1, S_3, S_7	Three sections in a force transducer, or three signals.
S_o	Slope of a channel bed, $S_o = \sin \beta$ in steep channels and $S_o = \tan \beta$ in mild ones.
Sd	Standard deviation.
sec	Second; a unit of time.
S.F; $(S.F)_d$	Shape factor; shape factor distribution of a stone mixture.
T; t	Duration of time a solid is exposed to a stream; time as a variable.
TM; $\overline{TM}$	A torque due to skin friction stresses distributed on the surface of a sphere; Mean torque.
$\overline{U}$	An average velocity of a solid during sliding, rolling or short saltations.
U_L	Under layer condition.
V_*	Shear velocity = $(\tau_o/\rho)^{\frac{1}{2}}$.
V_{*c}	Critical shear velocity = $(\tau_c/\rho)^{\frac{1}{2}}$.
$\overline{V}$	An average velocity of a stream.
V	Free stream velocity of an infinitely deep flow.
$\overline{V}_m$	An imaginary average stream velocity of an air-water mixture.
$\overline{V}_c$	A critical average stream velocity.
$v_{b\,c}$	A critical velocity near the bed of a channel.
v	Velocity of a stream at a depth y above the theoretical bed level.
V_g; $(V_g)_d$	The terminal fall velocity of a solid in still water; Fall velocity distribution of a stone mixture.
$\overline{V}_g$	Fall velocity of a stone whose size is D_{50} of a stone mixture.

List of Symbols Continued

$W,(W)_d$	The weight of an irregular solid; weight distribution of a solid mixture.
w	The weight of loose solids per layer per unit area of the channel bed.
w_k	Work rate per unit area of the channel bed.
x	Longitudinal distance measured from the leading edge of the flume along its centre line.
X_1, X_3, X_7, X_B, X_C	Distances shown in Fig. 4.1a .
X_n, X	The nth amplitude of a random wave.
$X(t)$	The amplitude of a variable X measured at any time t.
$X'_n(t)$	The nth amplitude of a stationary random wave with zero mean.
y	Elevation of a point in a stream above the theoretical bed level.
Y	A dependent variable.
z	A distance measured normal to the side wall of the flume
α	The angle of sliding friction.
α_1	The angle of internal friction.
β	The angle of inclination of a channel bed measured from the horizontal.
ε	Surface tension stress.
δ_l	Laminar boundary layer thickness.
δ_{tra}	Transition boundary layer thickness.
δ_{tur}	Turbulent boundary layer thickness.
δ'	Laminar boundary sublayer thickness.
λ	A resistance coefficient.
σ	Aeration factor.

List of Symbols Continued

τ	Shear stress at a unit area around a point in a stream.
γ_s	Dry weight density of solids.
ξ	Damping ratio.
τ_{*c}	Dimensionless critical shear stress.
τ_{*s}	Dimensionless critical shear stress adjusted for steep channel slopes.
τ_o	Shear stress at the channel bed.
τ_c	Critical shear stress at the channel bed.
μ	Viscosity of water.
ν	Kinematic viscosity of water.
$\rho; \rho(X)$	Mass density of water; probability density function of a variable X.
ρ_m	Mass density of an air-water mixture.
ρ_s	Mass density of solids.
Ω	Stream power per unit area of a channel bed.
Ω_c	Critical stream power per unit bed area.
Ω_{co}, Ω_{c1}	Critical stream powers that correspond to 0%dg and 1%dg respectively.

References

1. Apperley, L.W. (1968) "The Effect of turbulence on sediment entrainment". PhD thesis submitted to the University of Auckland, New Zealand.

2. Ashida, K., and Bayazit, M. (1973) "Initiation of motion and roughness of flow in steep channels". Proc. of 15th Congress of I.A.H.R., Vol. 1, pp. 475-484.

3. Bagnold, R.A. (1966) "An approach to the sediment transport problem from general physics". U.S Geological Survey, Professional Paper 422-J.

4. Bagnold, R.A. (1973) "The nature of saltation and of 'bed load' transport in water". Proc. Royal Society of London, Vol. 332, April.

5. Bendate, J.S., and Piersol, A.G. (1971) "Random data analysis and measurements procedures". Edited by John Wiley and Sons.

6. Blackman, R.B., and Tukey, J.W. (1958) "The measurement of power spectra". Dover Publications, New York, U.S.A.

7. Bogardi, J.L. (1968) "Sediment transportation in alluvial streams". Hydrological methods for developing water resources management, Subject 12, Budapest.

8. Brownless, K.A. (1965) "Statistical theory and methodology in science and engineering". John Wiley and Sons.

9. Charng-Ning-Chen and Carstens, M.R. (1973) "Mechanics of Removal of a spherical particles from a flat bed". Proc. of 15th Congress of I.A.H.R., pp. 225-233.

10. Cheng, E.D.H., and Clyde, C.G. (1972) "Instantaneous hydrodynamic lift and drag forces on large roughness elements in turbulent open-channel flows". Sedimentation, edited by Shen, W.H.

11. Chepil, W.S. (1958) "The use of evenly spaced hemispheres to evaluate aerodynamic forces on soil surfaces". Tr. American Geophysical Union, Vol. 39, No.3.

12. Chepil, W.S. (1959) "Equilibrium of soil grains at the threshold of movement by wind". Proc. Soil Science Society of America. Vol. 23, pp. 422-428.

13. Chepil, W.S. (1961) "The use of spheres to measure lift and drag on wind eroded soil grains". Proc. Soil Science Society of America. Vol. 25, No.5.

14. Einstein, H.A., and El-Samni, A. (1949) "Hydrodynamic forces on a rough wall". Review of Modern Physics, American Institute of Physics, Lancaster, Pa., Vol. 21, No.3, July, pp. 520-524.

15. Egiazaroff, I.V. (1957) "L'Equation generale des alluvions non cohesives par un courent fluide". Proc. 7th Congress of I.A.H.R.

16. Egiazaroff, I.V. (1965) "Calculation of non uniform sediment concentrations". Journal of ASCE, Vol. 91, No.HY4, Paper 4417, July, pp. 225-247.

17. Fortier, S., and Scobey, F.C., (1926) "Permissible canal velocities". Trans. ASCE, Vol. 89, pp. 940-984.

18. Francis, J.R.D. (1958) "A text book of fluid mechanics". Edward Arnold.

19. Francis, J.R.D. (1973) "Experiments on the motion of solitary grains along the bed of a water stream". Proc. of the Royal Society of London, Vol. 332, April.

20. Gessler, J. (1965) "The beginning of bed load movement of mixtures". Translated from German by Prych, E.A., Calif. Instit. of Technology, Pasadena, Calif., U.S.A.

21. Gessler, J. (1971) "Critical shear stress for sediment mixtures". 14th Congress of I.A.H.R., Vol. 3.

22. Graf, W.H. (1971) "Hydraulics of sediment transport". McGraw Hill.

23. Grass, A.J. (1970) "Initial instability of fine bed sand". Journal of ASCE Vol. 96, No.HY3, March.

24. Hartung, F., and Scheuerlein, H. (1967) "Macroturbulent flow in steep open channels with high natural roughness". 12th Congress of I.A.H.R., Vol. 1.

25. Hartung, F., and Scheuerlein, H. (1970) "Design of overflow rock-fill dams". Dixieme Congress des Grands Barages. Vol. 1.

26. Hjulstrom, F., (1935) "Studies of the morphological activity of rivers as illustrated by the River Fyris". Bulletin, Geological Institute of Upsala, Vol. XXV, Upsala, Sweden.

27. Kenn, M.J., and Zanker, K.J. (1967) "Aspects of similarity for air-entraining water flows". Nature, Vol. 213, No.5071, pp. 59-60, January.

28. Kenn, M.J. (1969) "Dynamic similarity for flow systems in which inertia effects are small". Jour.Inst.Water Eng.,Vol. 23, No.4, June

29. Kock, J.J.; Boiten, R.G.; Biermasz, A.L.; Roszbach, G.P. and Van Santen, G.W. (1952) "Strain gauges: theory and applications". Philips Technical Library.

30. Kramer, H. (1935) "Sand mixtures and sand movement in fluvial models". Tr. ASCE, Vol. 100.

31. Lane, E.W. (1955) "Design of stable channels". Tr. ASCE, Vol. 120, pp. 1234-1279.

32. Lelliavsky, S. (1955) "An introduction to fluvial hydraulics". Constable and Company Ltd., London.

33. Mantz, P.A. (1973) "Cohesionless, fine graded, flaked sediment transport by water". Nature, Vol. 246, November.

34. Mantz, P.A. (1975) "Low transport stages by water streams of fine, cohesionless, granular and flakey sediments". PhD thesis submitted to the University of London and Imperial College of Science and Technology, London SW7.

35. Mavis, F.T.,and Laushey, L.M. (1949) "Formula for velocity at beginning of bed load movement is reappraised". Civil Engineering, Vol. 19, January.

36. Neill, C.R. (1967) "Mean velocity criterion for scour of coarse uniform bed material". Proc. of the 12th Congress of I.A.H.R., Vol. 3, Paper C6.

37. Neill, C.R. (1968) "Note on initial movement of coarse uniform bed material". Journal of hydraulic research, Vol. 6, No.2.

38. Schlichting, H. (1955) "Boundary layer theory". Tr. from German by Kestin, J., Published by McGraw Hill Book Company.

39. Shields, A. (1936) "Anwendung der ahnlichkeitsmechanik und der turbulenz forshchung auf die geschiebebewegung". English Translation by Ottand, W.P., and Uchelen, J.C., Inst. of Techn. Pasadena, Cal., U.S.A.

40. Straub, L.G., and Anderson, A.G. (1960) "Experiments on self-aerated flow in open channels". Trans. ASCE, Vol. 125, pp. 456.

41. Task Committee ASCE (1961) "Aerated flow in open channels". Proc. ASCE, Vol. 87, No.HY3 (May), pp. 73.

42. Task Committee Report (1966) "Sedimentation transportation mechanics; initiation of motion". Journal of the ASCE, Vol. 92, No.HY2, Paper 4758, March

43. Valentine, H.R. (1969) "Applied hydrodynamics". Butterwurk and Company (Publishers) Limited.

44. Vanoni, V.A. (1964) "Measurement of critical shear stress". Calif. Instit. of Technology, Rep. No.KH R7.

45. White, C.M. (1940) "The equilibrium of grains on the bed of a stream". Proc. Royal Society of London, Series A, No.958, Vol. 174.

46. White, S.J. (1970) "Plane bed threshold of fine graded sediment". Nature, Vol. 228, pp. 151-153.

47. Yang, C.T. (1973) "Incipient motion and sediment transport". Journal of ASCE, No.HY10, October.

Appendix I

Curve Fitting by the Least Square Method

Let X_i; $X_1, X_2, \ldots X_n$ be a list of an independent variable X and Y_i; $Y_1, Y_2, \ldots Y_n$ be a list of a dependent variable Y, where n is the number of observations of each variable. Assume one of the following two algebraic functions to be fitted by the least square method to the above mentioned lists of variables:

$$Y = m_1 X + m_2 \qquad \ldots\ldots\ldots\ldots\ldots\ldots \text{Eq. I.1}$$

$$Y = m_3 X^{m_4} \qquad \ldots\ldots\ldots\ldots\ldots\ldots \text{Eq. I.2}$$

where m_1, m_2, m_3 and m_4 are constants to be determined from the least square fitting. The algebraic steps involved in the determination of those constants could be found in Brownless (1965). However, an expression for each of them is written below.

$$m_1 = \frac{\sum_{i=1}^{n} (X_i - \overline{X})(Y_i - \overline{Y})}{(X_i - \overline{X})^2}$$

$$m_2 = \overline{Y} - m_1 \overline{X}$$

where $\overline{Y} = \frac{\sum_{i=1}^{n} Y_i}{n}$ and $\overline{X} = \frac{\sum_{i=1}^{n} X_i}{n}$

$$m_4 = \frac{n \sum_{i=1}^{n} (\ln X_i \ln Y_i) - \sum_{i=1}^{n} \ln X_i \sum_{i=1}^{n} \ln Y_i}{n \sum_{i=1}^{n} (\ln X_i)^2 - (\sum_{i=1}^{n} \ln X_i)^2}$$

$$m_3 = \frac{\sum_{i=1}^{n} \ln Y_i - m_4 \sum_{i=1}^{n} \ln X_i}{n}$$

There is a restriction that Y_i and X_i should be positive only for the case of m_3 and m_4.

The coefficients of correlation of equations I.1 and I.2 are as respectively defined:

$$r_1 = \frac{\sum_{i=1}^{n} (X_i - \overline{X})(Y_i - \overline{Y})}{\left[\sum_{i=1}^{n} (X_i - \overline{X})^2 \sum_{i=1}^{n} (Y_i - \overline{Y})^2 \right]^{\frac{1}{2}}}$$

$$r_2 = \frac{n \sum_{i=1}^{n} \ln X_i \ln Y_i - \left(\sum_{i=1}^{n} \ln X_i \right)\left(\sum_{i=1}^{n} \ln Y_i \right)}{\left[\{ n \sum_{i=1}^{n} (\ln X_i)^2 - \left(\sum_{i=1}^{n} \ln X_i \right)^2 \} \{ n \sum_{i=1}^{n} (\ln Y_i)^2 - \left(\sum_{i=1}^{n} \ln Y_i \right)^2 \} \right]^{\frac{1}{2}}}$$

Appendix II

Computer Programs for the Statistical Analysis of Force Measurements

This appendix contains three sample computer programs which were written to facilitate the statistical analysis of the force measurements.

The instantaneous and simultaneous values of drag (FD), turning moment (TM), lift (FL) and angular acceleration (a) were calculated according to equations 4.1, 4.2, 4.3 and 4.14 respectively, where the three simultaneous records of the stress at sections S_1, S_3 and S_7 in the force transducer were digitized and stored in the computer memory for further statistical analysis. It was necessary to work out the combined calibration constants C_1, C_3 and C_7 (for the stress records at sections S_1, S_3 and S_7 respectively) resulting from the static calibration of the force transducer and the scale factor of the x-y digitizer.

Programs I, II and III contain subroutines BDS, RSO and ASA respectively, where the aforementioned subroutines are available in Statmat file at the Imperial College Computer Centre and the publisher is: Control Data 6000 Series Computer Systems Statistical Subroutines Reference Manual, Pub. No. 60135300

Control Data Corporation

Documentation Department

3145 Porter Drive

Pala Alta

California, U.S.A.

A brief description of the subroutines is presented below:

Subroutine BDS has three arguments which are discussed in their order from left to right:

1. One dimensional array of data points (the array should not be subscripted).

2. An integer indicating the number of data points.

3. A one dimensional array called STAT, which contains 8 locations. STAT(1) contains the mean value of the data points according to equation 4.4 , STAT(3) contains the third moment of the data points about their mean according to equation 4.6 , STAT(6) contains the standard deviation according to equation 4.5 and STAT(7) contains the skewness according to equation 5.1 .

Subroutine RSO has seven arguments which are described below:

1. A multi-dimensional array of numbers stored column-wise (like numbers arranged in a determinant). However, only one column was considerd in the present appendix.

2. An integer indicating the number of data points (m) in each column.

3. An integer indicating the number of columns of the matrix considered (this integer is 1 in this investigation).

4. An integer indicating the maximum number of rows in each column.

5. An integer indicating the index of the column of data points to be rank ordered.

6. A one dimensional array dimensioned to m locations. This argument rearranges a row column of data points in a descending order of magnitude.

7. A one dimensional array which contains m locations and stores the raw numbers in a column against the rank ordered numbers in argument number 6.

Subroutine ASA has six arguments which are described below:

1. An integer N equal to the number of data points in a one dimensional array.

2. An integer M equal to the maximum number of lag time steps in the autocorrelation and spectral density functions, $1 < M < N$.

3. A one dimensional (non subscripted) array containing the N data points.

4. One storage location for the mean value of the N data points. Call this location XB.

5. T1 is a two dimensional array dimensioned to T1(10,M + 1) locations where T1(7,p + 1) and p = 0,1,2,... M contain the auto-correlation coefficient, $\frac{R(r\Delta t)}{R(0)}$ and T1(9,p + 1) contains the estimates of the smoothed power density function according to equation 4.13 .

GRAFIT is a plotting subroutine available also at the Imperial College Computer Centre and has six arguments as described below:

1. One dimensional array containing the horizontal co-ordinates of the data points to be plotted.

2. One dimensional array containing the vertical co-ordinates of the data points to be plotted.

3. An integer indicating the maximum number of data points to be plotted.

4. An integer indicating the number of the first group of data points to be plotted as asterisks.

5. An integer indicating the number of the second group of data points to be plotted as crosses and the remainder of the data points will be plotted as O.

6. If zero is printed as the last argument, the computer will plot the data points as scattered symbols without joining between them.

Finally, samples of the three computer programs I, II and III are presented below.

Program I, Means, Standard Deviations and Skewnesses

```
      PROGRAM ARITH(INPUT,OUTPUT,TAPE5=INPUT,TAPE6=OUTPUT,TAPE62)
      COMMON    S1( 200),S3( 200),S7( 200)
      COMMON    FD( 200),FL( 200),TM( 200),ACC( 200)
      COMMON    STAT1(8), STAT2(8),STAT3(8),STAT4(8)
      COMMON T(200)
      READ (5,100) (S1(I),S3(I),S7(I),I=1, 200)
  100 FORMAT((12F6.0))
C     R.16 . SLOPE=23 PER CENT, PRTRUS. =3.835CM. Q= 90CM OF WATER
C       DENSITY '=2.65
C         THIS PROGRAM CALCULATES DRAG, LIFT AND TURNING MOMENT ON A
C     SPHERE PLACED IN A FAST SHALLOW STREAM. ALSO IT CALCULATES
C     THE MEAN, STANDARD DEVIATION, SKEWNESS AND KURTOSIS OF THE ABOVE
C     3MENTIONED VARIABLES. CALCULATE ALL INSTANTANEOUS VALUES OF
C     DRAG LIFT AND TURNING MOMENT.
C
      C1=+0.1973
      C3=-0.1311
      C7=+0.0827
      C8=-128.786
      DO 10 I =1, 200
      FD(I)=16.0+(C3*S3(I)-C1*S1(I))/1.93
      TM(I)=C3*S3(I)-10.07*(FD(I)-16.0)
      FL(I)=-66.7+(C7*S7(I)-TM(I)-12.05*(FD(I)-16.0))/4.194
      ACC(I)=0.960*FD(I)+0.841*FL(I)-0.503*TM(I)+C8
      T(I)=I*2.5
   10 CONTINUE
      WRITE (6,200) (FD(I) ,FL(I),TM(I),ACC(I),I=1, 200)
  200 FORMAT(1H1,10X,///,*DRAG/GM,LIFT/GM,T.M.GM-CM,ACC R/SEC/SEC*,//,1X
     1,(F17.3,F8.3,F10.3,F13.3)
C     CALL SUBROUTINES FROM STATMAT FILE TO COMPUTE MEAN.......STANDARD DEVIATIONS AND SKEWNESSES
      CALL BDS  (FD ,    200, STAT1)
      CALL BDS  (FL ,    200, STAT2)
      CALL BDS  (TM ,    200, STAT3)
      CALL BDS  (ACC,    200, STAT4)
C     WRITE OUT MEAN STANDARD DEVIATION , SKEWNESS AND KURTOSIS OF ALL VARIABLES.
```

Program I Continued

```
25.         WRITE (6,400) (STAT1(1) ,STAT1(6) ,STAT1(7) ,STAT1(8)
26.      400 FORMAT(1HO,10X,*DRAG AVERAGE,STANDARD DEVIATION,SKEWNESS,KURTOSIS*
            1,//////,(F21.3,F19.3,F9.3,F9.3))
27.         WRITE (6,500) (STAT2(1) ,STAT2(6), STAT2(7) ,STAT2(8)
28.      500 FORMAT(1HO,10X,*LIFT AVERAGE,STANDARD DEVIATION,SKEWNESS,KURTOSIS*
            1,//////,(F21.3,F19.3,F9.3,F9.3))
29.         WRITE (6,600) (STAT3(1),STAT3(6),STAT3(7),STAT3(8))
30.      600 FORMAT(1HO,10X,*MOMT AVERAGE,STANDARD DEVIATION,SKEWNESS,KURTOSIS*
            1,//////,(F21.3,F19.3,F9.3,F9.3))
31.         WRITE (6,700) (STAT4(1),STAT4(6),STAT4(7),STAT4(8))
32.      700 FORMAT(1HO,10X,*ACCE AVERAGE,STANDARD DEVIATION,SKEWNESS,KURTOSIS*
            1,//////,(F21.3,F19.3,F9.3,F9.3))
33.         CALL GRAFIT(T,FD,100,50,25,0)
34.         CALL GRAFIT(T,TM,100,50,25,0)
35.         CALL GRAFIT(T,FL,100,50,25,0)
36.         CALL GRAFIT(T,ACC,100,50,25,0)
37.         STOP
38.         END
```

Program II, Probability Distribution

```
      PROGRAM ARITH(INPUT,OUTPUT,TAPE5=INPUT,TAPE6=OUTPUT,TAPE62)
      COMMON    S1( 200),S3( 200),S7( 200)
      COMMON    FD( 200),FL( 200),TM( 200),ACC( 200)
      COMMON T(200),PR(200)
      COMMON    DZPI( 200),DMORN( 200),UZPI( 200),UMORN( 200),TZPI( 200)
     1,TMORN( 200),ACZPI( 200),ACMORN(200)
      READ (5,100) (S1(I),S3(I),S7(I),I=1, 200)
  100 FORMAT((12F6.0)
C     R.16 . SLOPE=23 PER CENT, PRTRUS. =3.835CM. Q=90 CM OF WATER
C       DENSITY '=2.65
C     THIS PROGRAM PLOTS A CURVE FOR EACH OF THE VARIABLES FD, FL,
C     TM,ACC,VS. THE PROBABILITY OF THE FORCE LEVEL OF EACH OF THE
C     FOUR VARIABLES. THIS PROGRAM CALCULATES DRAG, LIFT AND TURNING
C     MOMENT ON A SPHERE PLACED ON A FAST SHALLOW STREAM.
C
C
C
C
C
C
      C1=+0.1973
      C3=-0.1311
      C7=+0.0827
      C8=-128.786
      DO 10 I =1, 200
      FD(I)=16.0+(C3*S3(I)-C1*S1(I)/1.93
      TM(I)=C3*S3(I)-10.07*(FD(I)-16.0)
      FL(I)=-66.7+(C7*S7(I)-TM(I)-12.05*(FD(I)-16.0))/4.194
      ACC(I)=0.960*FD(I)+0.841*FL(I)-0.503*TM(I)+C8
      T(I)=2.5*I
   10 CONTINUE
C     CALL SUBROUTINE FOR RANK ORDER
      CALL RSO(FD, 200,1, 200,1,DZPI ,DMORN)
      CALL RSO(FL, 200,1, 200,1,UZPI ,UMORN)
      CALL RSO(TM, 200,1, 200,1,TZPI ,TMORN)
      CALL RSO(ACC,200,1, 200,1,ACZPI,ACMORN)
```

Program II Continued

```
24.       WRITE(6,800)(DZPI(JK),DMORN(JK),UZPI(JK),UMORN(JK),TZPI(JK),TMORN(
          1JK),ACZPI(JK),ACMORN(JK),JK=1, 200)
25.     800 FORMAT (1HO,10X,////,*ODR./GM,TDR/SEC,OLIF/GM,TLIF/SEC,OM/GM-CM,TI
          1MM/SEC,OACC/RAD/SEC/SEC,TIM ACC/SEC*,///,1X,(F8.2,3X,F8.2,3X,F8.2,
          23X,F9.2,3X,F9.2,3X,F9.2,3X,F9.2))
26.       CALL GRAFIT (PR,DZPI,200,50,25,0)
27.       CALL GRAFIT (PR,UZPI,200,50,25,0)
28.       CALL GRAFIT (PR,TZPI,200,50,25,0)
29.       CALL GRAFIT (PR,ACZPI,200,50,25,0)
30.       STOP
31.       END
```

Program III, Autocorrelation and Spectral Density Functions

```
      PROGRAM ARITH(INPUT,OUTPUT,TAPE5=INPUT,TAPE6=OUTPUT,TAPE62)
      COMMON    S1( 200),S3( 200),S7( 200)
      COMMON    FD( 200),FL( 200),TM( 200),ACC( 200)
      COMMON T(200)
      COMMON    T1(10,101),T2(10, 101),T3(10, 101)
      DIMENSION T17(101),T27(101),T37(101),T19(101),T29(101),T39(101)
      READ (5,100) (S1(I),S3(I),S7(I),I=1, 200)
  100 FORMAT(12F6.0))
C     R.16 . SLOPE=23 PER CENT, PRTRUS. =3.835CM, Q=90 CM OF WATER
C       DENSITY !=2.65
C          THIS PROGRAM CALCULATES DRAG, LIFT TURNING MOMENT AND ANGULAR  ACCELERATION ON A
C     SPHERE PLACED IN A FAST SHALLOW STREAM. THE AUTOCORRELATION  COEFFIC.  AND THE SMOOTHED
C     SPECTRAL DENSITY FUNCTIONS ARE ALSO CALCULATED AND PLOTTED.
C
C
C
      C1=+0.1973
      C3=-0.1311
      C7=+0.0827
      C8=-128.786
      DO 10 I =1, 200
      FD(I)=16.0+(C3*S3(I)-C1*S1(I))/1.93
      TM(I)=C3*S3(I)-10.07*(FD(I)-16.0)
      FL(I)=-66.7+(C7*S7(I)-TM(I)-12.05*(FD(I)-16.0)/4.194
      ACC(I)=0.960*FD(I)+0.841*FL(I)-0.503*TM(I)+C8
      T(I)=2.5*I
   10 CONTINUE
      CALL ASA   (  200, 100,FD ,XB1,T1,REL1)
      CALL ASA   (  200, 100,FL ,XB2,T2,REL2)
      CALL ASA   (  200, 100,TM ,XB3,T3,REL3)
C     WRITE OUT AUTOCORRELATION  COEFFIC. AND SMOOTHED SPECTRAL DENSITY
      WRITE (6,300 ) (T1(7,J) ,T1(9,J),T2(7,J),T2(9,J),T3(7,J),T3(9,J)
     1J=1, 100)
  300 FORMAT (1H1,10X,//// ,* (AUT.D  -  SPEC.  D. ), (AUT. L. SPE.L.)
     1 , (AUT.  TM - SPE. TM. ),(AUT.ACC-SRE.ACC)*,///,1X,(F16.2,5X,F16.
     22,5X,F16.2,5X,F16.2,5X,F16.2,5X,F16.2))
```

Program III Continued

```
      DO 20 J=1,100
      T17(J)=T1(7,J)
      T27(J)=T2(7,J)
      T37(J)=T3(7,J)
      T19(J)=T1(9,J)*1.0E-03
      T29(J)=T2(9,J)*1.0E-03
      T39(J)=T3(9,J)*1.0E-04
20    CONTINUE
      CALL GRAFIT (T,T17,100,50,25,0)
      CALL GRAFIT (T,T27,100,50,25,0)
      CALL GRAFIT (T,T37,100,50,25,0)
      CALL GRAFIT (T,T19,100,50,25,0)
      CALL GRAFIT (T,T29,100,50,25,0)
      CALL GRAFIT (T,T39,100,50,25,0)
      STOP
      END
```